NUCLEATION PHENOMENA OCCURRING IN AQUEOUS SOLUTIONS SUPERSATURATED WITH CALCIUM SULFATE

NUCLEATION PHENOMENA OCCURRING IN AQUEOUS SOLUTIONS SUPERSATURATED WITH CALCIUM SULFATE

By

RONALD E. MASSEY, B.Sc.

A Thesis

Submitted to the Faculty of Graduate Studies

in Partial Fulfilment of the Requirements

for the Degree

Doctor of Philosophy

McMaster University

October 1974

TO

MY PARENTS

who, by their example, gave me the direction

and to

DENISE

the encouragement of a loving wife

DOCTOR OF PHILOSOPHY (1974) McMASTER UNIVERSITY
(Chemistry) Hamilton, Ontario

TITLE: Nucleation Phenomena Occurring in Aqueous Solutions Supersaturated with Calcium Sulfate

AUTHOR: Ronald E. Massey, B.Sc. (McMaster University, Hamilton)

SUPERVISOR: Dr. O. E. Hileman, Jr.

NUMBER OF PAGES: xii,137

SCOPE AND CONTENTS:

An extensive study of the nucleation phenomena of $CaSO_4.2H_2O$ under various experimental conditions was undertaken. The droplet technique, a method of isolating mote-free portions of solution, was used along with a photomicrographic method of recording the results of nucleation within the droplet population.

Experiments performed at constant temperature, supersaturation and calcium-sulfate ratio, yielded unconfounded empirical relationships between various independent and dependent nucleation variables. The most significant of these was the relationship between the lag time and the nucleation rate. Recognition of a relationship between these variables led to an extension of the droplet technique to much lower supersaturations. Also, evidence was found for two distinct pre-nucleation processes, a lag and an induction time.

The functionality between the nucleation rate and the calcium-sulfate ratio was studied. It was concluded that the classical definition of supersaturation must include the calcium-sulfate ratio.

Classical thermodynamic parameters were calculated at four experimental temperatures. Most significant of these produced a solution phase diagram for $CaSO_4 \cdot 2H_2O$.

With the information obtained above, designs of droplet experiments with a variable driving force were evaluated, taking into account the changing supersaturation and the calcium-sulfate ratio with time. Mathematical models were also developed to handle the data collected from these experiments.

The mechanism of nucleation in aqueous solution was discussed in terms of a new non-classical model using, as a source of information, all the experimental results.

*ACKNOWLEDGEMENTS

The author would like to thank Dr. O. E. Hileman, Jr. for his advice and criticism. The informal relationship he created with his graduate students provided not only a lasting friendship but also the perfect atmosphere for creative thought.

Also the author wishes to thank Dr. Morrison and Dr. Walton for their advice.

I would like to thank the other members of our research group for the coffee, donuts, food, frizbee games and stimulating conversations.

The Province of Ontario and the National Research Council are also acknowledged for their financial support.

TABLE OF CONTENTS

LIST OF FIGURES

SYMBOLS AND NOTATION

a	activity of a solute
b	intercept
f	function
k	Boltzman constant = 1.38×10^{-16} ergs deg^{-1}
m	slope
n	number of molecules in an embryo or crystal
$n_{t,v}$	number of droplets of volume v crystallized at time t
r	radius of an embryo
t	time
t_g	growth time
t_i	induction time
t_n	nucleation time
v	average droplet volume in a droplet range
$\bar{v}$	molecular volume
A	the pre-exponential factor in the nucleation rate equation
A	the surface area of the embryo
B	a parameter
C	a parameter
D	a parameter
E_i	ith experiment
ΔG	change in Gibbs free energy
ΔG_a	free energy of activation for diffusion
ΔG_{extra}	free energy of activation for phase change
ΔH	change in enthalpy
J	rate of nucleation
K	a parameter

K_{sp}	solubility product
L	the lag time
M	the time required after appearance of crystal for the attainment of a steady-state rate
N	the number of droplets in a droplet range
S	supersaturation, the square root of the ratio of the ion product to the solubility product
ΔS	change in entropy
S_{ij}	shape energy level
T	absolute temperature
X	a parameter
Y	a parameter
W_{ij}	configuration of embryos
Z	a parameter
Z	Zeldovich factor
β	a function of temperature
μ	chemical potential
σ	excess surface free energy
τ	induction time

I INTRODUCTION

I-A NUCLEATION

Deposits formed naturally from aqueous solutions have in some instances been very beneficial to mankind and a nuisance in others. Their formation is but one example of several types of phase changes, a phenomena which has intrigued and puzzled man for many years.

Experimental limitations leading to ambiguity in interpretation of experimental data has generated lively controversy between proponents of various microscopic models of crystal formation from solution. One such dividing line is placed between those transformations which proceed spontaneously (homogeneous nucleation) and those which utilize a catalytic agent (heterogeneous nucleation). The experiments described here are attempts at observing the result of homogeneous phase transformations within systems by careful solution manipulation and by use of a screening technique (droplet technique). Together they have a high probability of eliminating extraneous information generated by motes or nucleation agents.

Just as a consensus among nucleationists is lacking on a statement of their understanding of phase changes on a micro scopic level so also are they divided over the appropriate thermodynamic linkage of macroscopic parameters in classical

nucleation theory. This has, as in most sciences, created a situation in which the experimental data collection far outstrips the development of sound theory. It is then most valuable to do an about face; to leave the ranks of the data collectors and statistically evaluate one method of measuring nucleation; namely, the droplet technique. If the method is a reliable one, it can be used to test the model of nucleation.

Developing a dependable model only builds a foundation. Using this footing it is then possible to move to the more interesting problem of phase change retardation or acceleration. Natural water contains sparingly soluble salts which form scale in batch systems when the bulk is concentrated by water loss. This problem occurs in desalinization ponds, in boilers, heat exchangers, natural ponds and lakes and in the human body. Until most recently, scale has been dealt with in two different ways; removal of the sparingly soluble salts before use or removal of the scale after it has formed. The former is both troublesome and expensive and the latter is destructive and very crude. More recent advances in the prevention of scale formation have, in some cases, allowed the use of natural water with at least a retardation of scale formation.

These new developments have posed new questions of how and why inhibitors prevent phase changes. It is then only natural to place more emphasis upon the method of measurement and model adequacy.

I-B NUCLEATION HISTORY

It has been known for some time that solutions can be supersaturated and melts of pure liquids undercooled. These observations were stumbled upon over 200 years ago.

At the beginning of the 18th century, Fahrenheit[1] was attempting measurements of the freezing point of water. This work initiated the study of phase equilibria and undercooling.

Lowitz[2] in 1775 observed that aqueous salt solutions could be supersaturated and, when compared with foreign crystals, crystals of that particular salt were the most effective nucleating agents.

New insight was gained in the mid 19th century when biologists[3], became aware of microorganisms which could be deposited from the air to supersaturated solutions. This observation aided in the understanding of heterogeneous nucleation (initiation on foreign growth centers) and homogeneous nucleation (unaided nuclei formation). These ideas were complemented by the work of Lecog de Boisbaudran[4] who found that spontaneous (homogeneous) nucleation only occurred at high supersaturation and not in solutions with low supersaturation.

A significant contribution was made by de Coppet[5] who measured average time lags, the time gap between initiation of supersaturation within a system and the appearance of crystallization.

W. Ostwald[6] distinguished two types of supersaturated solutions, metastable and labile. In the absence of foreign

nuclei or seed crystals a metastable solution remained unchanged for long periods of time whereas a labile solution exhibited spontaneous phase changes. The supersaturation corresponding to the metastable limit that point in supersaturation space beyond which homogeneous nucleation occurs is called the critical supersaturation. Miers and Isaac[7] proposed that at or near critical supersaturation the bulk properties of solutions undergo abnormal changes which account for homogeneous phase changes.

Ostwald's observations were repeated by several experimentalists[8] in 1900 working with small undercooled droplets of liquid metals. They observed rates of nucleation near zero below a certain undercooling (metastable melts) and spontaneous nucleation below this temperature (labile melts).

The effects of sample size on the nucleation event were observed by Desprez[9] in 1837 when he found that water in capillary tubes could be undercooled to lower temperatures than in larger vessels. This idea was reinforced by Dufour[10] who miniaturized the system by suspending droplets in an immiscible liquid and finding that smaller drops could withstand larger undercooling. This effect, according to Turnbull[11], is due to the isolation of mote-free droplets and to a kinetic effect[12].

I-C CLASSICAL NUCLEATION THEORY

I-C1 Fluctuations in Solution

It is convenient before a mathematical theory is developed to have a mental picture on the microscopic level of what liquid structure could be in a supersaturated solution.

As a solution becomes concentrated or the temperature is lowered, ordering in the liquid phase increases producing associated aggregates of solute molecules which influence the progress of phase changes. The presence of aggregates has been demonstrated in X-ray diffraction experiments but these experiments have left open the questions of whether these aggregates or embryos are charged or neutral or whether they are structured more like the liquid or the solid.

The classical model treats embryos as miniature crystals with bulk and surface energies. Embryos "Ai" grow or dissolve by gaining or losing a monomer "A_1" as shown below.

$$A_1 + A_1 \rightleftarrows A_2$$

$$A_2 + A_1 \rightleftarrows A_3$$

$$\cdots$$

$$A_{n-2} + A_1 \rightleftarrows A_{n-1}$$

$$A_{n-1} + A_1 \rightleftarrows A_n^* \xrightarrow{A_1} \text{growth}$$

An embryo will not grow to finite size by addition of monomers until the mother embryo is of a definite critical size called the nucleus "A_n^*". The rate controlling step in the phase change is the addition of one unit to the nucleus, i.e., $A_n + A_1 \rightarrow A_{n+1} \rightarrow$ Xtal. This model predicts that embryos of size greater than the nucleus are extremely unstable and are consequently non-existent in solution.

An alternative point of view considers embryos as fluctuations of solute density in solution i.e., they have a liquid structure. This model, shown below, differs from the classical model in a number of ways.

$$A_1 + A_1 \rightleftharpoons A_2$$

$$A_2 + A_1 \rightleftharpoons A_3$$

$$\cdots$$

$$A_{n-1} + A_1 \rightleftharpoons A_n \longleftrightarrow \begin{cases} A_n^+ \\ A_n^* \text{ (solution)} \longrightarrow A_n^* \text{ (crystal)} \longrightarrow \text{growth} \\ A_n^\bullet \end{cases}$$

$$A_n + A_1 \rightleftharpoons A_{n+1}$$

$$\cdots$$

$$A_i + A_1 \rightleftharpoons A_{i+1}$$

Since embryos "A_i" are more liquid-like, very small embryos, i.e. $i < n$ should be more stable than their crystal counterparts. The distribution of embryo concentration should be smooth over a wide range of sizes and allows embryos to exist which have $i > n$. The rate controlling step is not simply a unit addition to the nucleus but a rearrangement of the structure of the critical sized embryo "A_n" into "A_n^*" which then undergoes a phase change to a crystal "A_n^*" (crystal) which will grow by addition of monomers. This model allows configurational changes of embryos i.e., A_n^+ and $A_n^\bullet$ but these species will not undergo a phase change because of an unfavourable orientation. Thus it is necessary to consider four processes on the microscopic scale for the liquid-like model; density fluctuations, configurational changes, phase change and addition.

The classical and "non-classical" models are two extremes, both with useful qualities. The classical model uses miniaturized crystals which allows mathematical calculation of macroscopic thermodynamic parameters, whereas, the liquid-like embryo has no such definable properties.

The "non-classical" model is enticing because it predicts a smooth distribution of embryo sizes unlike the classical model which truncates when the number of monomers in the embryo is greater than the critical size.

The classical model restricts embryo configuration, whereas, loose structure "liquid embryos" have degrees of freedom which allow different oreintations.

Both models are attempts at describing homogeneous nucleation, that is those phase changes which occur without the aid of an agent (usually a solid surface) which reduces the energy barrier to the change. The classical model resembles nucleation via a heterogeneous route because monomers add to a preformed surface, whereas, the non-classical model distinguishes between homogeneous and heterogeneous nucleation since a solution phase clicks into a crystal phase.

Note that both schemes, as depicted, are misleading because they illustrate embryo formation and breakdown as macroscopic equilibria in solution. One may believe from this that embryos are long lived i.e., embryos are particles that "float around" in solution. On the microscopic scale embryos are very short lived. If one could take a time averaged

count of embryo concentrations, the concentration of the i^{th} embryo is a constant independent of time. In statistical mechanics this is called a time independent ensemble average. The fact that embryo life times are quite short on the microscopic level is an important concept in developing a new model for nucleation. This new model must account for lag times, induction times, non steady-state rates of nucleation and the term "critical" supersaturation.

I-C2 Energy Barrier to Phase Changes

If an embryo is a density fluctuation in the liquid, it will have a gradation of properties in structure and density radiating from a point of origin in solution. One simplification used in classical theory rests on the treatment of the embryo as a piece of crystal having a well defined crystal-liquid boundary and crystal structure which facilitates the description of bulk and interfacial properties. The energy difference between monomers in solution and in the bulk, called ΔG_v the "volume free energy", is easily approximated by the energy difference between the solid and liquid phase (macroscopic thermodynamic properties).

According to the classical theory, at constant temperature and volume, the Helmholtz free energy of formation of an embryo from the bulk liquid is

$$\Delta F = \frac{4}{3} \pi r^3 \Delta\phi + 4\pi r^2 \sigma \qquad (1)$$

where $\Delta\phi$ = volume interaction between the cluster and the bulk,

r = the radius of the embryo, and

σ = surface energy/unit area.

If the net volume change in the liquid is zero as embryos form, then the Gibbs and Helmholtz energies may be equated; i.e.,

$$\Delta G = \frac{4}{3}\pi r^3 \Delta G_v + 4\pi r^2 \sigma \qquad (2)$$

where $\Delta G_v = \mu_{solid} - \mu_{liquid}$ is the excess free energy relative to the surroundings.

If the equilibrium equations of the model presented in the previous section are considered, the formation of an embryo may be expressed in terms of the embryo dissociation constant K_x.

$$G^\circ = -KT \ln K_x = -KT \ln[N_x(N_1 + \sum_{2}^{x} N_x)^x/(N_1 + \sum_{2}^{x} N_x)Ni] \qquad (3)$$

where N_x is the number of embryos with X monomers and N_1 is the number of monomers. If the nucleating phase is weakly associated, then

$$N_x \sim N_1 \exp(-\Delta G_x^\circ/KT). \qquad (4)$$

In the case of pure liquids it is possible, with this model, to equate ΔG_x°, the energy barrier to nucleation, with the Gibbs free energy of embryo formation

$$\Delta G_x^\circ = V\Delta G_v + A\sigma^3. \qquad (5)$$

Assuming spherical embryos, the critical energy of formation is

$$\Delta G^* = \frac{16\pi\sigma^3}{3(\Delta G_v)^2}. \qquad (6)$$

The volume free energy term ΔG_v is described by the following equation.

$$\Delta G_v = \Delta\mu = \mu_{embryo} - \mu_{monomer}$$

From the Gibbs-Kelvin equation, the chemical potential of an embryo is

$$\mu_{embryo} = \mu_o + \frac{(2M\beta)\bar{\sigma}}{3\rho\ell} \qquad (7)$$

where μ_o = is the chemical potential of the bulk,

M = molecular weight,

β = geometric shape factor,

$\bar{\sigma}$ = mean interfacial energy,

ρ = density of nucleating phase, and

ℓ = edge length.

The chemical potential of the monomer in solution of activity "a" is:

$$\mu_{monomers} = \mu_o' + \nu\, RT\, \ell n\, a \qquad (8)$$

where ν is the number of ions in a neutral molecule.

If μ_{embryo} is equated with $\mu_{monomer}$ (i.e., describing equilibrium situation) then,

$$\Delta G = \frac{RT}{\bar{\nu}} \cdot \ell n \frac{a}{a_o} = \frac{2\beta\bar{\sigma}}{3\ell} \qquad (9)$$

which gives,

$$\Delta G_x^* = \frac{16\,\pi\sigma^3\nu^2}{3\,k^2T^2\ell n\, a^*/a_o} \qquad (10)$$

In classical theory, the concept of critical energy in the formation of the nucleus is confusing. An expression for ΔG_n, the Gibbs free energy of formation of an embryo of size n, is given in equation (11).

$$\Delta G_n = -n\Delta G_v + n^{2/3}\sigma \quad . \qquad (11)$$

The surface free energy will increase with the number in the embryo but the per particle surface energy will decrease as the crystal becomes larger. This relationship is represented by the dotted line in Figure I-1(a). The volume free energy term represents the free energy per molecule in the bulk. The term $n\Delta G_v$ will linearly increase with n, represented in Figure I-1(a) by the dashed line. The solid line represents the combination of $n^{2/3}\sigma$ with $-n\Delta G_v$ and should give the change in free energy of an n-size embryo as a function of n. The corresponding value of n when ΔG_n is a maximum is called the critical size, n*. Embryos with a size $n<n^*$ will not grow, whereas those with $n>n^*$ grow to macroscopic size.

Using the classical model of nucleation to describe the energy barrier to nucleation is too restrictive. It is very hard to believe that (1) embryos are crystals floating in solution, (2) embryos grow by a step by step addition of monomers, (3) the pathway to nucleation involves only addition to a critical size and (4) embryo distributions are non-existent beyond a critical size. It is much more satisfying to use the dynamic non-classical model to understand a critical free energy and critical size.

If embryos are considered more solution-like, i.e. formed from solution density fluctuations with a resulting smooth size distribution, then critical sized embryos requiring minimum energy in crystal formation are the key to the phase change. Since embryos are not crystals, smaller ones are more stable

Figure I-1 The dependence of the Gibbs free energy of formation, ΔG on the size of the embryo for (a) classical model and (b) a non-classical model.

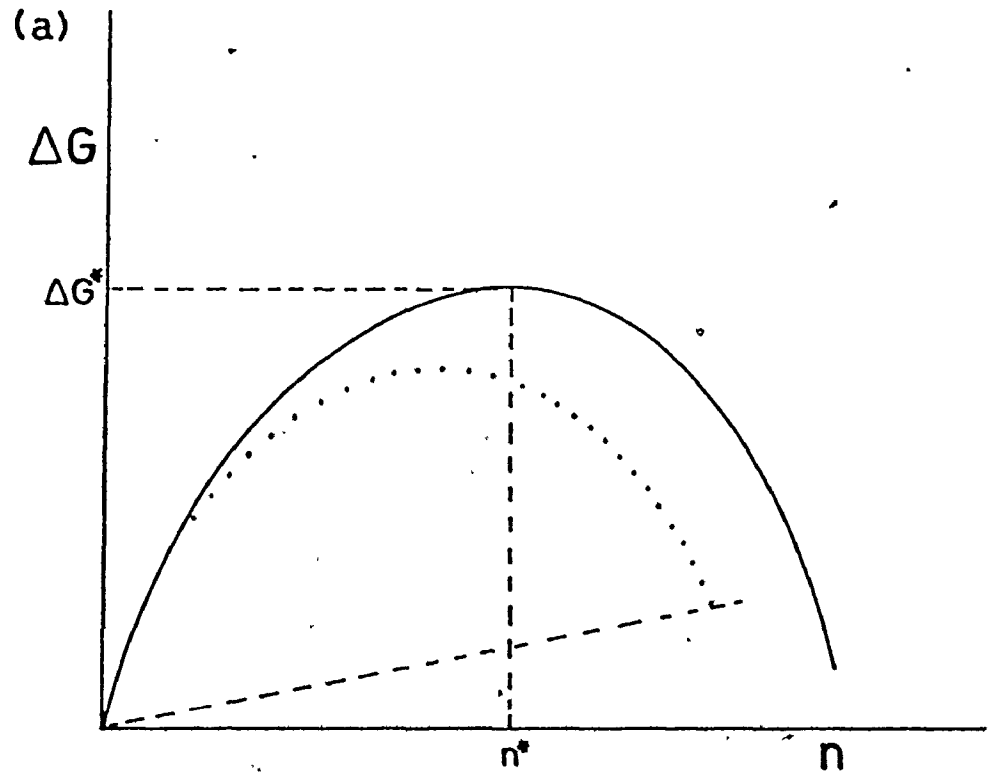
(a)
ΔG
ΔG*
n*
n

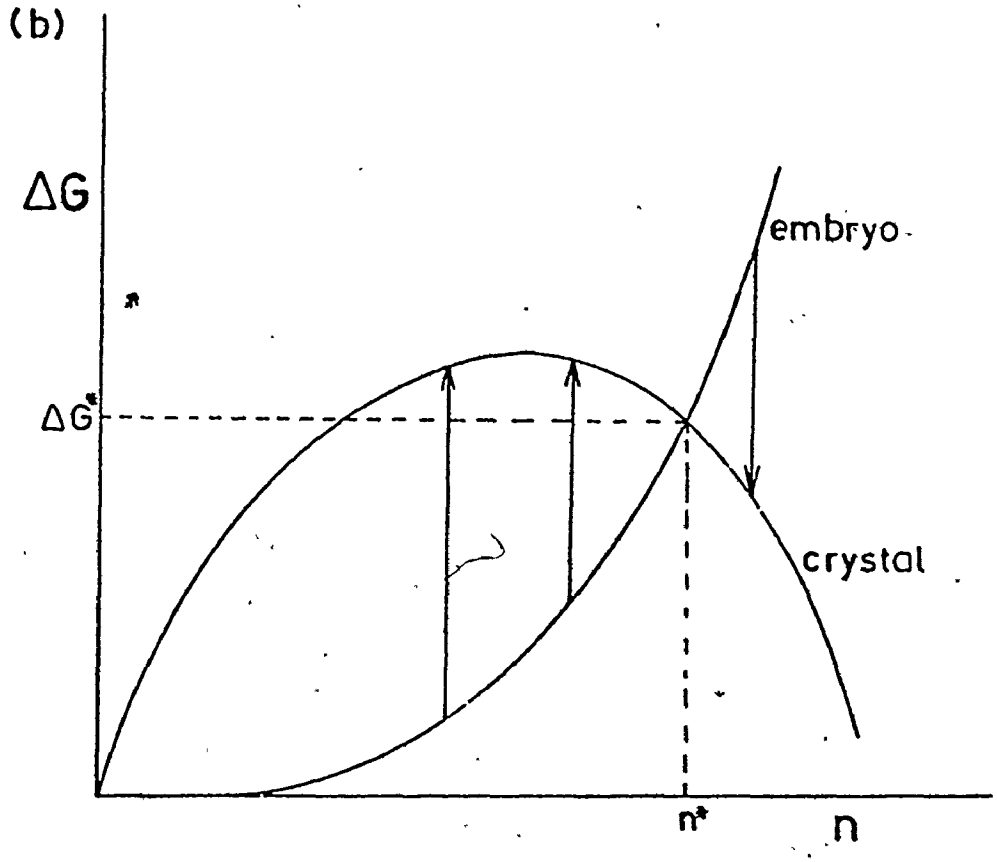
(b)
ΔG
embryo
ΔG*
crystal
n*
n

thermodynamically than larger ones. This is shown in Figure I-1(b) by the solid line. Let us also plot the energy, according to the Gibbs-Thomson equation, of hypothetical crystals of varying sizes (shown by the dotted curve). The length of the arrows joining the two curves represents the difference in energy between an embryo of size n and a crystal of size n. The energy difference is a minimum when the two curves meet and this should be the critical size. Embryos smaller than this critical size are thermodynamically stable with respect to crystal formation whereas embryos larger are thermodynamically unstable.

One predicts a spontaneous phase change when $n>n^*$ and there is a negative free energy difference between the embryo and the crystal shown in Figure I-1(b). The rate of conversion of embryos to crystals however may be kinetically controlled preventing embryos with $n>n^*$ from undergoing a phase change. Explanation of kinetic control usually makes use of an activated complex requiring extra free energy (activation energy) and an energy barrier to the phase change (Figure I-2). The change in free energy of the activated complex of an embryo of size n is

$$\Delta G_n^* = \Delta G_n + \Delta G_{extra}. \qquad (14)$$

The phase change can be represented by the following

$$An \rightarrow An^* \rightarrow An(xtal)$$

where An* is the activated complex.

ΔG_{extra} could have components of rearrangement of the structure of the embryo, loss of water, formation of the surface,

Figure I-2 The activation energy barrier between an embryo of size n and a crystal of size n

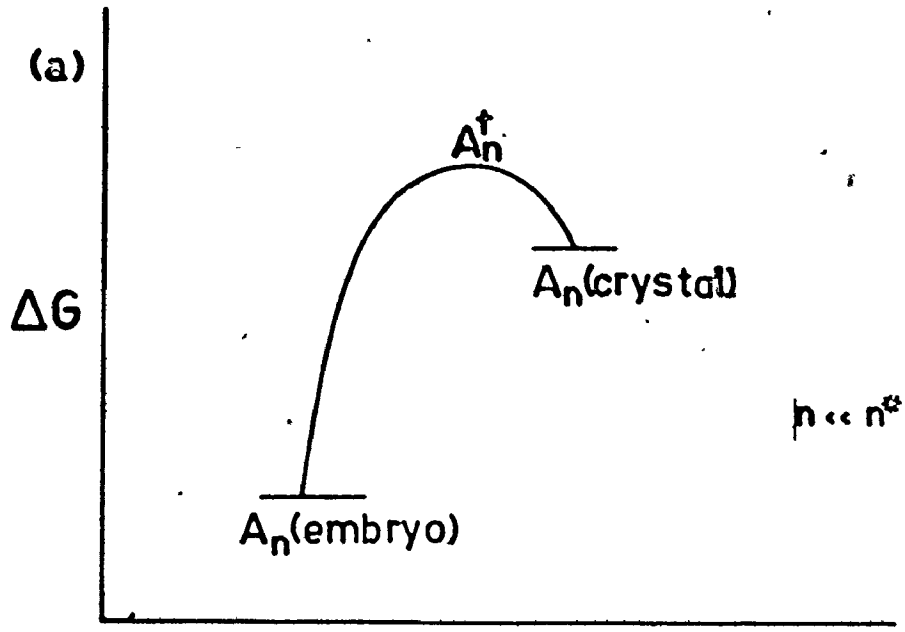
(a)
$A_n^\dagger$
A_n(crystal)
ΔG
$n \ll n^*$
A_n(embryo)

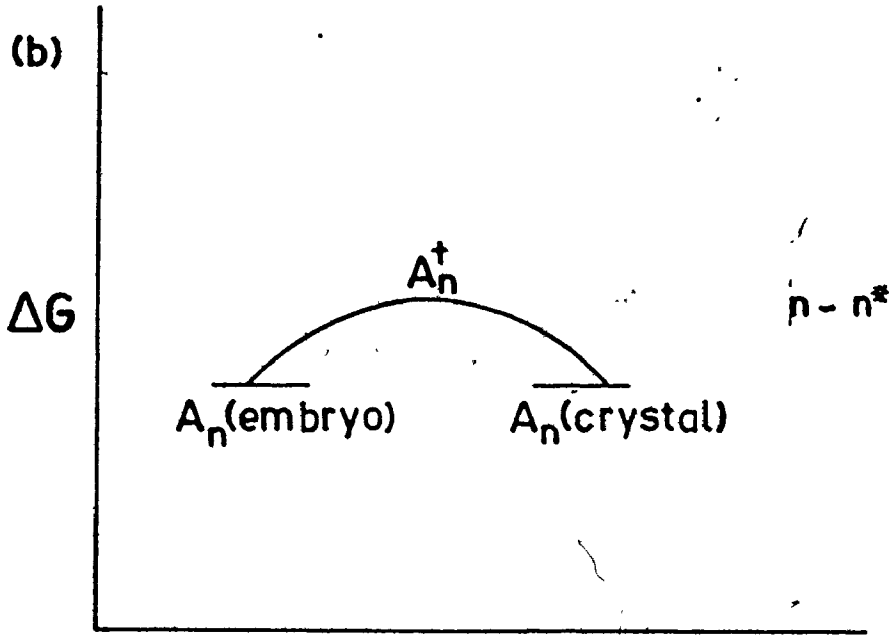
(b)
$A_n^\dagger$
ΔG
$n \sim n^*$
A_n(embryo)
A_n(crystal)

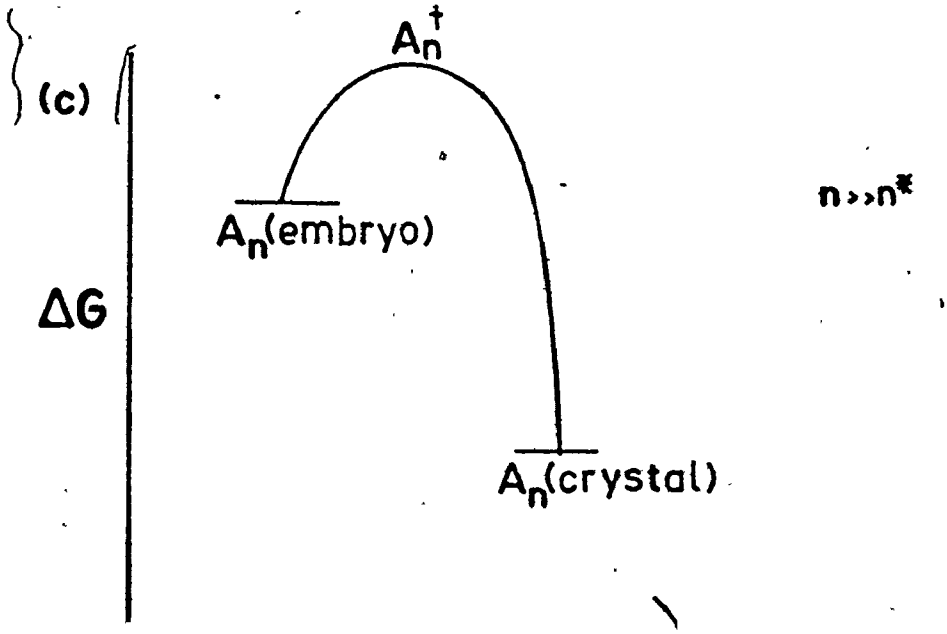
(c)
$A_n^\dagger$
$n \gg n^*$
A_n(embryo)
ΔG
A_n(crystal)

loss of entropy and others. ΔG_{extra} would vary with the embryo size, being small when n is small and large when n is large compared with the activation energy of the nucleus. Figure I-3 shows hypothetical curves of both ΔG_n and ΔG_{extra} plotted against the number of monomers in the embryo. The number in the nucleus should correspond to a minimum in the sum of ΔG_n and ΔG_{extra}.

An important point to note about the description above is that the phase change is independent of embryo growth steps and embryo life-times.

I-C3 The Classical Nucleation Rate Equation

The development of an equation for the rate of nucleation is dependent upon a number of assumptions. In the previous section, the concept of a formal barrier inhibiting the formation of critical-sized embryos has allowed calculations of the density of clusters of a certain size. The loss of nuclei through a phase change is, however, neglected. It is also assumed that growth is initiated by the addition of a single unit to the nucleus. This rate of addition is assumed first order in monomer concentration.

The nucleation rate is represented by

$$J = R_i S^* N^*. \qquad (15)$$

where: R_i = bombardment rate of monomers,

S^* = surface area of the critical cluster, and

N^* = concentration of N_x^*.

The bombardment rate of monomers upon a critical embryo is equated

Figure I-3 The free energy of formation of a crystal of size n from an embryo of size n.

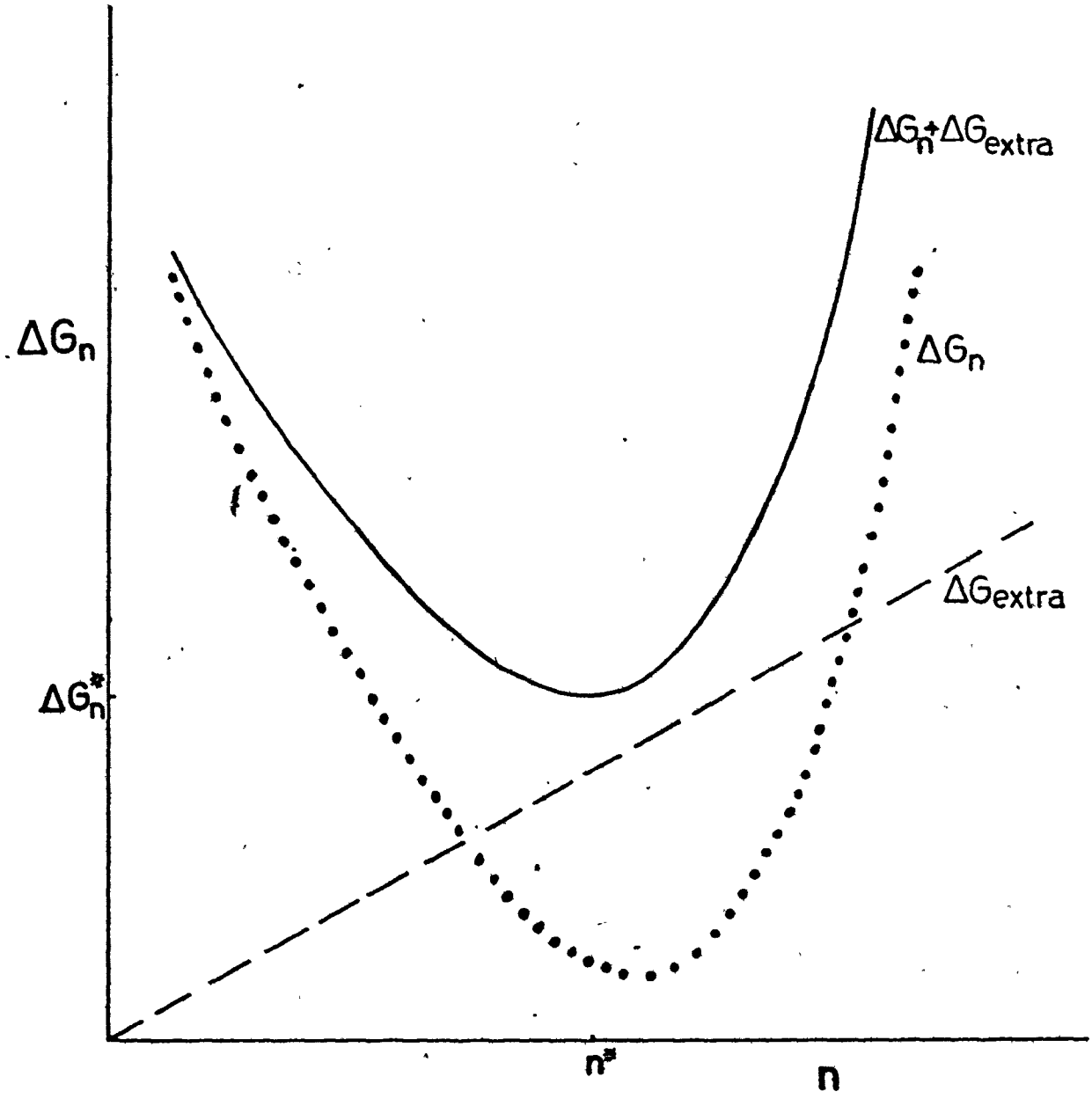
$\Delta G_n + \Delta G_{extra}$
ΔG_n
ΔG_n
ΔG_{extra}
ΔG_n^*
n^*
n

to the rate of transport of monomer across the solid-liquid interface.

$$R_i = \frac{kT}{h} \exp(-\Delta G_a/kT) \qquad (16)$$

where: ΔG_a is the activation energy barrier to transport, and

$\frac{kT}{h}$ is the frequency factor.

In the classical theory the addition step, the collision of a monomer with a small piece of matter, becomes the kinetic rate controlling step.

Replacing N* from equation (4) and R_i from equation (16) yields

$$J = \frac{kT}{h} S^* \exp(-\Delta G_a/kT) \cdot N_i \exp(-\Delta G^*/kT) \qquad (17)$$

ΔG_a is usually taken as the energy barrier to diffusion of monomers from bulk solution to the cluster.

Equation (17) has been modified in the steady-state treatments of Becker[13,14], Döring[13], Farkas[15], Zeldovich[16], and others, who have attempted to make equilibrium thermodynamics applicable to a kinetic situation.

$$J = Z \frac{kT}{h} S^* \exp(-\Delta G_a/kT) \cdot Ni \cdot \exp(-\Delta G^*/kT) \qquad (18)$$

Where: Z is the Zeldovich factor which accounts for the fact that not all nuclei form crystals -

$$Z = \left[\frac{\Delta G^*}{3\pi kTX^2}\right]^{1/2} = \frac{\bar{V}\Delta G_v^2}{8\pi\sigma(\sigma kT)^{1/2}} \cdot \qquad (19)$$

Replacing Z in equation (18) with equation (19) gives

$$J = \frac{2\bar{V}(kT\sigma)^{1/2}}{h} \cdot Ni \cdot \exp(-\Delta G_a/kT)\exp\left[\frac{-16\pi\sigma^3\bar{V}^2}{3k^3T^3(\ell nS)^2}\right],$$

or

$$= A \exp\left[\frac{-16\pi\sigma^3\bar{V}^2}{3k^3T^3(\ell nS)^2}\right] . \qquad (20)$$

From equation (20) one expects that the rate "J" is very sensitive to both temperature and supersaturation. The surface tension "σ"is calculated from the slope of ℓnJ vs $(\ell nS)^{-2}$ plots. The assumption is made that embryos are microscopic crystals having a spherical shape.

The critical supersaturation "S*", the condition for breakdown of the metastable state, is defined mathematically as that supersaturation which just causes a rate of nucleation of $1/sec\ cm^3$.

With the use of S* and equation (20) it is possible to derive the following:

$$n^* = \frac{32\pi\sigma^2\bar{V}^2}{3(kT\ell nS^*)^3} , \qquad (21)$$

$$r = \frac{2\sigma\bar{V}}{kT\ell nS^*} . \qquad (22)$$

Where n* is the number of units in the nucleus, and

r* is the radius of the nucleus.

An estimate of σ can be obtained using equation (23)

$$\sigma = \left(\frac{-16\pi\bar{V}^2}{3k^3T^3}\right)^{-1} \left[\frac{\partial \ell nJ}{\partial(\ell nS)^{-2}}\right]_T = \left(\frac{-16\pi\bar{V}^2}{3k^3(\ell nS)^2}\right)^{-1} \left[\frac{\partial \ell nJ}{\partial\ 1/T^3}\right]_{I.P.,K_{sp}} . \qquad (23)$$

I-C4 Induction Times

There are two peculiarities that have been observed in studies of the initial stages of nucleation. The first phenomenon involves the observation of the time lapse between initiation of a supersaturation and crystal appearance and secondly the observation of increasing initial rates of precipitation to a final steady-state rate. These induction times or time lags, as they are sometimes referred to, are very large in the metastable region (in the absence of foreign particles) but shorten as the supersaturation increases in the labile region. Classical nucleation theory does not lead one to expect a time gap between the time of attainment of supersaturation within the system and the appearance of crystals.

The induction time, given the symbol τ, is usually attributed to one or more of the following; t_i, the time required for attainment of a steady-state embryo distribution, t_n, the time required for nucleation, and t_g, the growth time of a post critical nucleus to detectable size.

$$\tau = t_i + t_n + t_g. \qquad (24)$$

Various workers[16-19] have considered t_i to be the major component in τ. Using the rates of formation and destruction of embryos and assuming that the number of monomers is not significantly changed during the formation of embryos Kantrowitz[6] derived an equation for the rate of nucleation.

$$J_{y,t} = 2N(D/\pi t)^{1/2} \sum_{m=1}^{\infty} \exp[-y^2/4D + (2m-1)^2] \qquad (25)$$

where N = total number of monomers,

D = diffusion of monomers across the phase boundary,

y = number of units in nucleus, and

m = an integer with values from 1 to ∞.

For small t,

$$J_{y,t} = 2N(D/\pi t)^{1/2} \exp(-y^2/4Dt). \qquad (26)$$

It has been shown from this equation that the nucleation rate only becomes appreciable at a time $\tau \sim y^2/4D$ and that the rate depends upon the diffusion rate of monomers across the solid-liquid boundary and the number of monomers in the cluster.

Garten and Head[20], in their studies on nucleation from solutions of very soluble salts attributed the observed induction time to the time required for nucleation t_n. They believe that these salt solutions contain non-crystalline glassy sub-nuclei responsible for the phenomenon of light emission known as crystallo-luminescence. These glassy particles are said to click into solid releasing a photon ($t_n = 10^{-8}$ sec) and begin to grow. If this is true in most systems, induction times would be independent of the nucleation time.

Garabedian and Strickland-Constable[21] in their collision breeding experiments have attempted measurements of the time required for the nucleus to grow to macroscopic size. The growth rate of crystals in supersaturated solutions is usually very high indeed. If it is assumed that the growth rate of the nucleus is as fast, the required time to grow to detectable size would be very short. These authors contend, however, that crystal imperfections are the cause of high growth rates.

Post-critical embryos should have more perfect lattice structures thus lengthening their growth time.

Nucleation techniques have proven to be nondiscriminative in sorting out the components of the induction time. Most measurements of induction times have been carried out at very high supersaturations (far above the critical supersaturation) and in bulk solution (susceptible to contamination). Krantowitz's attempt at describing τ mathematically is very dependent upon its being very small in magnitude and does not account for a lag in crystal appearance.

In the literature there seem to be two distinct pre steady-state rate phenomena, the induction time τ, the time elapsed between attainment of a supersaturation and a steady-state nucleation rate, and the lag time L, the time required after the attainment of a supersaturation for a new phase to appear. The pre steady-state phenomena depend upon the nature of the species being precipitated, the degree of supersaturation and other considerations. Special solution conditions govern magnitudes of L and τ. Three possible observations are shown in Figure I-4. In (a) the results seem to coincide with a time dependent build up of embryo concentration and leads one to believe that $\tau = t_i$. If the observed results resemble (b), the lag time L could be caused by a slow growth of nuclei to detectable size and $L = \tau = t_g$. In (c) both lag and induction times are observed giving $\tau = t_g + t_i$. Both growth and induction times can be used to describe τ.

Figure I-4. Some pre steady-state rate phenomena reported in the literature.

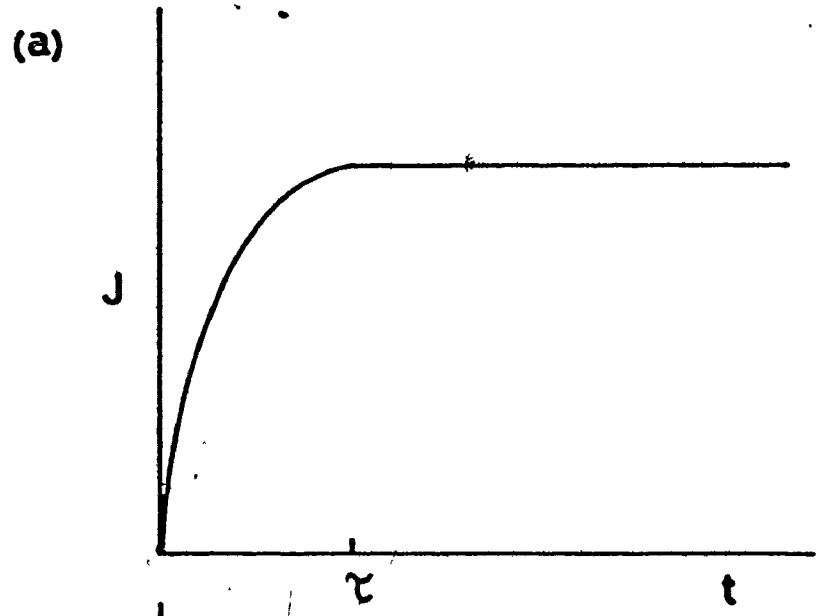
(a)
J
τ
t

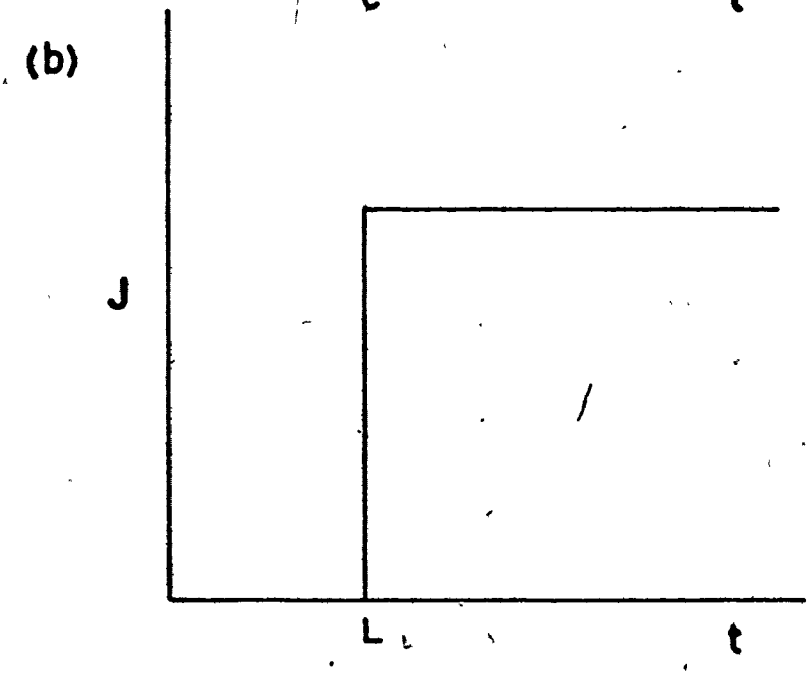
(b)
J
L
t

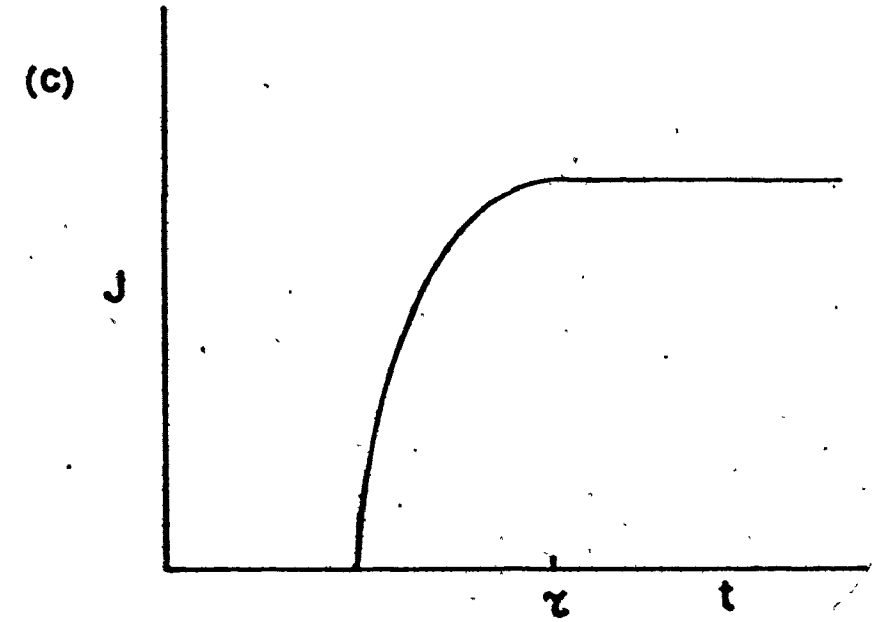
(c)
J
τ
t

I-D ASSUMPTIONS WITHIN THE CLASSICAL THEORY

Calculation of the free energies of embryos assumes that thermodynamic properties of macroscopic crystals apply to microscopic embryos. The nucleus is described in rigid body terms plus surface terms. Very small crystals have surface and edge corrections found especially in the microscopic surface entropy. Hindmarsh and Holian[22] found that the intensive properties of bulk crystals have a 1/N dependence but nuclei-sized crystals would have surface and edge corrections to the entropy terms called "non-thermodynamic" terms of the order of $(1/N)^{1/2}$ and $(1/N)^{2/3}$. These corrections greatly affect the statistical mechanical nuclear partition function giving small errors in the Helmholtz energy. Small errors in F (1/4 RT) lead to very large errors in the rate (10^{10}).

In the classical theory rotational and vibrational contributions to the free energy of an embryo are neglected. The above authors also contend that F depends upon size in a relatively simple way but on shape in a complicated way. In classical theory the nucleus is treated as if it were a sphere. This makes calculations much simpler but errors in the shape factor β in equation (20) are reflected in calculations of the surface tension σ.

Since present experimental techniques of rate measurement are so crude, rate errors can be neglected and consequently the present thermodynamic theory accepted as adequate.

Classical theory neglects configurational entropy corrections to the free energy of the embryos. In a recent review Frank[23] contends that there is no "critical embryo" but crystals form from embryos larger and smaller than n*. Each of these important embryos has multiple configurations of low excitation energy. With n monomers contained in an embryo there could be W_j distinct configurations with varying energy

$$N_x = \Sigma W_{xj} \exp(-\Sigma_{nj}/RT) \quad . \qquad (27)$$

Configurational entropy will depend upon the size of the nucleus n*. If n* is very small configurations have very low excitation energy, whereas, very large embryos have configurational energy levels split far apart. Configurational entropy lowers the surface tension.

In the expression for the concentration of embryos, it was assumed that a formal barrier to crystal formation exists, thus preventing nucleation and allowing equilibrium conditions. In other words the equilibrium must be attained very quickly relative to the appearance of the first crystals, i.e., t_i must be small. The concentration of critical clusters will be reduced by sub-critical clusters and by the nucleation process as well. This demand on the system necessitates the use of very high supersaturations in rate measurements in bulk solutions. At lower S, nucleation events will not be independent of each other but dependent upon what has happened already in solution.

Classical theory was developed for the simplest system - the condensation of pure gas. When used to describe nucleation

in a solvent the theory has been adequate because measurement is difficult. When a sound model of solution chemistry is developed and experimental techniques made more sensitive, a better theory can evolve from the resulting data.

I-E NUCLEATION AND SOLUTION PROPERTIES

Nucleation theory was adapted for the condensation of vapour, a quite simple system. It would be interesting to return to the question of liquid structure and how it affects nucleation. The effect of liquid structure would be greatest upon ΔG^*, the energy barrier to nucleation and A the pre-exponential factor. There are three major properties of solutions which may modify each of these, namely; viscosity, entropy, and foreign substances.

The relationship found in Equation (20) represents reasonably well the nucleation characteristics of both vapours and solutions. In some systems however it does not hold for high values of S. Tamman[8], working with organic melts, found that the number of nuclei increased with the degree of supercooling but, reached a maximum and then decreased. He suggested that this sequence was a result of the formation of a glassy state due to a sharp increase in viscosity, restricting molecular movement and inhibiting ordered crystal structure. More recently Turnbull and Fisher[24] modified equation (20) to account for viscosity

$$J = A' \exp\left[\frac{-16\pi\sigma^3 V^2 N}{3k^3T^3(\ell nS)^2} + \frac{\Delta G'}{kT}\right] \qquad (28)$$

where $\Delta G'$ is the activation energy for transport across the phase interface. $\Delta G'$ becomes the dominating factor for highly viscous liquids and glasses. Mullin and Leci[25] have observed the same behaviour in supercooled citric acid solutions. They claim that citric acid molecules possess a large degree of hydrogen bonding which structures the supersaturated solution. The structuring involves the formation of chains and clusters inhibiting reorientation of the solution to the crystal structure.

The entropy effects within solutions are of two types, solution structure and ion and cluster hydration. In the former the volume free energy of the cluster with respect to the matrix depends upon the liquid and solid packing. If nuclei are solid-like and liquid and crystalline structures are very similarly ordered (similar entropies), then σ will be less than it would be if ordered crystals originate from a very disordered solution structure. If nuclei are structured more like the liquid then ΔG^* will be very low and entropy changes on a rearrangement step would be high.

Many charged ions (e.g., Ca^{2+} and Mg^{2+}) are highly hydrated in aqueous solution. Unlike the gas phase, the embryos have a choice of being built up from either desolvated species or very loosely bound hydrated aggregates. Scheme A below represents embryos as desolvated species. The equilibria are very similar to gas phase equilibria except that desolvation would further increase the embryo free energy of formation. The rate controlling step for the nucleation process would require

rearrangement of the embryo structure, phase change and desolvation of adding monomers.

SCHEME A

$$A_1 \cdot n(H_2O) + A_1 \cdot n(H_2O) \rightleftharpoons A_2 + 2n\ H_2O$$

$$A_2 + A_1 \cdot n(H_2O) \rightleftharpoons A_3 + n\ H_2O$$

$$A_{n-1} + A_1(nH_2O) \rightleftharpoons An \begin{cases} An^+ \\ An^*_\circ \\ An \end{cases} \longrightarrow An^*(\text{crystal}) \longrightarrow \text{growth}$$

$$A_n + A_1(nH_2O) \rightleftharpoons An\text{-}1 + n\ H_2O$$

Scheme B represents equilibria of solvated embryos. The critical embryo $An \cdot n^2H_2O$ is forced to undergo possibly three processes before it becomes a crystal. Not necessarily in order the three processes are rearrangement, phase change, and addition.

SCHEME B

$$A_1 \cdot n\ H_2O + A_1 \cdot n\ H_2O \rightleftharpoons A_2 \cdot 2n\ H_2O$$

$$A_2 \cdot 2n\ H_2O + A_1 \cdot n\ H_2O \rightleftharpoons A_3 \cdot 3n\ H_2O$$

$$\circ\ \circ\ \circ$$

$$An\text{-}1(n\text{-}1)nH_2O + A_1 \cdot nH_2O \rightleftharpoons Ann^2H_2O \xrightarrow{-H_2O} An + An^* \xrightarrow{A_1} \text{growth}$$

The last of the major factors which affect nucleation is the presence of foreign substances called motes. These particles can act as sites for growth, changing the pathway to crystal formation and effectively reducing the energy barrier to phase changes. This type of phase change (heterogeneous) will be discussed in Section I-F.

An adverse effect upon measurements of the energy barrier to the nucleation of ionic salts in solution stems from

the definitions of the supersaturation. S, a gross thermodynamic term, depends upon the ion product and the solubility product as shown by Equation (29).

$$S = \left(\frac{\text{ion product}}{\text{solubility product}}\right)^{1/2} . \qquad (29)$$

The cation-anion ratio, however, may take on many values while the I.P. remains the same. Classical theory, by definition, predicts a rate independent of the cation-anion ratio. If the rate is dependent upon cation/anion, it will become evident in the measurements of σ, A, and S* from variable driving force experiments. Experiments measuring the rate of nucleation at constant supersaturation will be affected too. For a family of experiments conducted at constant T_1 and $(\text{cation/anion})_1$ and varying I.P., the measured values of σ, A, and S will vary from those obtained at T_1, and $(\text{cation/anion})_2$ since $J = J$ (cation/anion).

Equation (20) predicts that the rate of nucleation should be constant for any combination of ionic species giving a constant ion product. However, when one inspects this on the microscopic level, various ratios of cation to anion are going to greatly affect the distribution of embryos and the rate of nucleation.

There are other physical properties of liquids which are thought to have a slight influence on nucleation. These are dielectric constant, solvent molecular weight, solvent surface tension, and solvent density. The individual effect of changing

these parameters is usually confounded and masked by the major effects of supersaturation and temperature.

I-F HETEROGENEOUS NUCLEATION

Heterogeneous nucleation is the name given to a process of phase change catalyzed by some foreign substance called a mote or heteronucleus. When the heteronucleus is in contact with a supersaturated solution it provides a site of high energy and effectively reduces the energy barrier to the phase change.

Both a thermodynamical and a statistical approach have been applied to heterogeneous nucleation theory.

According to the thermodynamic theory, the rate of nucleation is a function of particle diameter, surface properties, supersaturation, and interfacial free energies. Nielsen[26] has developed an expression for the energy barrier for heterogeneous nucleation. The interfacial tension between the crystal to be formed and the heteronucleus must be considered. Letting the surface tension between the crystal and solution be σ, between heteronucleus and solution σ_1 and between the two solids σ_2, the free energy change of nucleation upon a square site $\ell \times h$ is:

$$\Delta G = -n\Delta G_v + \sigma(\ell^2 + 4h\ell) + \sigma_2\ell^2 - \sigma_1\ell^2$$

$$= -n\Delta G_v + 2\sigma_o\ell^2 + 4h\ell\sigma \qquad (30)$$

where $2\sigma_o = \sigma - \sigma_1 + \sigma_2$.

Assuming the volume of the active site is fixed, $V = \ell^2 h$, the most probable ratio between h and ℓ is found by minimizing ΔG

with respect to ℓ (equation (31)).

$$\Delta G = -n\Delta G_v + 6(\sigma_o\sigma^2V^2)^{1/3} \quad \text{(heterogeneous)}$$
$$\Delta G = -n\Delta G_v + 6\sigma V^{2/3} \quad \text{(homogeneous)} \qquad (31)$$

If the surface of the active site "resembles" the crystal, σ_o is small and the free energy change of nucleation is lower for a heterogeneous phase change thus it may take place at a lower supersaturation. For a site to "resemble" the crystal it is more important to have agreement in lattice type and atomic distances than chemical similarity.

Information of more practical valuc can be obtained using a statistical treatment. Thijssen et al[27] have made two observations while performing water droplet freezing experiments. If droplets are cooled to a certain undercooling (i) at high undercooling there is a constant rate of nucleation vs time and (ii) at low undercooling there is an initial period of constant rate after which time it begins to decrease (see Figure I-5). These observations can be explained by the following. Assume there are two distinct probabilities of nucleation, Ps,nu and Ps,cr. Ps,nu is the probability that a particular solid particle is able to cause nucleation under equilibrium conditions, and Ps,cr, that equilibrium is attained in a unit time interval. Ps,nu is a function of particle properties or the potency of the heteronuclei and the supersaturation, whereas, Ps,cr is a function of the supersaturation only. Ps,nu is also related to the frequency of nucleus formation in thermodynamical relationships of Turnbull and Fisher[24] and Fletcher[28].

Figure I-5. The effects of heteronuclei on the nucleation rate in water droplets at high and low undercooling.

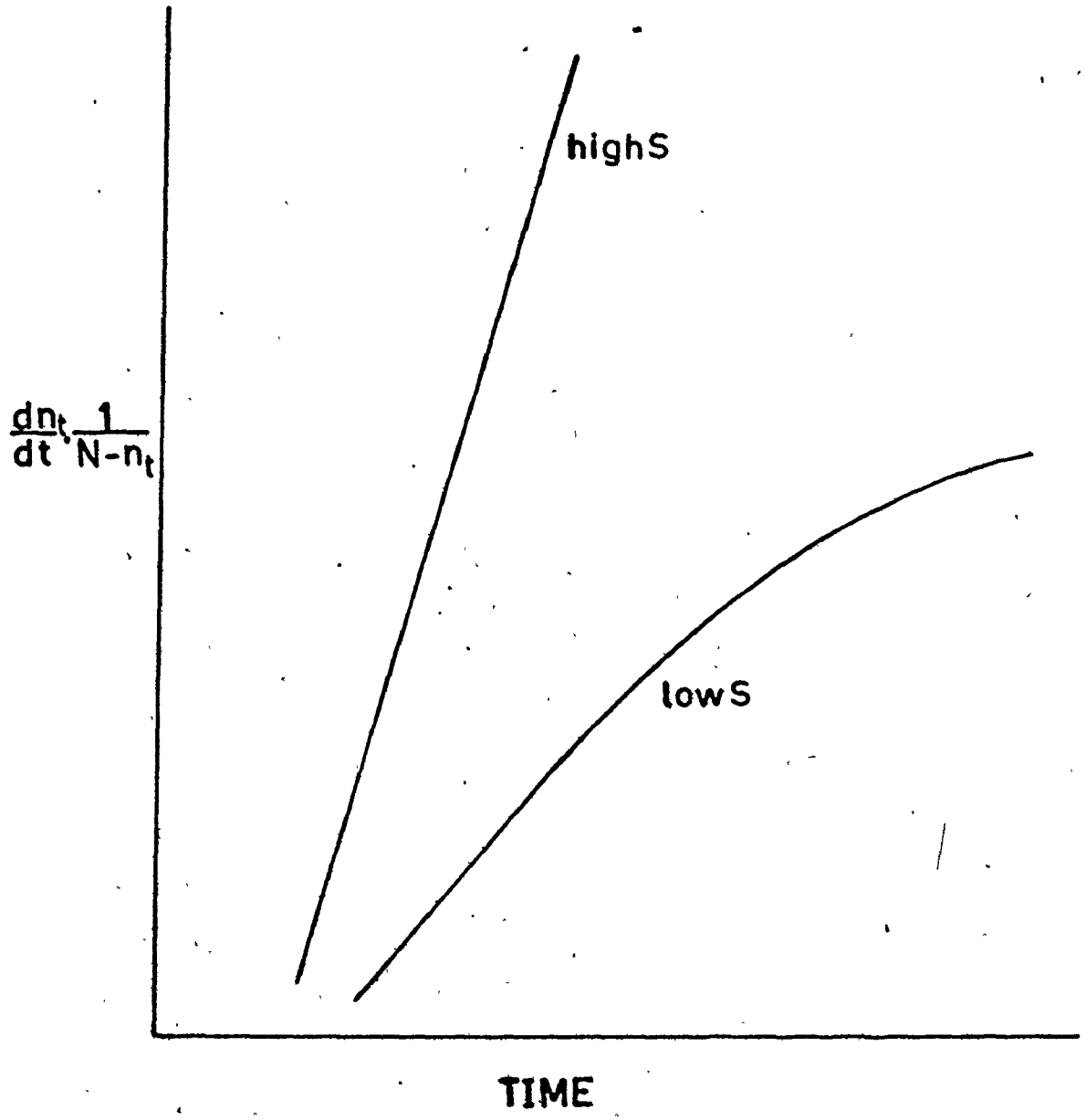
highS
lowS
$\frac{dn_t}{dt}\frac{1}{N-n_t}$
TIME

The probability of nucleation of a particle with critical supersaturation S*, Pn(S*,S), in a unit time interval is

$$Pn(S^*,S) = Ps,nu(S^*,S)Ps,cr(S). \qquad (32)$$

If $n(\theta)$ is the concentration of particles with a critical supersaturation S*, and assuming $n(\theta)<<1$, the probability Psg of having one or more of those particles in a volume V is

$$Psg = 1 - \exp(-n(\theta)V). \qquad (33)$$

The probability of having one or more particles with S* between S and S+dS in a volume V is

$$Psg' = 1 - \exp\left(-V \frac{dn(\theta)}{d\theta} \cdot d\theta\right). \qquad (34)$$

The probability of nucleation of a sample with volume V at a supersaturation S in unit time is

$$P = \int_{S^*}^{S} Psg'(S^*)Pn(S,S^*) \qquad (35)$$

When droplets are cooled rapidly to a constant temperature, and there is a large undercooling all heteronuclei become active (i.e., Pn(S,S*) is the same for all droplets) and the distribution of active sites is constant throughout the population. When the undercooling is small, fewer sites are active, (i.e. Pn(S,S*) is low) and the probability Psg of having one or more of these sites in a volume V is low. The spread in the number of active sites per drop, therefore, is significant. From Equation (35) it can be predicted that all droplets in the population do not have the same probability at low supersaturation.

Markov and Kaschiev[29] have extrapolated the above ideas to include a non-discriminating mechanism for homogeneous and heterogeneous nucleation. As the supersaturation increases, even the weakest sites become active until even collections of parent phase atoms act as self nucleating sites. This supersaturation is the critical supersaturation of homogeneous nucleation. It is nothing special, only a limiting case. This approach predicts no abrupt change or critical point between metastable and labile zones since these concepts only hold in special cases. Nucleation of real solutions which are dirty and very complicated is more understandable when the above ideas are embraced.

The above authors introduce the term "screening zone". Around a heteronucleus there is a screening zone, a volume that increases with time, in which other sites are deactivated. The zone volume depends upon the potency of the site, the weaker sites requiring a larger volume than for more active ones. The following examples of screening zones have been reported: temperature gradients from crystallization from melts[30], concentration gradients from vapour growth[31-36] and the appearance of a potential drop around electrolytically growing nuclei[37].

Heterogeneous nucleation may seem like a nuisance factor because it may hasten the precipitation of unwanted scale. Controlled heterogeneous nucleation techniques, however, have found application in nucleation inhibition. As far back as 1936[38], it was known that parts per million of sodium hexametaphosphate, added to irrigation water, prevented calcium

carbonate precipitation even when ammonia was added. Subsequently, polyphosphates have found use in industry to control calcium carbonate scale formation in recirculating cooling water systems, heat exchangers, and boiler lines. Many other examples have been reported[39-42]. The effect is called "threshold treatment", because only a fraction of the amount required for sequestration of calcium was required.

Glasner's mechanism of the threshold effect, reported by Elliot[43], uses the classical model as a basis. The additive acts as a catalyst to embryo formation, reducing monomer concentration. The number of embryos increases but their average size decreases. Elliot reports that crystals formed in the presence of a threshold inhibitor take much longer to form, are larger, have phosphorous contamination and have distorted shapes.

The threshold effect may be more adequately described by site activity and/or screening zones using a "non-classical" model of embryo build up. If threshold inhibitors are heteronuclei with very weak potency relative to the catalysis of crystal formation, they may be effective only in reducing the energy barrier to embryo formation. The small embryo population is increased and must compete for available monomers. The screening zone concept predicts the same outcome since weak sites have very large screening zones which overlap and render all heteronuclei ineffective in producing crystals. If additives of higher site potency are present, the concentration of sites must be increased to obtain the same zone overlap. Phase

change is accelerated by a lowering of the critical embryo size and by the existence of smaller screening zones. In the case of potent heteronuclei then, monomers compete for active sites. One could imagine a hypothetical experiment in which the experimenter measured the rate of nucleation from a solution with a certain supersaturation. At his disposal he has a jar of nucleation sites with the same potency. The rate is observed to increase with small additions of the sites, then, levels off with the addition of more, and declines again when the site concentration becomes high. As more sites are added,he would find a certain concentration of sites which would prevent nucleation.

Care must be taken to distinguish between nucleation inhibition and growth inhibition. Rolfe[44] has reported scale inhibition by a polymer of acrylic acid, and Smith[45], the inhibition of gypsum formation by polyacrylic acid. Both have observed that the precipitate exhibited a modification in crystal habit. The crystals were smaller, distorted, and appeared in greater numbers. The authors proposed a mechanism which involves the adsorption of the additive onto the surface of the crystals (embryos or macroscopic crystals) reducing the free energy of embryo formation, and increasing the number of effective nuclei.

These results are more easily explained by growth inhibition. Loss of mass from an unstable supersaturated solution may be completed by growth or formation of new growth sites. The inhibitors block growth which forces new crystals to form.

A nucleation inhibitor is a substance that alters either the rate of nucleation or the induction time or both. The induction time measurements, however, can be susceptible to large crystal growth components. The rate of nucleation, in this case, would remain the same but its observation would be delayed by a longer growth time of the nucleus to detectable size. Rate measurements discriminate between nucleation inhibition and growth inhibition.

I-G NUCLEATION TECHNIQUES

There are a number of experimental techniques used to study nucleation from aqueous solution. All of them are based on the measurement of the appearance of macroscopic crystals. No one has claimed to actually observe or measure the critical embryo which may be composed of only 20 atoms.

Lack of reproducibility of results observed within sets of "equivalent" nucleation experiments have been reported throughout the history of the subject. Recently researchers came to the conclusion that aqueous solutions, no matter how carefully they were prepared, contain heteronuclei. There are normally between 10^6 and 10^8 impurity particles per ml of aqueous solution. Most filtering techniques will only reduce this number to approximately 100/ml, causing the embarrasing conclusion that nucleation from bulk solution involves heterogeneous nucleation at moderate supersaturations and a mixture of homogeneous and heterogeneous nucleation at higher supersaturations. Efforts then turned towards the examination of

nucleation in droplets, nucleation on reproducible surfaces, and the design of discriminating bulk solution experiments.

A summary of the techniques used to observe and/or measure nucleation phenomena is given in Table I-1.

In the so-called "beaker" experiments, the supersaturations must be very high, such that $J_{homogeneous} >> J_{heterogeneous}$. The rate of crystal appearance at these high supersaturations may be as much as 10^8 crystals/cm^3.sec. and are very difficult to measure. The errors in the rate measurements lead to large confidence limits in the derived thermodynamic parameters such as in A, σ, and S*.

Heterogeneous nucleation measured by surface techniques is more reproducible due to the fact that the surface is reproducible. Wide ranges of supersaturations have been used and quantitative parameters calculated.

Miniaturization techniques are less susceptible to heterogeneous nucleation because the probability of finding heteronuclei in very small volumes is extremely small. The absence of these catalysts allows the use of a wide range of supersaturations and measurable rates between 10^3 and 10^8 crystals/cm^3sec. The separation of homogeneous and heterogeneous nucleation is very distinct at lower supersaturations, leading to more accurate measurements of the critical supersaturation of homogeneous nucleation.

Homogeneous nucleation, as discussed previously, could be identical to the process of heterogeneous nucleation without

TABLE I-1

Techniques used to observe and/or measure nucleation phenomena

Method	Subclass	Generation of Supersaturation	Detection	Response	Comments
"Beaker" Techniques	1. Bulk (46) nucleation	direct mixing	dilatometry	τ, J	The presence of heteronuclei hinder measurement of the homogeneous nucleation rate.
		chemical generation *in situ*	light scattering		
		solvent removal by boiling	crystalloluminescence	t_n	Usually high supersaturations are used resulting in poor measurement of τ and J.
	2. Collision (47) breeding	introduction of seeds to a supersaturated solution	microscope	t_g	
Surface Techniques	(48) Electrochemical	electrochemical impulse followed by growth at a lower current	microscope	L, J, τ	Heterogeneous nucleation is measured. The results are reproducible on one surface but not from surface to surface.
Miniaturization Techniques	1. Sealed tube	undercooling of saturated solutions	microscope	qualitative	Miniaturization techniques suffer from population deficiencies. Since an apparent droplet crystallization rate is volume dependent volume ranges must be dealt with individually
	2. Droplet (49)(50) Technique	chemical generation *in situ*	microscope	$L, J_{homo}, \tau, J_{hetero}$	
		solvent removal			

catalysis. It might be argued that this special case has no real relevance to practical chemistry. The importance of attaining and measuring homogeneous nucleation, however, lies in the fact that the mechanism of this process and that of heterogeneous nucleation are probably the same. Experimentally, techniques measuring homogeneous nucleation are reproducible, unlike most heterogeneous-measuring methods, the results of which are sometimes meaningless.

STATEMENT OF THE PROBLEM

The precipitation of calcium sulfate from aqueous solution is important in a host of processes which continually concentrate it in its natural water. The convenience of basing a study of nucleation on $CaSO_4 \cdot 2H_2O$ lies in the fact that, with a good control of experimental conditions, the response can be measured as a function of single independent variables; such as T, S, and Ca^{2+}/SO_4^{2-}.

The droplet technique is a powerful method of measuring homogeneous nucleation from aqueous solution because heteronuclei seldom appear in the droplets. The difficulty with the technique lies in the manipulation of the experimental conditions, I.P., T, Ksp, pH, t, and Ca^{2+}/SO_4^{2-}.

The purpose of experimental design is to extract the greatest amount of reliable data from a minimum number of experiments. In the case of calcium sulfate, an experimental design will be constructed for measurement of nucleation phenome-

non of ionic salts precipitated isothermally with chemically generated supersaturation and a decreasing calcium-sulfate ratio.

Experiments will be designed that will vary one of the following independent variables while keeping the rest essentially constant; I.P., T, Ca^{2+}/SO_4^{2-}, and pH. The responses that will be measured will be the rate of nucleation, J, and the induction time τ. The results of these experiments will be used to calculate, using classical equations, the thermodynamic parameters S^*, σ, A, n^*, r^*, and ΔG^* as a function of the unconfounded independent variables. Along with these, the entropy change for the nucleation of calcium sulfate will be calculated.

A second use of the results will be to find a mathematical relationship between the rate, J, and the lag time, L. The lag time may play an extremely important role in rate measurements.

These results will also form a base from which to comment upon postulates of the classical and non-classical models of nucleation. In particular, the components of lag and induction times will be studied.

Armed with the above information, variable driving force experimental designs will be made.

II EXPERIMENTAL

The development of a process which generates a supersaturation in situ was of premier importance to this project. Sulfate ion was produced in a homogeneous aqueous solution in the presence of a constant calcium ion concentration. To be useful, the chemical reactions had to have the following characteristics:

1) The chemical reaction had to be fast enough to generate a supersaturation high enough so that crystals of gypsum would appear in a reasonable amount of time (30 min), but not so fast as to cause a crystallization rate too fast for recording.
2) The reaction must proceed in aqueous solution.
3) $CaSO_4$ or $SrSO_4$ should be the only species that precipitate.

The reduction of peroxydisulfate with thiosulfate or iodide produces sulfate ion at a moderate rate.

$$S_2O_8^{2-} + 2S_2O_3^{2-} \rightarrow 2SO_4^{2-} + S_4O_6^{2-}$$

$$S_2O_8^{2-} + 2S_2O_3^{2-} \rightarrow 2SO_4^{2-} + I_2$$

Both of these reactions were used to generate sulfate and the required supersaturation.

II-A SOLUTIONS

II-A1 Reagents

Solutions were prepared by dissolving appropriate amounts of the following in deionized water. $Ca(NO_3)_2 \cdot 4H_2O$ (Baker, re-

agent), $K_2S_2O_8$ (Allied, reagent), $Na_2S_2O_3 \cdot 5H_2O$ (BDH, reagent), NH_4I (Baker, reagent), and $Sr(NO_3)_2$ (Allied, reagent).

All solutions were pressure filtered through a 0.3 μ PVC filter (Sartorius Membrane filter, Germany) in a filter holder supplied by the Millipore Co., Montreal.

The calcium or strontium salts, together with the peroxydisulfate, were used to prepare solution "A" and thiosulfate or iodide to prepare solution B. The amounts of each salt were selected so that mixing equal volumes of each solution produced the desired initial concentrations.

II-A2 Measurement of Generation Rates

a) Reduction with thiosulfate: The production of sulfate was not measured directly, but the change in thiosulfate concentration with time was measured using a polarographic technique. The free dissolution wave of mercury was used at $E_{1/2}$ = -0.2 volts (vs SCE) in 0.1 M KNO_3 and 0.1% Triton X-100.

A calibration curve was prepared as follows: A thiosulfate solution was prepared and standardized against $K_2Cr_2O_7$; 0, 5, 10, 20, and 25 ml of this solution were pipetted into separate 250 ml volumetric flasks and polarograms were run over a +0.1 to -0.5 voltage range (vs SCE).

Solutions A and B, previously described, were mixed and at certain time intervals 3.0 ml of the solution were trans-

ferred into 250 ml volumetric flask containing 200 ml of water to quench the reaction. After addition of KNO_3 and Triton-X100, the polarograms of these solutions were run. The diffusion currents of the above solutions were measured over the same voltage range as the standards. The diffusion current of the first aliquot was observed and recorded over a period of two hours.

b) Generation of sulfate in the presence of Sr^{2+}: Sulfate ion was generated by the reduction of peroxydisulfate by iodide. The sulfate ion concentration was not measured directly but the iodine concentration was monitored using standard $S_2O_3^{2-}$ titrations. Aliquots of the reaction mixture were removed at certain times, the reaction quenched by dilution, and I_2 was titrated to a blue to colourless end point using starch indicator.

c) Step function generation of sulfate in the presence of Ca^{2+}: The sulfate ion was generated using iodide as a reducing agent. Sulfate ion concentration was measured directly as described in section II-A2(b). Some preliminary experiments were performed to determine rates of sulfate ion production at various initial iodide concentrations and $[S_2O_8^{2-}] = 0.102$. Changes in the iodine concentration, which increased with time, were followed spectrophotometrically at 610 mμ. 100% transmission was set with deionized water blanks, whereas 0% transmission was set with a mixture of solutions A and B after the reaction had reached equilibrium. 0% transmission

was adjusted by changing the wavelength.

II-A3 Solubility Measurements

a) Calcium Sulfate: For the experiments conducted at room temperature and variable driving force, a synthetic matrix was prepared which contained the following: $Na_2S_4O_6$, 0.2 M and $Na_2S_2O_3$, 0.05 M. Excess calcium sulfate precipitate was added and the solution was stirred for 24 hours, pressure filtered and aliquots removed. Calcium ion was determined by titration with EDTA, 0.01 M using EBT indicator. This procedure was carried out four times.

b) Calcium Sulfate: The solubility of calcium sulfate at various temperatures and at constant driving force was measured using the same technique as above. The matrix solution prepared contained KNO_3, 0.204 M, NH_4NO_3, 0.204 M and NH_4I, 0.146 M. The solutions were stirred with excess calcium sulfate in a 100 ml beaker which was wrapped in aluminum foil and had an outside jacket through which water was pumped from a constant temperature bath (Forma Scientific, U.S.A.). These solutions were stirred for 12 hours, pressure filtered and aliquots withdrawn. The molarity of calcium ion was determined indirectly by adding a known excess of 0.01 M EDTA solution followed by a back titration with a standard magnesium solution.

c) Strontium Sulfate: The solubility of strontium sulfate was taken from the literature.

II-A4 Temperature Measurements

Measurements of the temperature of the heavy mineral oil at the bottom of the Nessler cups were taken using a fine wire thermocouple (iron-constantan), attached to a calibrated potentiometer (Leeds-Northrup). Both the temperature of the constant temperature bath and the oil were noted. Measurements were taken to determine the length of time required for the oil to reach terminal temperature after the flow of water from the constant temperature bath was initiated.

II-A5 Form of the Precipitate

250 mls of a dilute solution of $S_2O_3^{2-}$, $S_2O_8^{2-}$ and Ca^{2+} was allowed to react for two days. The precipitate was collected, washed and dried. Some of this product was weighed on an analytical balance and dissolved in deionized water. This solution was titrated for calcium ion with 0.01 M EDTA.

II-B THE DROPLET TECHNIQUE

The droplet technique applied to nucleation from aqueous solution requires that very small droplets of a homogeneous solution be produced, a certain size range of droplets isolated and then transferred to an optically flat surface for observation. Large populations of these droplets can be observed visually and any phase changes that occur in the droplets photographically recorded.

II-B1 Apparatus

Dispersions of the aqueous solutions were made with the aid of a Virtis micro-homogenizer (Fisher Scientific, Toronto)

in a 6 ml homogenizing flask.

Isolation of certain droplet size ranges was accomplished by using a centrifuge (International Clinical Centrifuge, Boston) and a 15 ml centrifuge tube.

The observation vessels were Nessler cups. These cups were 31 mm OD, 26 mm high and had an optically flat bottom. The bottom inside surface was made hydrophobic with a coating of Drifilm SC-87 (Pierce Chemical Co., Illinois).

One of the two microscopes used for observation and recording was a Vickers M15 polarizing microscope (Vickers Instruments, Toronto) with a magnification of 75× (5× objective, 10× eyepiece, 1-$\frac{1}{2}$× analyser). The light source was a 500 watt super-high pressure mercury vapour lamp (Philips Electronics, Toronto). Cooling water was pumped through a water jacket housing the lamp and primary condenser, and the polarizer was protected by two heat absorbing filters (Wild Scientific).

The other microscope used was a Vickers M41 (Vickers Instruments, Toronto), with a magnification of 200× (250×) [20× objective, 10× eyepiece, 1.00× (1.25 ×) analyser]. The light source was a 12 volt 100 watt tungsten-halogen lamp (Philips, Holland). The lamp unit had its own heat and light filters. The dark field illumination technique was used.

Nessler cups were fitted into cell holders and onto a micrometer stage (Vickers Instruments, Toronto) equipped with a micrometer dial (Metutoyo, Japan) with a range of 0.01 to 20 mm.

A thermostatted cell holder, which would hold a Nessler

cup was manufactured from an aluminum rod. A schematic diagram of it is shown in Figure II-1. A tight fitting O-ring was attached to the Nessler cup and placed in the cell holder. An outside collar, with a hole in its top large enough for the Nessler cup to pass, was screwed down, forcing the O-ring onto a lip and sealing the inner compartment formed by the walls of the Nessler cup and the cell holder. Through this compartment, thermostatted water would pass via nozzles placed at 180° to each other. The outlets were attached to the water pump hoses leading to the constant temperature bath. The base of the cell holder, made from aluminum plate, had a 25 mm diameter window into which a thin quartz circular cover glass was affixed.

The camera, an Autowind 35 mm (Vickers Instruments, Toronto), was controlled by an autoexposure unit J-35 (Vickers Instruments, Toronto).

The film used was Anscochrome D-500 and D-200 colour reversal film (G.A.F., Toronto). Exposed films were processed by Benjamin Labs (Toronto).

The photomicrographs were projected upon a pinboard (2×3) feet covered by a large sheet of white paper, with either a Pradovit projector (Lietz, West Germany), equipped with a 150 mm or a 50 mm lens or an Ansochrome 940 projector (G.A.F., Toronto), equipped with a 150 mm lens.

II-B2 Procedure

Both solution A, containing calcium and peroxydisulfate, and solution B, containing either thiosulfate or iodide, were

Figure II-1. The thermostatted cell holder for droplet observation under the microscope.

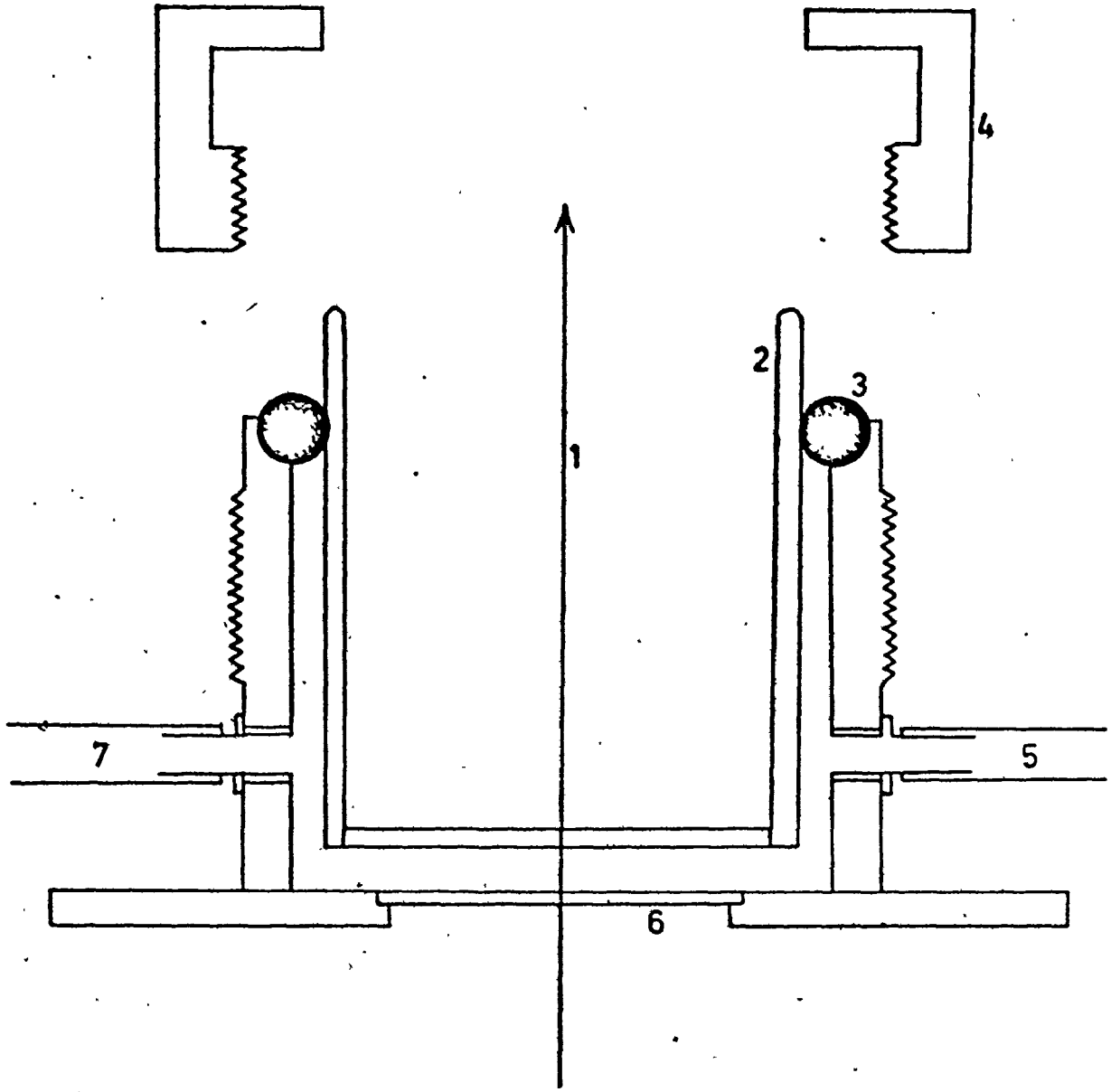

1 optical axis

2 Nessler cup

3 o-ring

4 collar

5 inlet

6 window

7 outlet

pressure filtered through a 0.3 μ PVC filter. Aliquots of each were withdrawn and thoroughly mixed. This solution was drawn up into a dropping pipette and 2 drops placed in a 6 ml homogenizing flask containing 5 ml of DC 20-200 c.s. oil. The solution was dispersed by means of a micro-homogenizer rotating at approximately 40,000 r.p.m. for 10 seconds. The contents of the homogenizing flask were then poured into a 15 ml centrifuge tube containing 11 ml of D.C. 200-100 c.s. oil. This mixture was rotated at 4000 r.p.m. in a centrifuge for 2-5 min. Three to four milliliters of the heavier oil was taken up into an eye dropper and transferred to the bottom of a Nessler cup which contained 1 ml of the heavier oil. Cup and contents were rotated at 4000 r.p.m. for 3-4 min and then most of the oil was decanted off until a depth of 3 mm remained.

The observation cup was placed in a cell holder. The cell holder was placed on the microscope stage and fields of view were selected for observation. Micrometer dial settings for each field of view were noted so that accurate readjustment for observation of multiple fields of view was possible.

Each field of view was photographed at certain time intervals and the time, relative to experimental time zero (t_o), was recorded. Data recording was terminated when most of the droplets contained crystals or at the end of a predetermined time interval. Finally a photograph was taken of a millimeter slide, using the same magnification factor.

II-B3 Data Collection

The slides were sorted into fields of view, then arranged into the correct time sequence, labelled, and mounted in slide trays. The absolute droplet sizes were measured by comparing their diameters with the distance measured between rulings on the projected millimeter slide.

A slide of the droplets of one field of view was then projected on the screen and the droplet population divided into volume ranges. The droplets in each range were tagged with coloured pins. All the slides of the one field of view were projected in correct time sequence. As each slide was displayed, a search was made for those droplets containing a crystal not visible in the previous slide. If the droplets contained a crystal, the pin associated with it was removed and placed in a container holding all those removed for that particular slide. This procedure was followed for all slides of this field of view.

The above procedure was then repeated for all remaining fields of view.

Tables of number of droplets of a certain volume v per time interval between slides in which crystals have appeared ($\Delta n_{t,v}$) were constructed at corresponding times. The data from all fields of view were lumped together according to volume and time. These data were then summed with time, equation (36), to give $n_{t,v}$, the total number of droplets of volume v containing crystals at time t.

$$\sum_{t=0}^{t} \Delta n_{t,v} = n_{t,v} \qquad (36)$$

II-C EXPERIMENTAL RESUME

An outline of the experiments that were performed, including all experimental variables, is shown in Tables II-1, 2, and 3.

TABLE II-1

Experimental variables used in the variable driving force experiments

Variables \ Experiment Number	E_1	E_2	E_3
T°C	22	22	22
$[Ca^{2+}]_i$	0.250	0.475	-
$[Sr^{2+}]_i$	-	-	-
$[S_2O_8^{2-}]_i$	0.100	0.157	0.00633
$[S_2O_3^{2-}]_i$	0.250	0.433	-
$[I^-]_i$	-	-	0.0420
$[K^+]$	0.200	0.314	0.0420
$[Na^+]$	0.500	0.866	-
$[NH_4^+]$	-	-	0.0840
μ	1.55	2.72	0.139
S_f	7.6	13.7	25.8

$[Ca^{2+}]_i$ = the initial concentration of calcium.

μ = the ionic strength.

S_f = the final supersaturation.

TABLE II-2

Experimental variables used in the constant driving force experiments

Variables \ Experimental Number	E_4	E_5	E_6	E_7	E_8	E_9	E_{10}	E_{11}	E_{12}	E_{13}	E_{14}	E_{15}
T°C	21.8	28.1	34.3	40.4	21.8	28.1	34.3	40.4	21.8	28.1	34.3	40.4
$[Ca^{2+}]_i$	.175	.175	.175	.175	.204	.204	.204	.204	.233	.233	.233	.233
$[SO_4^{2-}]_f$	.175	.175	.175	.204	.204	.204	.204	.204	.233	.233	.233	.233
$[S_2O_8]_i$	.0875	.0875	.0875	.0875	.102	.102	.102	.102	.117	.117	.117	.117
$[K^+]$	.175	.175	.175	.175	.204	.204	.204	.204	.233	.233	.233	.233
$[NO_3^-]$	.350	.350	.350	.350	.408	.408	.408	.408	.466	.466	.466	.466
μ_f	1.31	1.31	1.31	1.31	1.47	1.47	1.47	1.47	1.63	1.63	1.63	1.63

$[SO_4^{2-}]_f$ = final sulfate concentration. μ = final ionic strength. pH = 3.23, NH_4I = 0.35 M, $[Ca^{2+}]/SO_4^{2-}] = 1.0$.

TABLE II-3

Experimental variables used in cation-anion ratio experiments

Variables \ Experimental Number	E_{16}	E_{17}	E_{18}	E_{19}	E_{20}	E_{21}	E_{22}	E_{23}	E_{24}	E_{25}	E_{26}	E_{27}	E_{28}
$[Ca^{2+}]_i$	.101	.124	.136	.143	.166	.175	.214	.232	.248	.303	.350	.175	.175
$[S_2O_8^{2-}]_i$	.152	.124	.113	.107	.0923	.0875	.0715	.0661	.0614	.0505	.0438	.0875	.0875
$[Ca^{2+}]/[SO_4^{2-}]$	.33	.50	.60	.75	.90	1.0	1.5	1.75	.20	3.0	4.0	1.0	1.0
$[K^+]$	.303	.248	.226	.214	.185	.175	.143	.132	.124	.101	.0876	.175	.175
$[NO_3^-]$	.202	.248	.272	.286	.332	.350	.428	.464	.496	.606	.700	.350	.350
μ	1.41	1.34	1.30	1.32	1.31	1.32	1.35	1.38	1.40	1.51	1.62	1.32	1.32
pH	3.23	3.23	3.23	3.23	3.23	3.23	3.23	3.23	3.23	3.23	3.23	3.23	7.60

$[NH_4^+] = [I^-] = 0.35$ M . T = 34.3°C . I.P. = 0.03063 . μ = ionic strength.

III RESULTS AND DISCUSSION

The results and discussion section will be divided into four separate parts. Section III-A deals with the variable driving force experiments, E_1, E_2 and E_3, of calcium sulfate and strontium sulfate. Thermodynamic parameters are calculated and the effects of $\frac{dS}{dt}$ and S on their magnitudes will be examined.

The second section, III-B, will include a study of the inter-relationships between the rate, lag time, and two independent variables T and I.P. The results of experiments E_4 through E_{15} are examined.

Section III-C contains the study of the relationship between the nucleation rate and various calcium-sulfate ratios, the results of experiments E_{16} to E_{26}. Comments are made about the applicability of the classical expression of supersaturation for ionic salts. As well, the results are discussed from the point of view of a non-classical model.

The last part, section III-D, records measurements of J and L for experiments E_{27} and E_{28} as a function of pH. The growth rate effect upon the lag time will be discussed.

III-A NUCLEATION EXPERIMENTS WITH A VARIABLE DRIVING FORCE

Observations of phase changes occurring in droplets were made at two values of $\frac{dS}{dt}$ for calcium sulfate and one for

strontium sulfate. The supersaturation was generated by the reaction of peroxydisulfate with thiosulfate for calcium sulfate and with iodide for strontium sulfate. The solubility product and sulfate ion concentration were measured and the molecular formula determined in each case. Phase changes occurring in the droplets were photomicrographically recorded. Thermodynamic parameters were calculated and compared. This led to a critical discussion of rate measurement of nucleation with a variable driving force.

II-A1 Experimental Design

Generation of Sulfate Ion: Excess thiosulfate was used to reduce peroxydisulfate in the presence of a constant calcium concentration. All products of the oxidation-reduction reaction were very soluble compared to calcium sulfate. CaS_4O_6, the second least soluble, has a Ksp 10^2 times as large as that of $CaSO_4 \cdot 2H_2O$. The initial concentrations of reactants after mixing were:

Experiment	$[Ca^{2+}]$	$[S_2O_3^{2-}]$	$[S_2O_8^{2-}]$	Final S
E_1	0.250 M	0.250 M	0.100 M	7.6
E_2	0.475 M	0.433 M	0.157 M	13.7

Thiosulfate was not suitable for generation of sulfate in the presence of strontium because strontium thiosulfate is very insoluble. Potassium iodide was used as the reducing agent since it forms no insoluble salts with any of the cations present in solution and its reaction with peroxydisulfate was

much faster at the lower concentration required. The initial reactant concentrations were:

Experiment	$[Sr^{2+}]$	$[I^-]$	$[S_2O_8^{2-}]$
E_3	0.00633 M	0.0420 M	0.0210 M

Measurement of Sulfate Ion Concentration with Time: The sulfate ion concentration, generated by the reaction of thiosulfate and peroxydisulfate, was measured using the technique described in section II-A2(a). It was discovered, however, that $S_2O_8^{2-}$ interfered with the free dissolution wave of thiosulfate. This was remedied by the addition of $S_2O_8^{2-}$ to the standard thiosulfate solution to give a $[S_2O_3^{2-}]/[S_2O_8^{2-}]$ identical to the initial mixture of solutions A and B. The standard solution was diluted 1:10 and then 0, 5, 10, 15, 20, and 25 ml aliquots were diluted to 250 ml. The dilution factor of approximately 1:250 ensured that the oxidation-reduction reaction had a negligible rate in the standard solutions and in the kinetic sample solutions. The quenching of the reaction was confirmed by the measurement of the diffusion current of the most concentrated standard over a period of four hours. The wave height remained constant.

The sulfate ion concentration was calculated from $S_2O_3^{2-}$ vs. time measurements, ion products using the constant calcium concentration, and the supersaturation from equation (36). The supersaturation is plotted against time in Figure III-A1.

Figure III-A1. Plots of the supersaturation vs time for experiments E_1 and E_2

- ○ E_1
- □ E_2

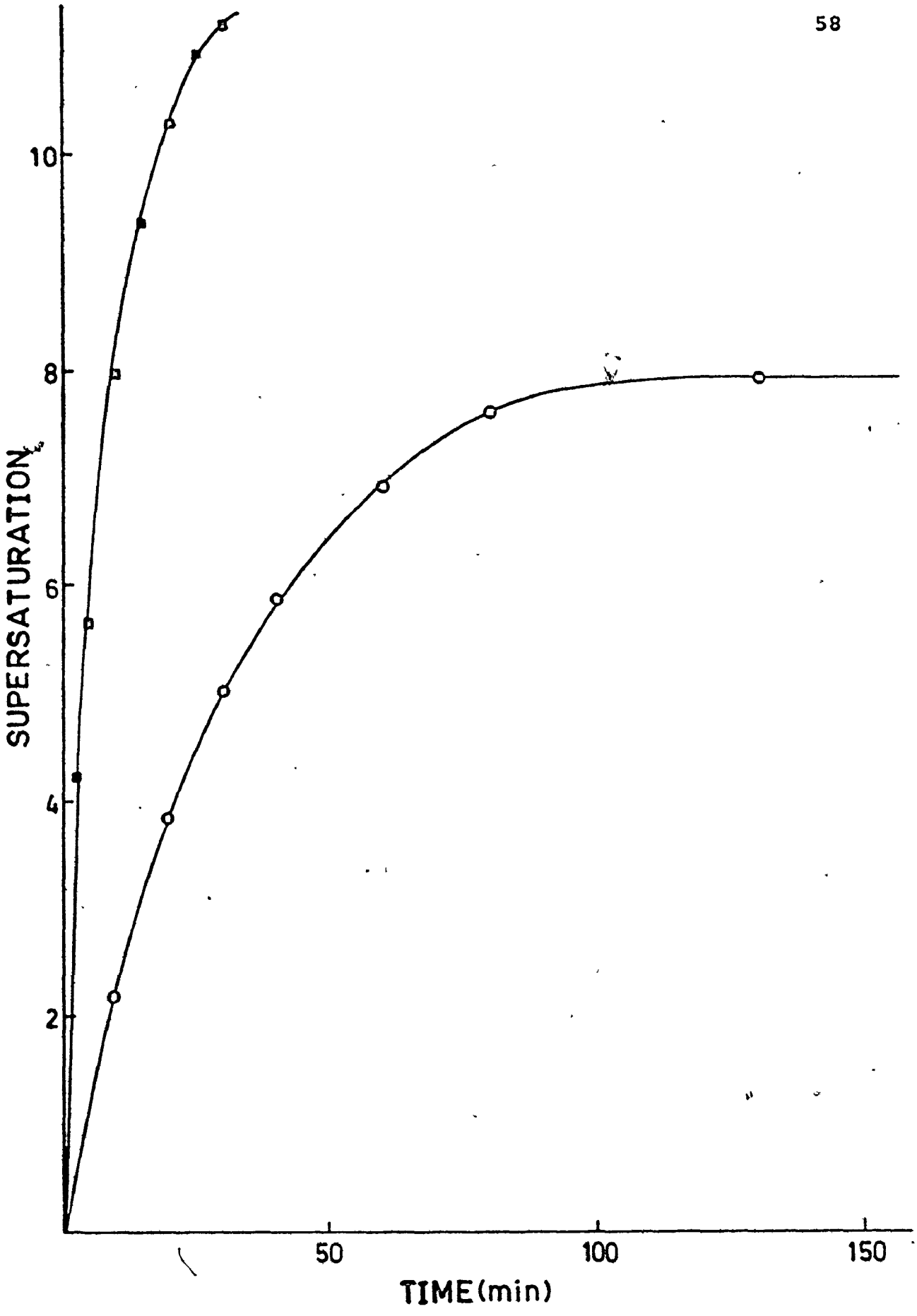
10
8
6
4
2
SUPERSATURATION
50
100
150
TIME(min)

Sulfate ion measurements for the iodide-peroxydisulfate reaction were made using the technique described in section II-A2(a). The supersaturation-time curve is displayed in Figure III-A2.

Solubility Measurements: The solubility of $CaSO_4 \cdot 2H_2O$ was measured using the technique described in section II-A3(b). The concentrations of species present in the matrix solution into which excess calcium sulfate would be added were identical to those present in a mixture of solutions A and B at infinite time after mixing. The Ksp for $CaSO_4 \cdot 2H_2O$ was found to be 8.47×10^{-4}.

The Ksp of $SrSO_4$ (4.0×10^{-7}) was taken from the literature[51].

Precipitating Form: The molecular formula of the precipitate, $CaSO_4 \cdot nH_2O$, was determined by weighing out some of the product of the beaker reaction, dissolving it, and titrating the calcium ion with standard EDTA solution. This procedure gave n = 2.087, indicating that the precipitate was gypsum ($CaSO_4 \cdot 2H_2O$).

When $SrSO_4$ precipitates from aqueous solution, it forms needle shaped crystals of $SrSO_4 \cdot 2H_2O$[52]. The 2-hydrate undergoes a very rapid transition to the anhydrous form and this results in a more compact grainy precipitate.

III-A2 Nucleation Experiments

Droplets were made as described in section II-B2. Approximately 20 photomicrographs were taken for experimental durations of 240, 30, and 45 min. for experiments E_1, E_2 and E_3 [illegible]. In [illegible] III-A3, 4, and 5, n vs [illegible]

Figure III-A2. A plot of the supersaturation vs time for experiment E_3

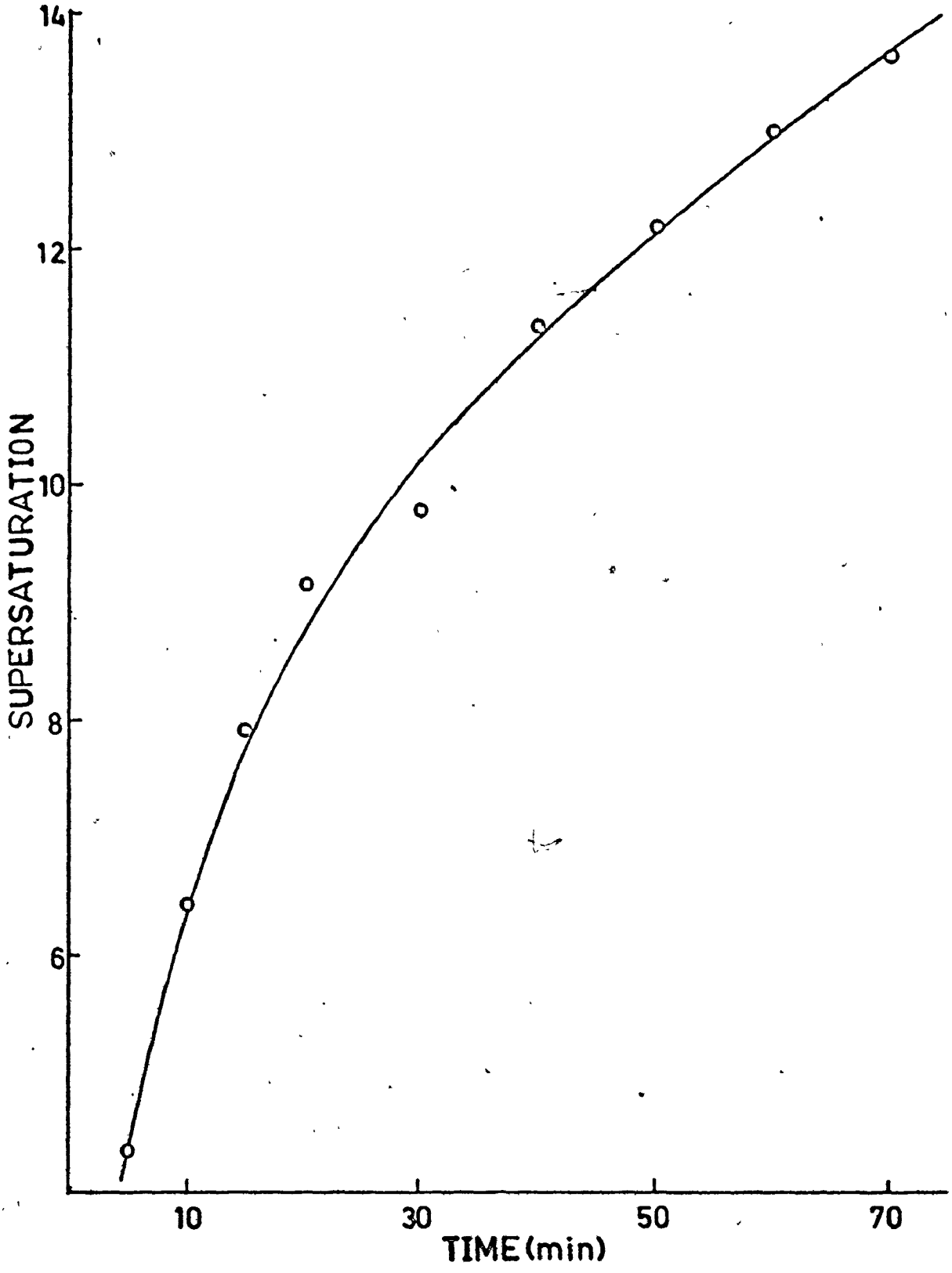
14
12
10
8
6
SUPERSATURATION
10
30
50
70
TIME (min)

Figure III-A3. Plots of $n_{t,v}$ vs time measured for three volume ranges in experiment E_1

Legend ● $v = 2.57 \times 10^{9}$ cm^3

■ $v = 4.85 \times 10^{-9}$ cm^3

▲ $v = 8.18 \times 10^{-9}$ cm^3

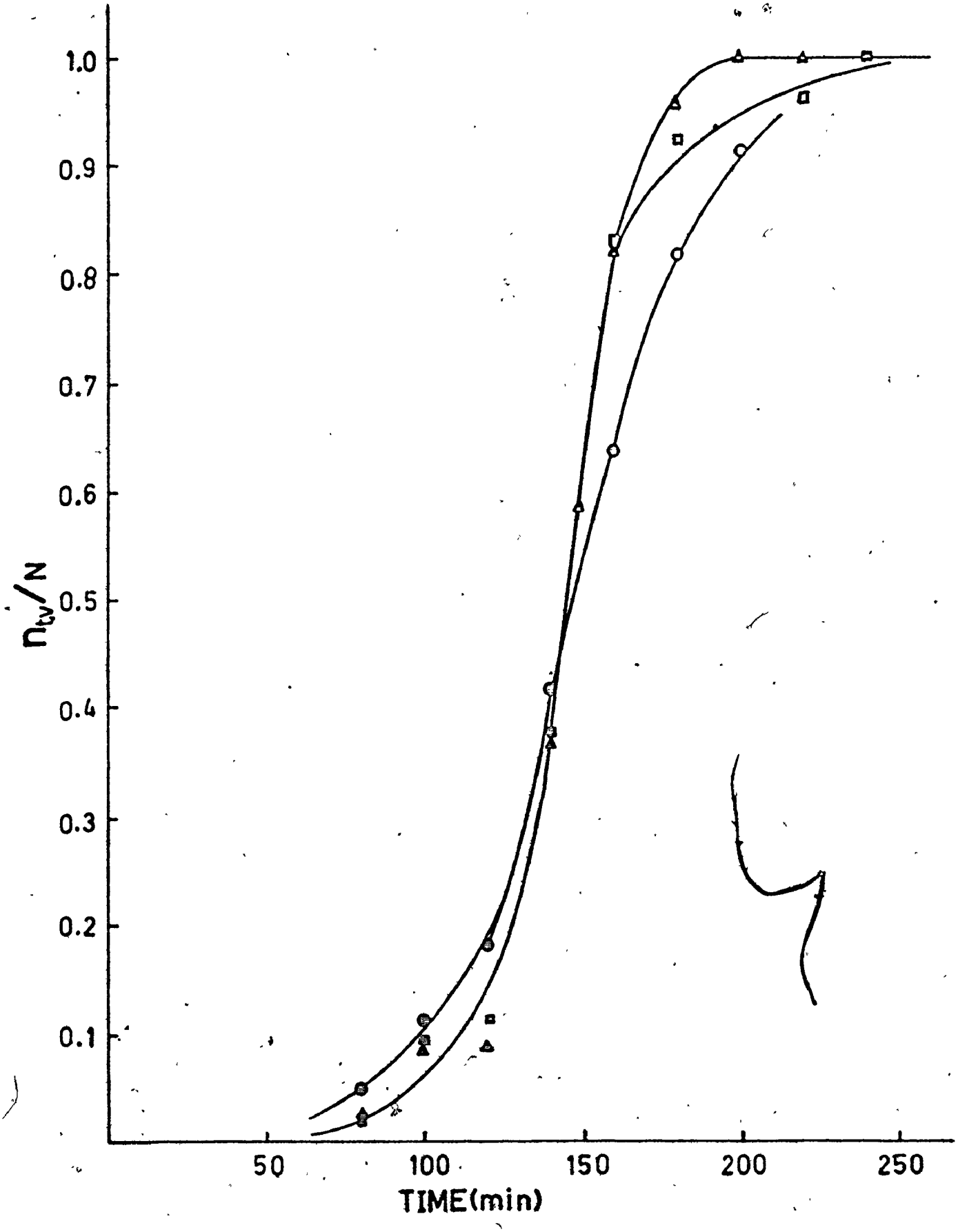
1.0
0.9
0.8
0.7
0.6
0.5
0.4
0.3
0.2
0.1
n_{tv}/N
50
100
150
200
250
TIME(min)

Figure III-A4. Plots of $n_{t,v}$ vs time measured for three volume ranges in experiment E_2

Legend: ● $v = 5.24 \times 10^{-10}$ cm^3

■ $v = 4.19 \times 10^{-9}$ cm^3

▲ $v = 1.41 \times 10^{-8}$ cm^3

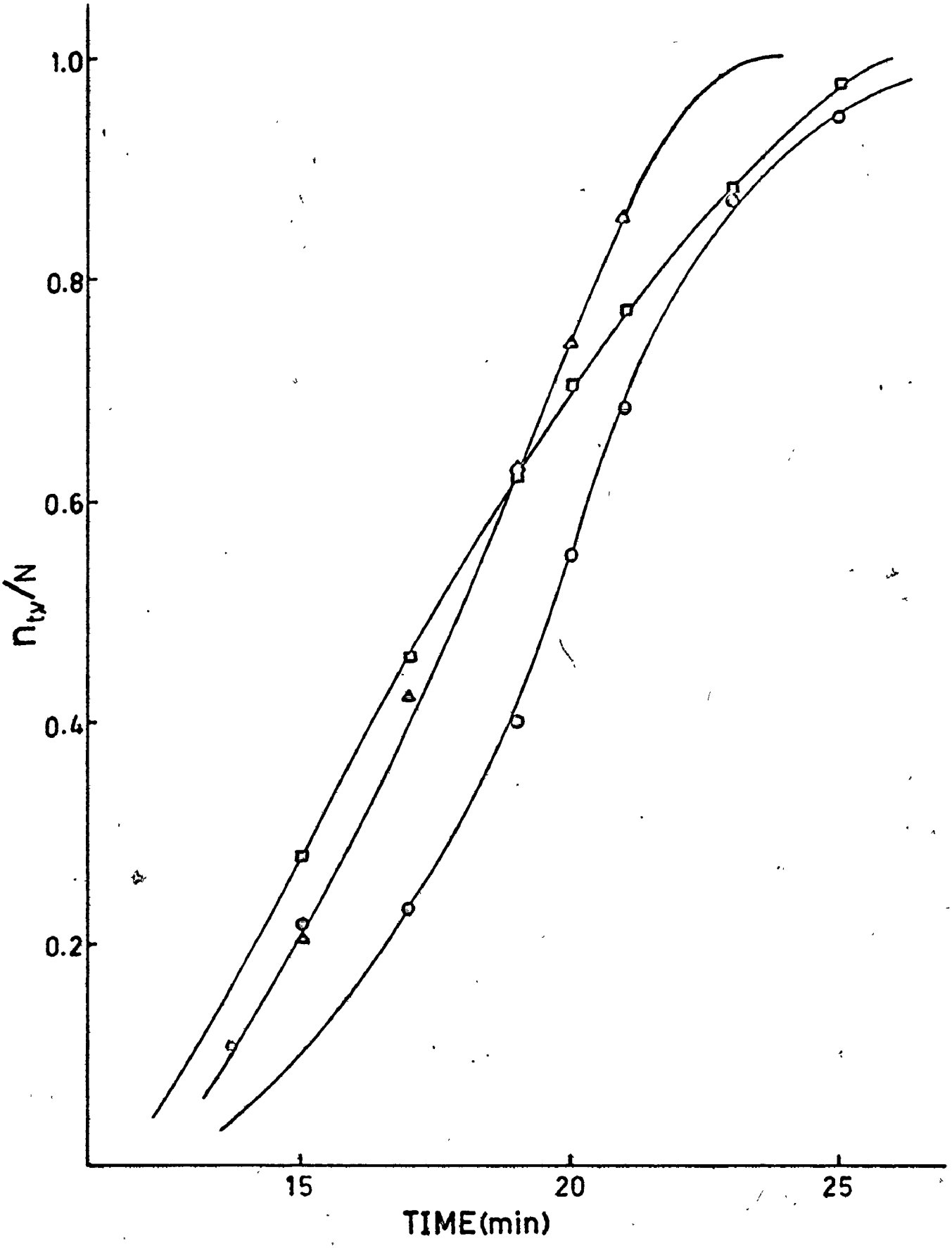
1.0
0.8
0.6
0.4
0.2
$n_{t,y}/N$
15
20
25
TIME(min)

Figure III-A5. Plots of $n_{t,v}$ vs time measured for three volume ranges in experiment E_3

Legend: ○ $v = 1.58\times10^{-9}$ cm^3

□ $v = 2.88\times10^{-9}$ cm^3

▲ $v = 4.75\times10^{-9}$ cm^3

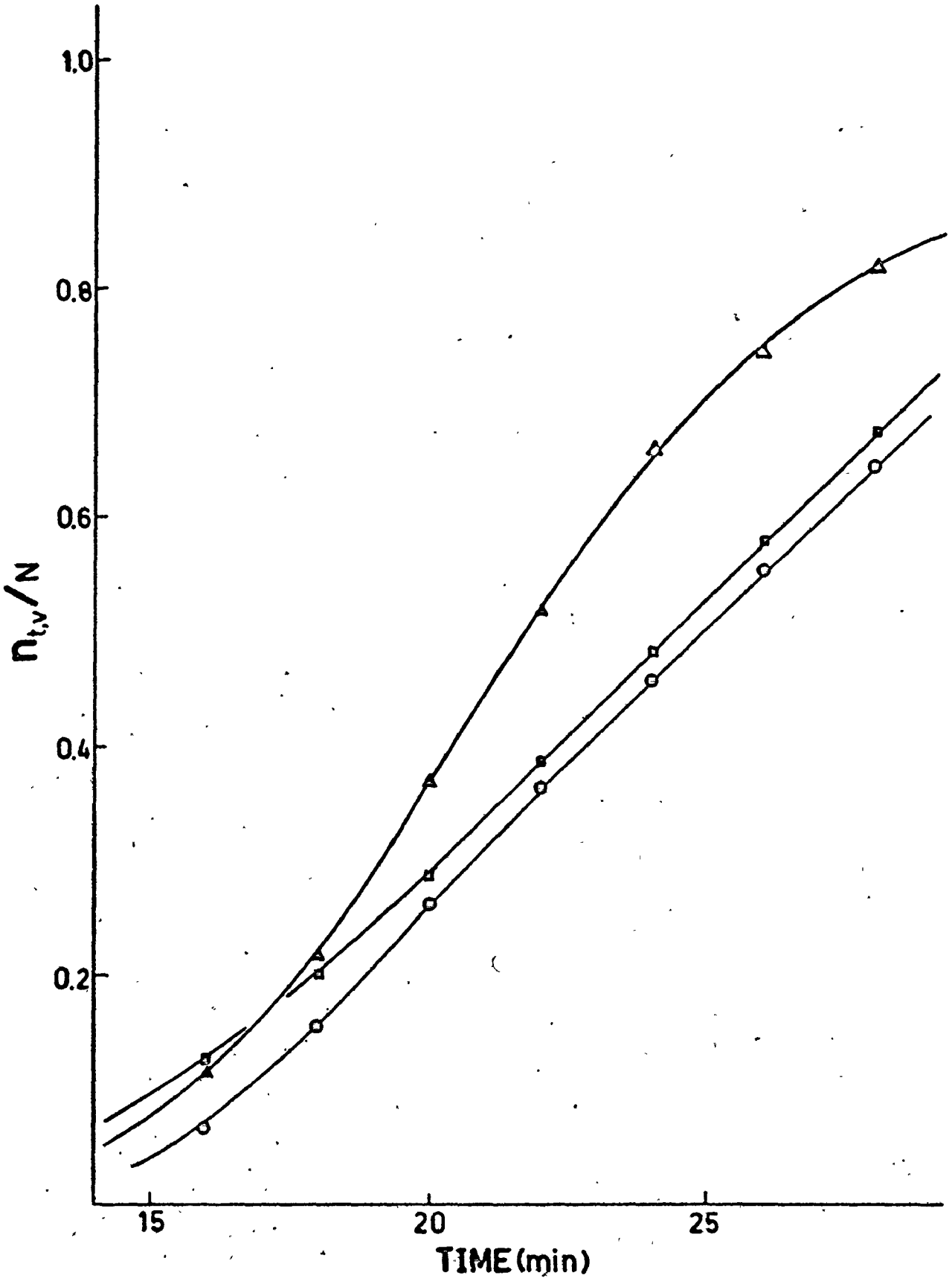
1.0
0.8
0.6
0.4
0.2
$n_{t,v}/N$
15
20
25
TIME (min)

curves are drawn from the information obtained from slides processed as described in section II-B3.

Rate Calculations: The rate of nucleation, J, is defined as the number of nuclei formed per unit volume (cm^3) and unit time (sec.). Values of $n_{t,v}$, however, are measurements of the droplet crystallization rate J'. J' is the number of droplets of volume v having a crystal appear in them per second. The relationship between J and J' is given in equation (37).

$$J = J'/v \quad . \tag{37}$$

The rate of nucleation was calculated using equation (38).

$$J = \frac{1}{v} \cdot \frac{1}{N-n_{t,v}} \cdot \frac{dn_{t,v}}{dt} \tag{38}$$

where v is the volume of the average droplet in a volume range, and N is the total number of droplets in the volume range. Equation (38) becomes identical to that derived by Carte[53] if both numerator and denominator are divided by N. Using this equation, rate measurements that are independent of the induction time can be made if the supersaturation is not changing. Equation (38) is also useful for calculating steady and non-steady state rates.

Bigg[54] reports that $n_{t,v}$ data obtained from observation of nucleation events in a droplet population with a variety of volume ranges can be lumped together if the mean crystallization time of each volume range is reduced to that of a droplet of standard size. This is possible if the assumption

is made that all $n_{t,v}$ curves have the same shape independent of the volume, and only differ in their mean crystallization times. It is important, however, that rate calculations be performed on droplet volume ranges individually. This is the conclusion which follows from the argument below.

If the supersaturation is constant, equation (38) can be integrated with time to give equation (39).

$$n_{t,v} = N[1 - \exp(-Jvt)]. \qquad (39)$$

In this case, the mean crystallization time is defined as $n_{t,v}/N = 0.5$. If we let $J = 10^6$/sec and $v_1 = 10^{-10}$ cm^3 and $v_2 = 5\times10^{-10}$ cm^3, the mean crystallization times would be 6930 and 1380 sec. respectively. Eighty-five percent crystallization times are 19,000 and 3,820 for v_1 and v_2. Curves, generated using Equation (39) and different values of v, shown in Figure III-A6(a), do not have the same shape. If the mean crystallization time of droplets of the smaller volume is reduced to that of the larger, i.e. 5550 sec. is subtracted from all t_1, the $n_{t,v}$ vs time plots would look like Figure III-6A(b). Summation at this point produces S-shaped curves with a time of crystal appearance in minus experimental times and a non-steady state rate in the initial stages of crystallization.

Let us take two droplet ranges with mean volumes v_1 and v_2 having N droplets each. Assume there is no lag or induction time. At constant supersaturation the $n_{t,v}$ curves of each are

Figure III-A6. (a) The $n_{t,v}$ vs time plots of two droplet populations V_1 and V_2. (b) The mean crystallization time of V_1 reduced to that of V_2

Legend ● $V_1 = 1.0 \times 10^{-10}$ cm^3

■ $V_2 = 5.0 \times 10^{-10}$ cm^3

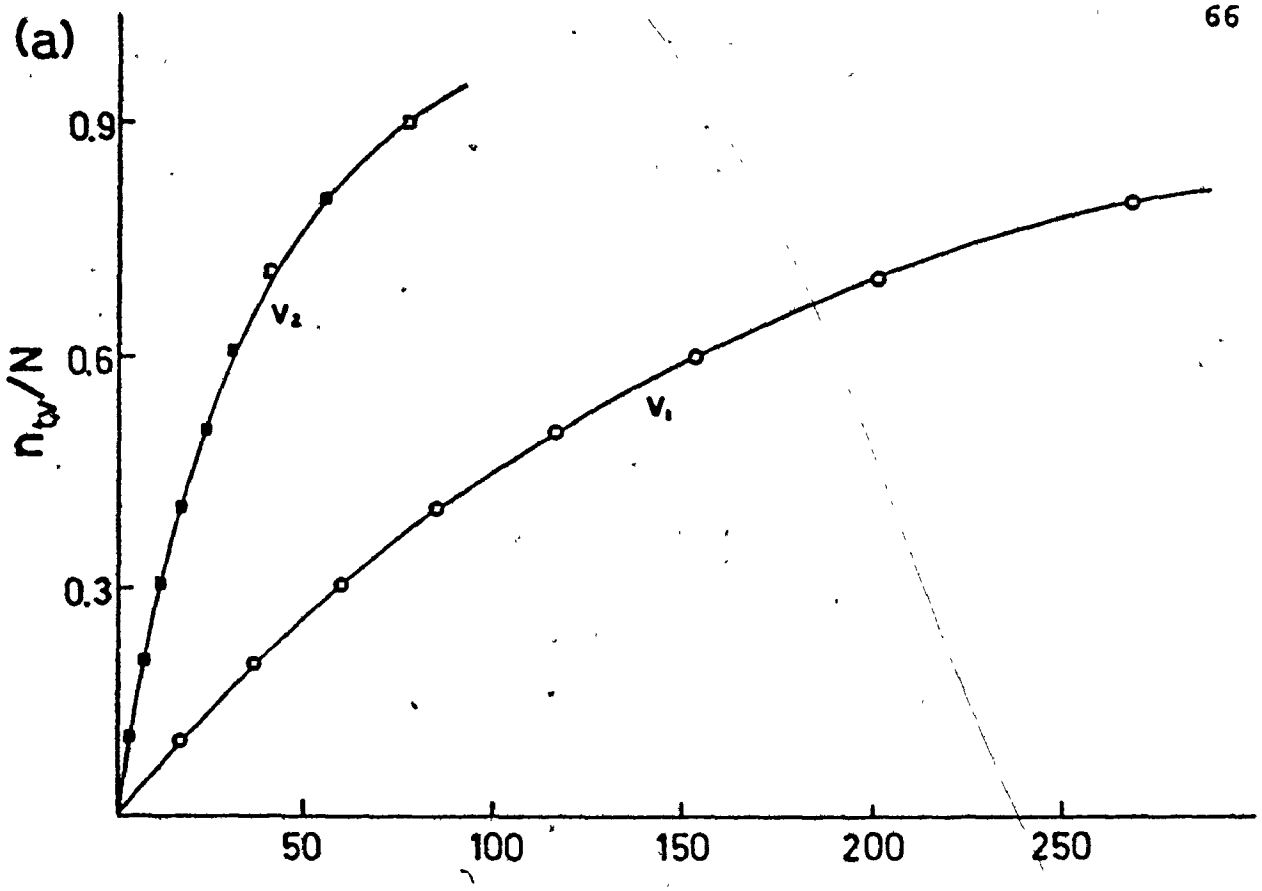
(a)
0.9
0.6
0.3
$n_{t,v}/N$
v_2
v_1
50
100
150
200
250

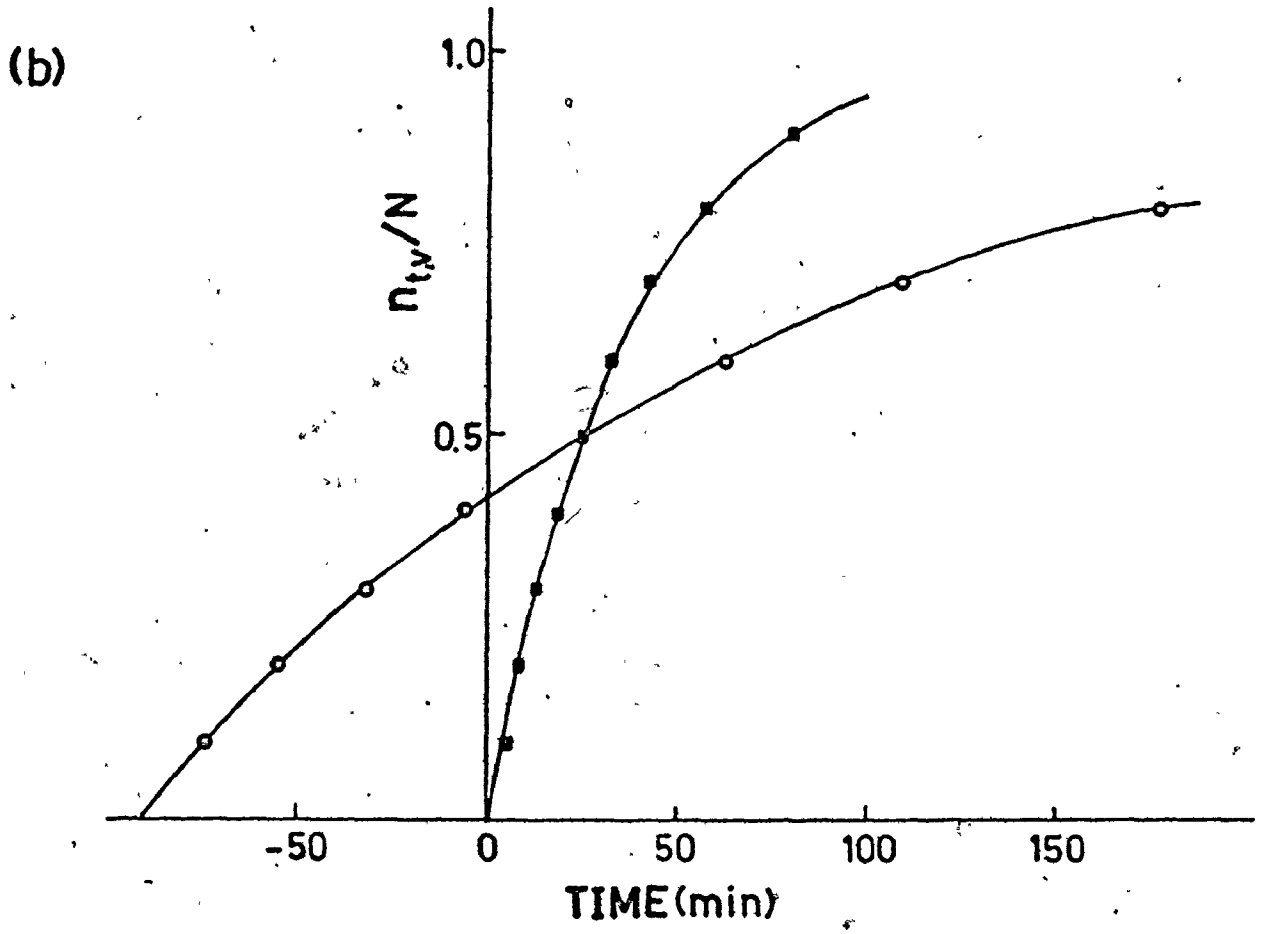
(b)
1.0
0.5
$n_{t,v}/N$
-50
0
50
100
150
TIME(min)

$$n_{t_1,v_1} = N[1-\exp(-Jv_1t_1)] \quad \text{and}$$

$$n_{t_2,v_2} = N[1-\exp(-Jv_2t_2)].$$

Equating the above we have

$$N[1-\exp(-Jv_1t_1)] = N[1-\exp(-Jv_2t_2)] \tag{40}$$

and

$$t_1 = \frac{v_2}{v_1} \cdot t_2 . \tag{41}$$

If there is a lag time, L, then

$$(t_1-L) = \frac{v_2}{v_1} (t_2-L). \tag{42}$$

If the droplet populations were not the same, then

$$t_1 = \frac{v_2}{v_1} \cdot t_2 + \frac{\ell n\ N_1/N_2}{Jv} . \tag{43}$$

Equation (43) breaks down when the supersaturation changes since J is a function of S.

The mean crystallization times of a droplet population with a number of volume ranges has little relevance to nucleation rate measurements. Bigg's assumptions, therefore, are not useful for the interpretation of the data.

Thermodynamic Parameter Estimation: In Figure III-A7 ℓnJ vs ℓnS curves are plotted for both $CaSO_4 \cdot 2H_2O$ experiments. The intercepts on the ℓnS axis give values of S*. These values A 6.13 (high $\frac{dS}{dt}$) and B 7.2 (low $\frac{dS}{dt}$) correspond to values obtained by extrapolation of ℓnJ vs (ℓnS)

In Figures III-A8 and 9, ℓnJ is plotted against $(\ell nS)^{-2}$ and ℓnS respectively for $SrSO_4$. The calculated values are listed in Table III-A1.

Figure III-A7. Plots of ℓnJ vs ℓnS for experiments E_1 and E_2

- ● E_1
- ◘ E_2

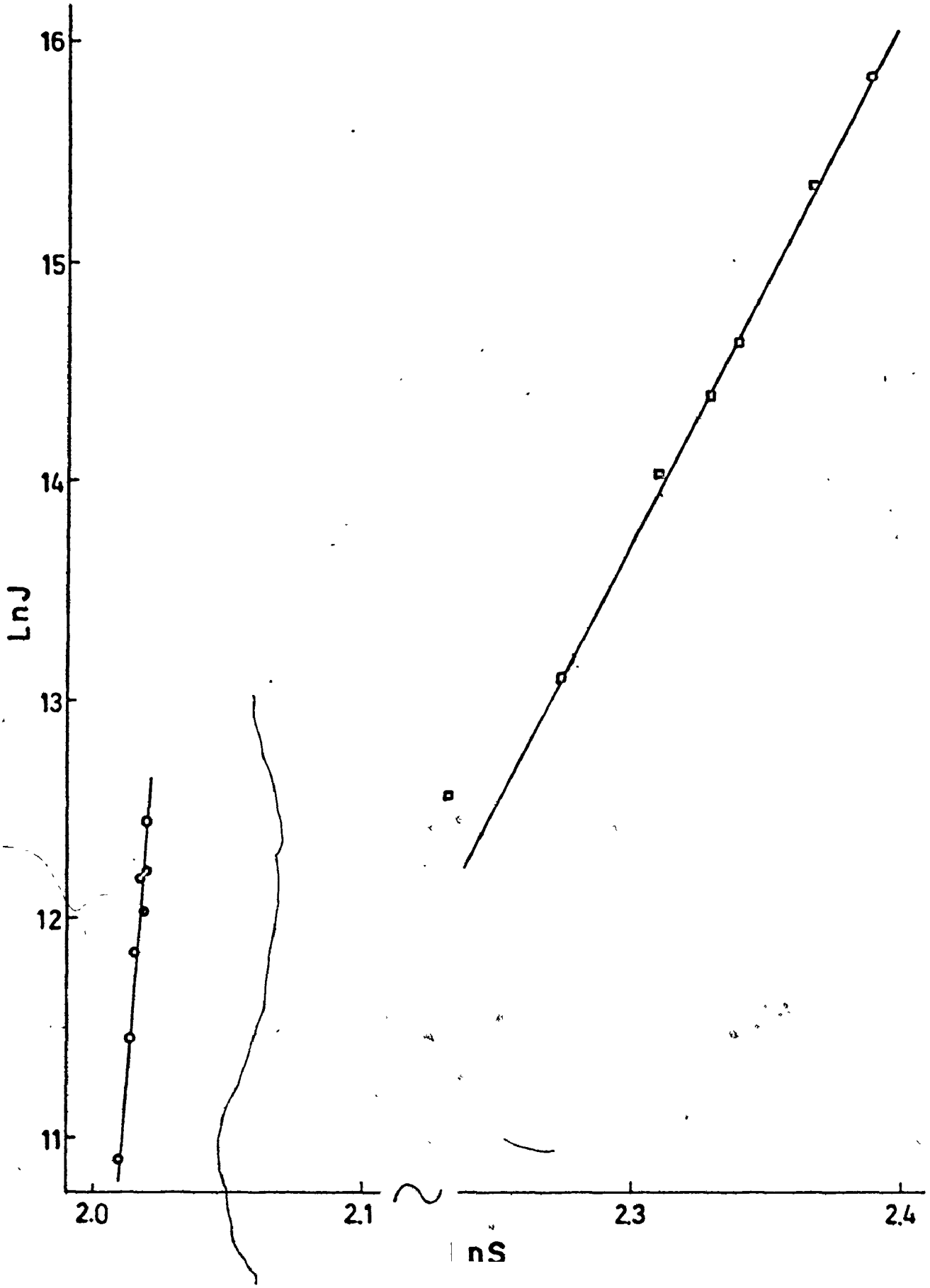
16
15
14
13
12
11
LnJ
2.0
2.1
2.3
2.4
nS

Figure III-A8. Plot of ℓnJ vs $(\ell nS)^{-2}$ for $SrSO_4$, experiment E_3

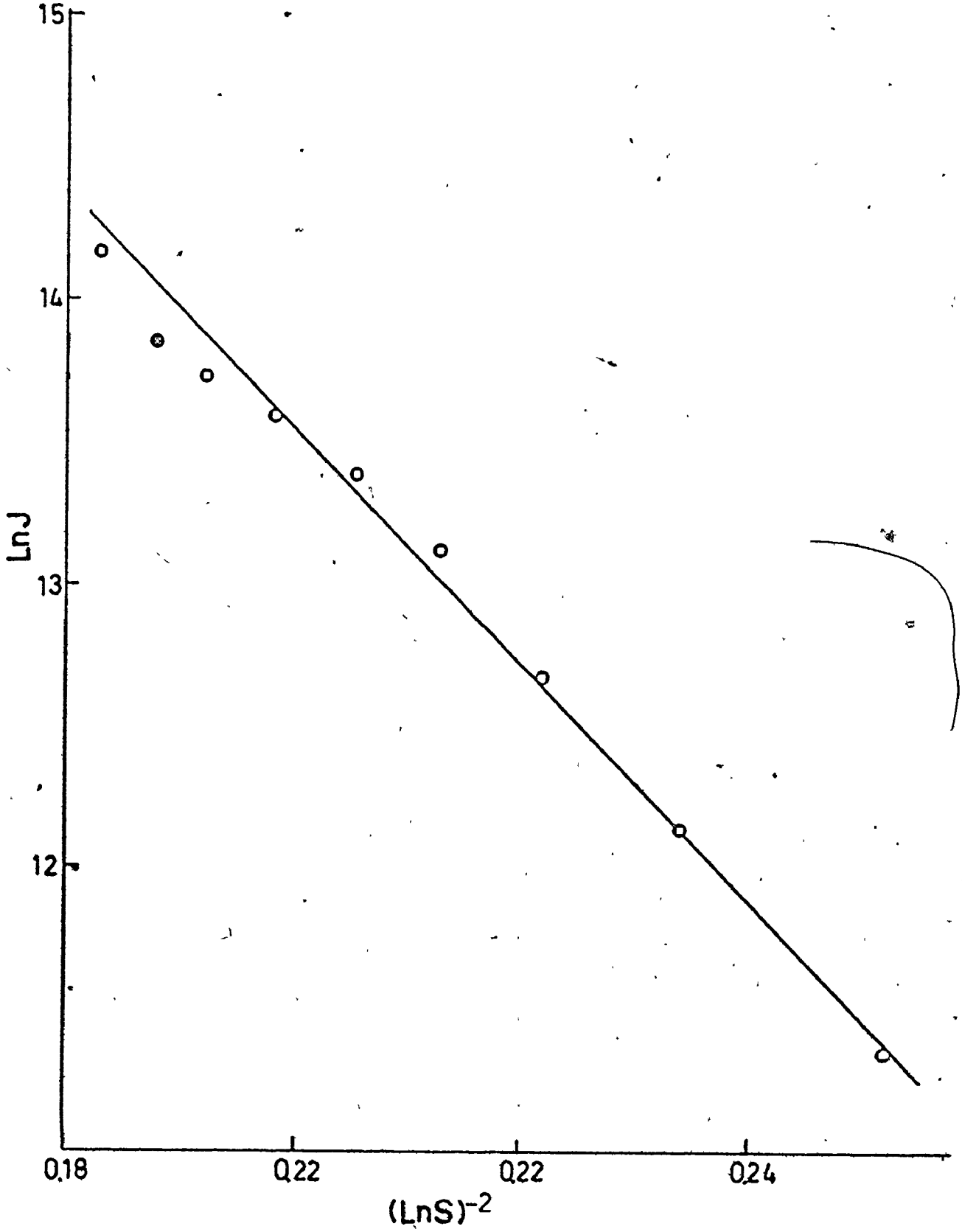
15
14
13
12
LnJ
0.18
0.22
0.22
0.24
(LnS)⁻²

Figure III-A9. Plot of ℓnJ vs ℓnS for experiment E_3

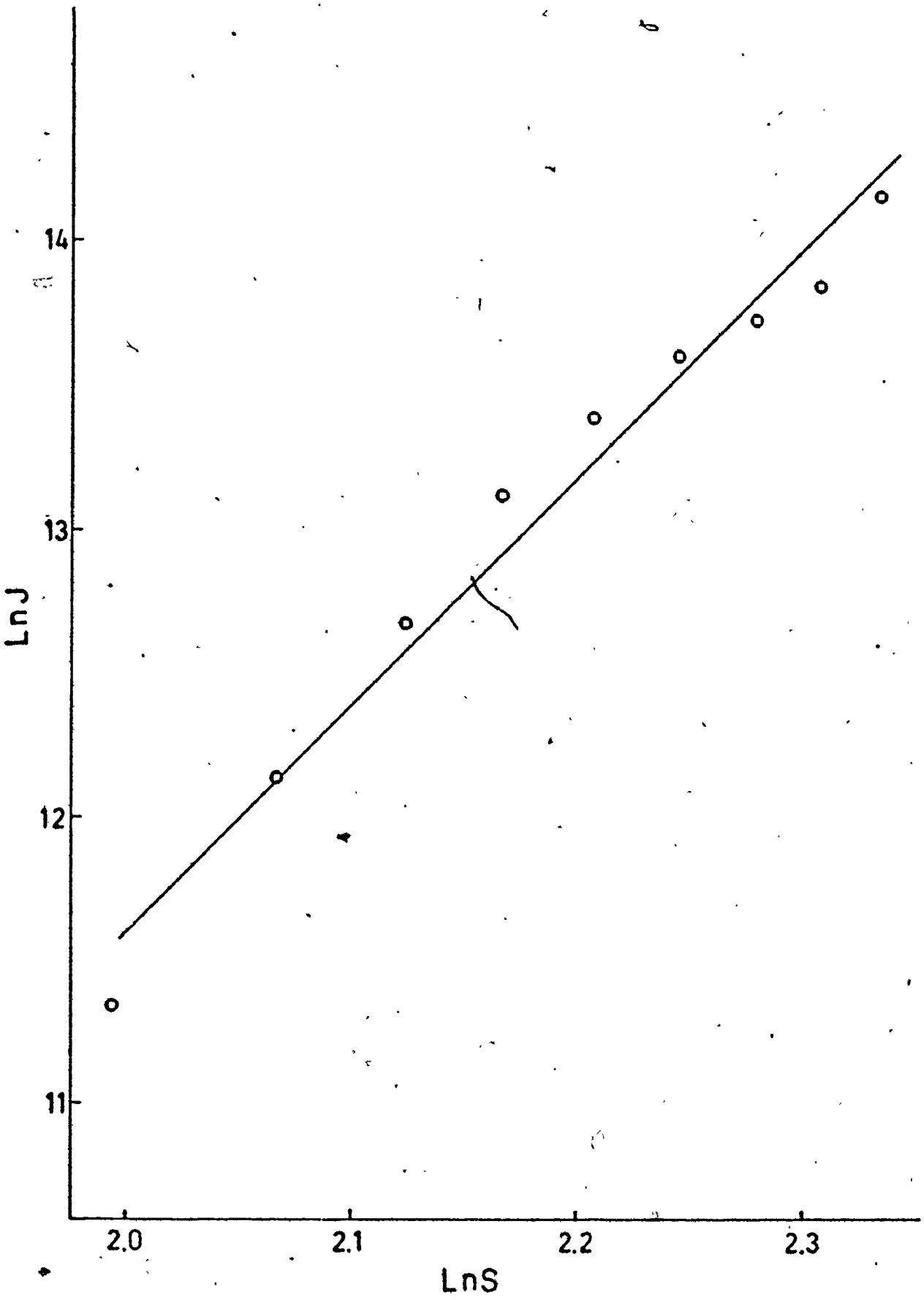
14
13
12
11
LnJ
2.0
2.1
2.2
2.3
LnS

TABLE III-A1

Various Thermodynamic Parameters for Experiments E_1, E_2 and E_3

Parameters \ Experimental Number	E_1	E_2	E_3
*Droplet volume ranges (cm^3)$\times 10^9$	(1.77-3.59) (3.59-6.37) (6.39-10.31)	(0.659-1.77) (1.77-8.21) (8.21-22.4)	(.467-1.11) (1.11-2.16) (2.16-3.74) (3.74-5.95)
σ(ergs$\times 10^9$)	56.8±1.7	34.4±1.0	30.9±0.8
S*	7.02±0.35	5.57±0.33	4.04±0.07
ℓnA	78.9±4.8	42.7±2.6	22.3±.4
n*	186. ±37	45.0±9	198. ±40
r*(Å)	17.6±1.4	11.0±0.9	8.37±0.7
ΔG^*(ergs)$\times 10^{12}$	7.39±0.8	1.74±0.2	0.907
S_b^*	7.2 ±.2	6.13±.11	2.42±0.20

S_b^* = critical supersaturation from ℓnJ vs ℓnS plots.

*Note: It was not necessary to select identical volume ranges. See section III-A2.

In Figures III-A10 and 11, ℓnJ vs $(\ell nS)^{-2}$ was plotted for $CaSO_4 \cdot 2H_2O$, observed at two rates of generation of supersaturation. From the slope and the intercepts, σ, ℓnA and S^* were calculated. The derived parameters n^* and r^* were calculated using equations (21) and (22). The results are found in Table III-A1.

The results seem to depend upon two factors; the rate of change of the supersaturation with time and/or the supersaturation. The following are true for experiments E_1 and E_2:

$$\left(\frac{dS}{dt}\right)_{E_2} > \left(\frac{dS}{dt}\right)_{E_1} \text{ and } S_{E_2} > S_{E_1}$$

The effect of the magnitude of $\frac{dS}{dt}$ is manifested in the mathematics involved in the calculation of the nucleation rate. Results may be dependent upon the supersaturation in that lag time, calcium-sulfate ratio and non-steady state rate depend upon the supersaturation and influence nucleation rate calculations. The rate, calculated in equation (38) is assumed to be a function of the supersaturation only. Carte[55], and later Kuhns and Mason[56], have derived an expression, shown as equation (44), which is claimed to be applicable to the calculation of rates of nucleation from data for the freezing of water droplets, cooled at a steady state rate

$$J(S) = \frac{1}{v} \cdot \frac{1}{N-n_{t,v}} \cdot \frac{dn_{t,v}}{\partial S} \cdot \frac{\partial S}{\partial t} \qquad (44)$$

It will be shown below that equation (44) is only applicable when the rate of change of supersaturation is small.

Figure III-A10. Plot of ℓnJ vs $(\ell nS)^{-2}$ for $CaSO_4 \cdot 2H_2O$ experiment E_1

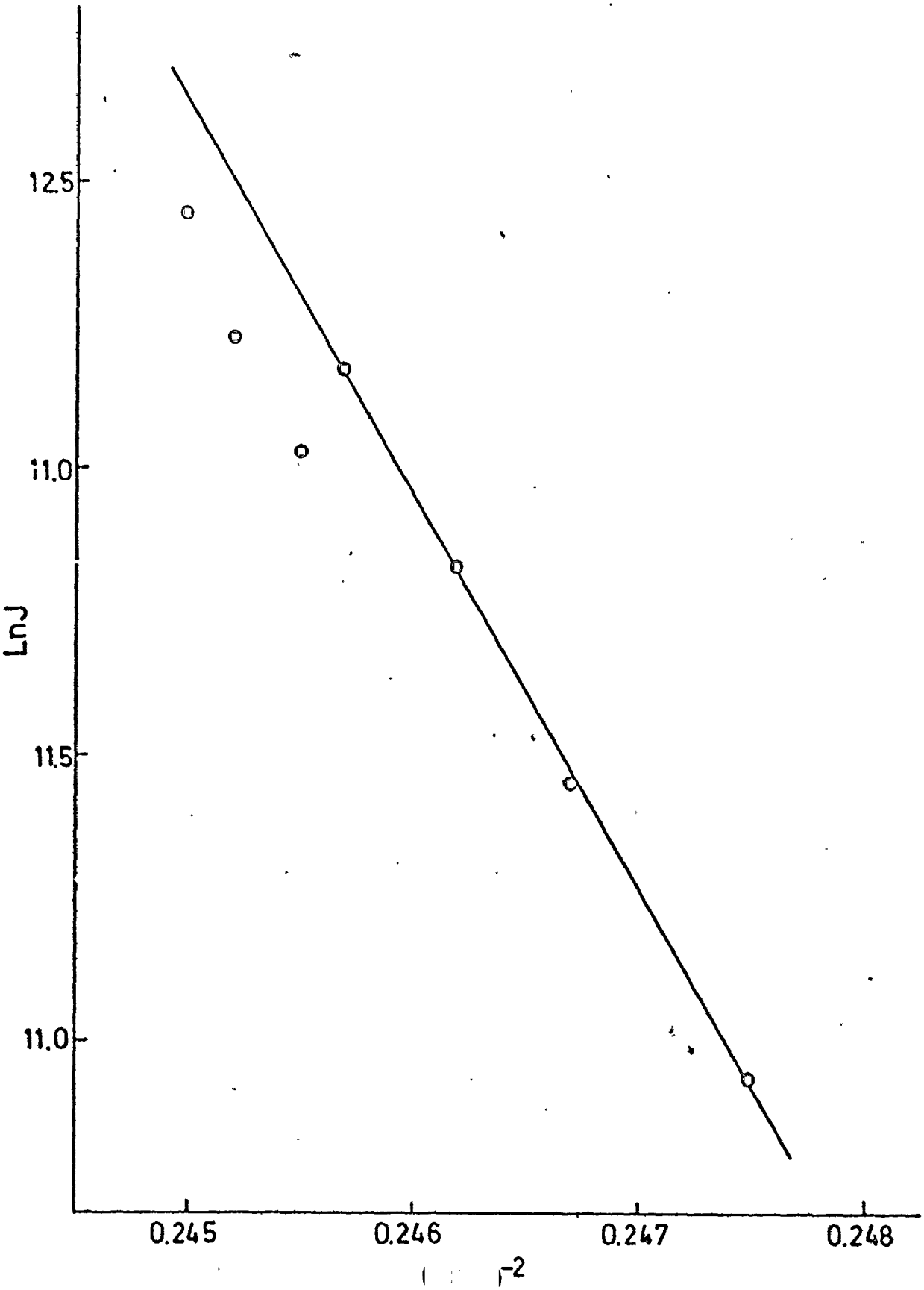
12.5
11.0
11.5
11.0
Ln J
0.245
0.246
0.247
0.248
I -2

Figure III-A11. Plot of ℓnJ vs $(\ell nS)^{-2}$ for $CaSO_4 \cdot 2H_2O$, experiment E_2

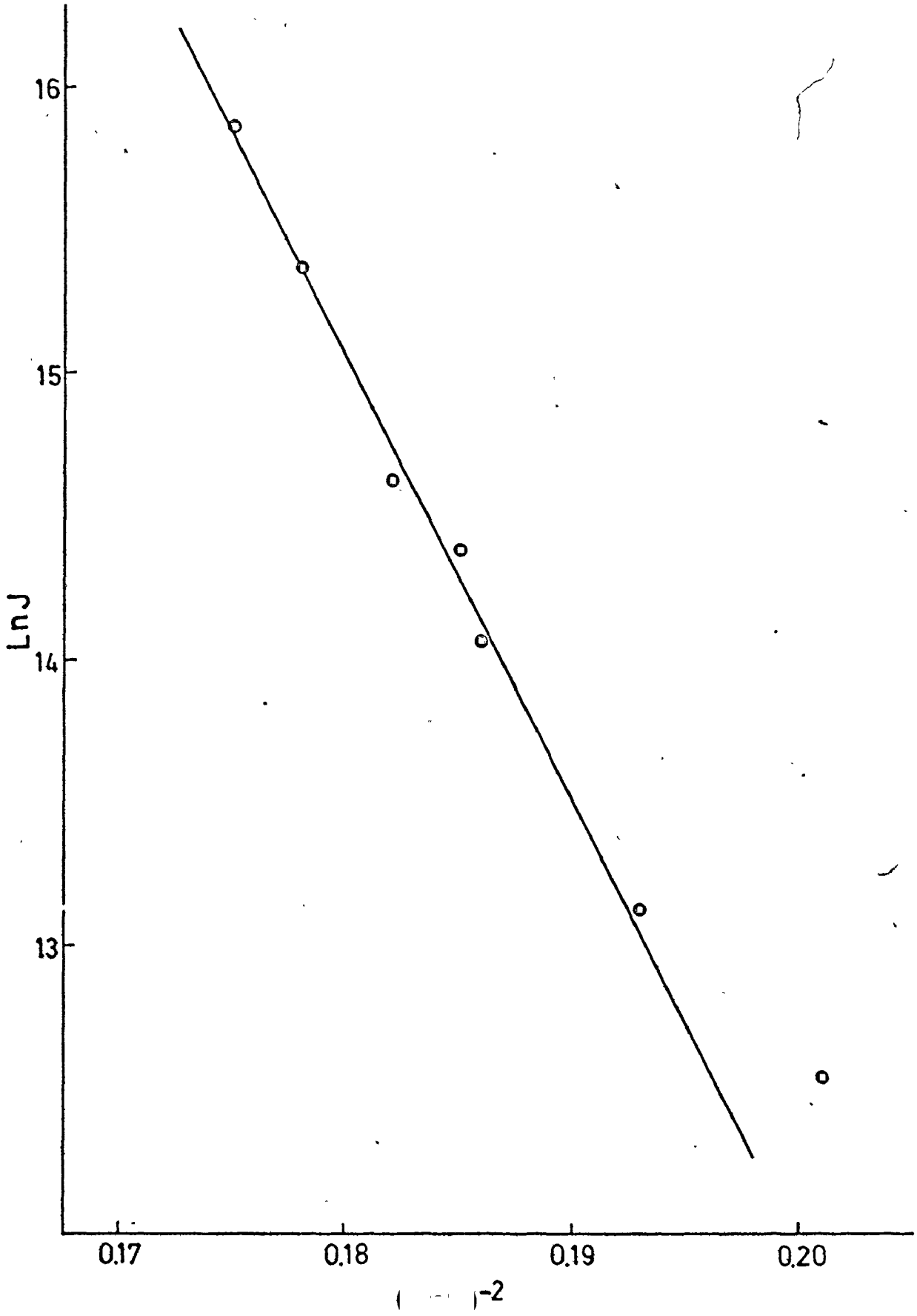
16
15
14
13
LnJ
0.17
0.18
0.19
0.20
-2

Figure III-A12 depicts, in three dimensions, the interrelationships between $n_{t,v}$, t and S in an experiment that has a variable driving force. The derivative of $n_{t,v}$ in the n-t plane is $\partial n/\partial t$, in the n-S plane $\partial n/\partial S$, and in the s-t plane $\partial n/\partial z$. These derivatives are a measure of the rate. $\partial n/\partial t$ represents the rate of nucleation as a function of time, $\partial n/\partial S$ as a function of the supersaturation, and $\partial n/\partial z$ as a function of both variables. The physical meaning of $\partial n/\partial z$ is not clear. A mathematical expression, however, for the rate of nucleation can be derived as a function of the z co-ordinate. The components of dz on the t and S axes are dt and ds respectively. If we let θ represent the angle that dz makes with the t axis, the following triginometric functions can be derived;

$$\frac{\partial t}{\partial z} = \cos\theta \qquad \frac{\partial n}{\partial z} = \frac{\partial n}{\partial t} \times \cos\theta \qquad (45)$$

$$\frac{\partial S}{\partial z} = \sin\theta \qquad \frac{\partial n}{\partial z} = \frac{\partial n}{\partial S} \times \sin\theta \qquad (46)$$

and

$$\frac{dS}{dt} = \tan\theta.$$

Substituting the following into equations (45) and (46)

$$\frac{1}{\cos^2\theta} = \tan^2\theta + 1$$

$$\sin^2\theta = \frac{\tan^2\theta}{1 + \tan^2\theta}$$

we get

$$\frac{\partial n}{\partial z} = \frac{\partial n}{\partial t}\sqrt{\frac{1}{\left(\frac{dS}{dt}\right)^2 + 1}}, \qquad (47)$$

and

Figure III-A12. The inter-relationships between $n_{t,v}$, t and S in an experiment that has a variable driving force.

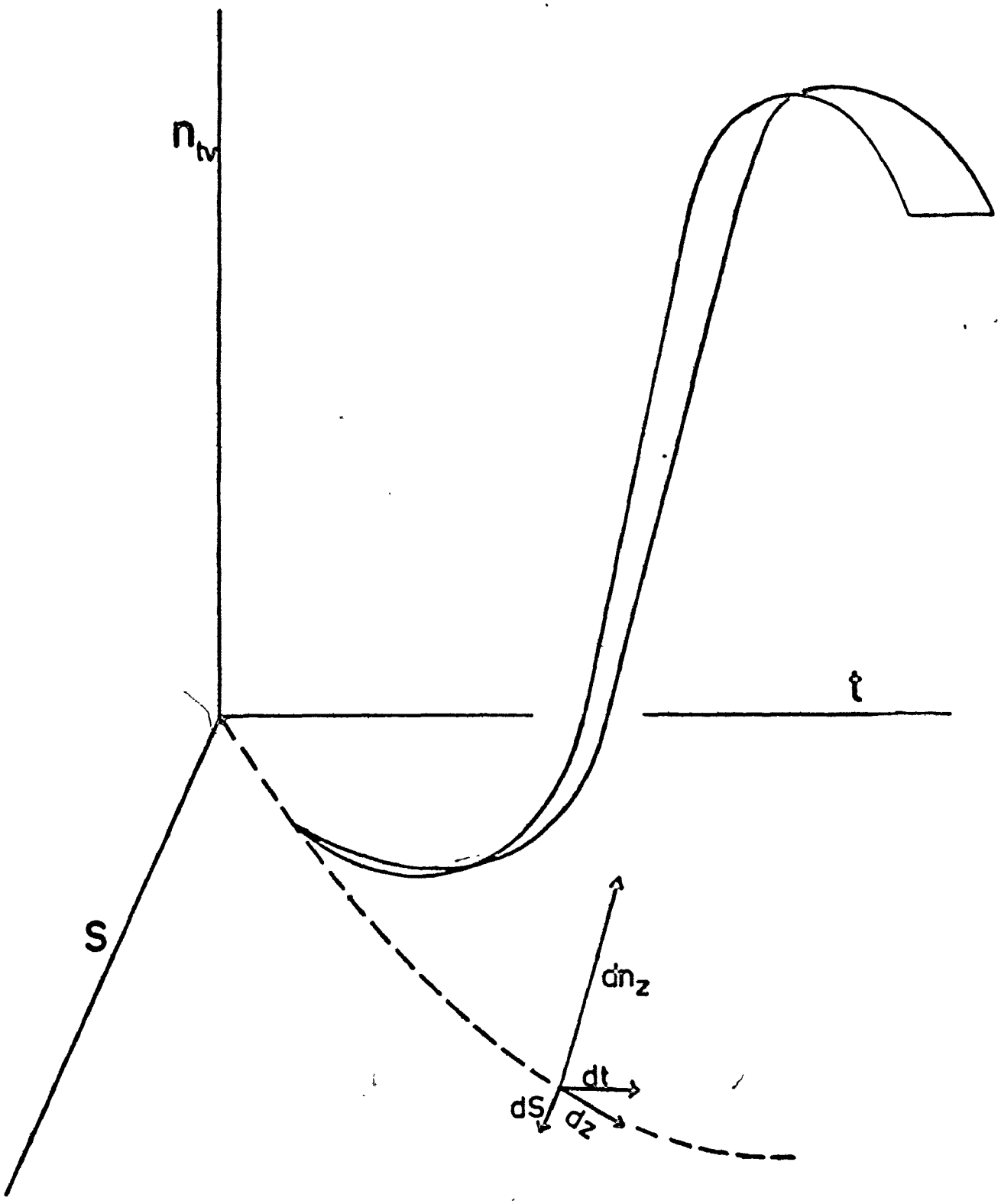
n_{tv}
t
S
dn_z
dt
dS
d_z

and

$$\frac{\partial n}{\partial z} = \frac{\partial n}{\partial S} \sqrt{\frac{(\frac{dS}{dt})^2}{1 + (\frac{dS}{dt})}} \qquad (48)$$

To an observer in the S-t plane as a point of reference for measuring the change in $n_{t,v}$, the apparent rate of nucleation would be adequately described by equation (49).

$$J(z) = \frac{1}{v} \cdot \frac{1}{N-n_{t,v}} \cdot \frac{\partial n_{t,v}}{\partial z} \qquad (49)$$

Substituting (47) and (48) into equation (49) gives

$$J(S,t) = \frac{1}{v} \cdot \frac{1}{N-n_{t,v}} \cdot \frac{\partial n_{t,v}}{\partial t} \left[(\frac{dS}{dt})^2 + 1\right]^{-\frac{1}{2}} \qquad (50)$$

and

$$J(s,t) = \frac{1}{v} \frac{1}{N-n_{t,v}} \frac{\partial n_{t,v}}{\partial S} \left[(\frac{dS}{dt})^{2-} + 1\right]^{-\frac{1}{2}} . \qquad (51)$$

At very low $\frac{dS}{dt}$

$$J(S) = \frac{1}{v} \cdot \frac{1}{N-n_{t,v}} \cdot \frac{\partial n_{t,v}}{\partial t} . \qquad (52)$$

or

$$J(S) = \frac{1}{v} \cdot \frac{1}{N-n_{t,v}} \cdot \frac{\partial n_{t,v}}{\partial S} \cdot \frac{dS}{dt} . \qquad (53)$$

At very high $\frac{dS}{dt}$

$$J(S) = \frac{1}{v} \cdot \frac{1}{N-n_{t,v}} \cdot \frac{\partial n_{t,v}}{\partial t} \cdot \frac{dS}{dt} \qquad (54)$$

or

$$J(S) = \frac{1}{v} \cdot \frac{1}{N-n_{t,v}} \cdot \frac{\partial n_{t,v}}{\partial S} \qquad (55)$$

Equation (44), therefore, is only a special case of a more general expression for the rate of nucleation. The $(\frac{dS}{dt})^2$

values at the initial stages of crystallization for calcium sulfate were 1.74×10^{-9}, for experiment E_1, and 1.22×10^{-5} for experiment E_2. This confirms that equation (38) was used legitimately. Equation (51), while being mathematically equivalent to equation (50) is, however, rather poor, because it requires the multiplication of a very large number, $(\partial n/\partial S)$, by a very small number, $\frac{dS}{dt}$.

It may be concluded that the $\frac{dS}{dt}$ effects seem to be negligible in the case of $CaSO_4\cdot2H_2O$ and cannot account for the large discrepancies in the thermodynamic parameters calculated from the data of E_1 and E_2.

The effects of supersaturation on the nucleation events are manifested through the lag time the cation-anion ratio and non steady-state rates of nucleation.

(1) Lag Time Effects: Large lag times occurring at supersaturations used in variable driving force experiments deal a decisive blow to the results. Since the lag time varies inversely as the supersaturation, the rate calculations will lag S measurements considerably more at lower supersaturations. The resulting σ values taken from plots of ℓnJ vs $(\ell nS)^{-2}$, will always be too high. The preexponential factor, A, will also be too high and $(\ell nS^*)^{-2}$ too low resulting in a high measurement of the critical supersaturation. The lag times will also tend to force ℓnJ vs $(\ell nS)^{-2}$ to deviate from linearity. When designing a variable driving force experiment one must

know the magnitude of L and its rate of change with S, so that experiments which yield meaningful results can be designed.

(2) Ca^{2+}/SO_4^{2-} effects: Calcium ion was in excess from the beginning of experiments E_1 and E_2 and Ca^{2+}/SO_4^{2-} approached 1.0 as the experiment proceeded. In section III-C, it will be reported that the rate at one I.P. varies with the calcium-sulfate ratio. Measurement of the rate of nucleation as the cation-anion ratio was increasing would have the effect of tilting the ℓnJ vs $(\ell nS)^{-2}$ plot in the direction of increasing slope and making it curve downwards. The curve will also be shifted upwards if the critical supersaturation is reached when that calcium-sulfate ratio giving a maximum rate is approached.

(3) Non-steady-state rate effect: Non-steady state rates of nucleation of calcium sulfate generally occurred at very low supersaturations and high values of the calcium-sulfate ratio. These effectively lengthen the lag time - which in turn causes measured values of σ, A and S* to be high.

The design of variable driving force experiments depends upon a comparison between the effects of supersaturation and the rate of change of supersaturation. The S-effects are major at lower supersaturations whereas problems arising from $\frac{dS}{dt}$ increase as it increases. In some cases, then, it is necessary to trade off the latter for the former. For calcium sulfate studies with variable driving force, it is necessary to use high supersaturations which give $L \simeq 0$, or $\frac{\partial L}{\partial S} \sim 0$ and no change of non-steady state rate effects. Also, the calcium-sulfate ratio must be approximately unity when the critical nucleation phenomena are occurring.

III-B NUCLEATION EXPERIMENTS AT CONSTANT S AND T

A chemical reaction producing sulfate ion, exhibiting a concentration-time curve resembling a step function, was developed so that the observed nucleation events occurred at a nearly constant supersaturation. The need for temperature control was satisfied with the use of a thermostatted cell holder. The rate of nucleation and the lag time, then, were studied as a function of temperature and supersaturation.

III-B1 Experimental Design

The necessity of controlled temperature experiments can be appreciated when one estimates the variance in the rate of nucleation with supersaturation and temperature. The classical nucleation equation (20) can be expanded in a Taylor series (Appendix A) about some supersaturation and temperature, and then components of variance separated.

$$\mathrm{Var}(\ell nJ) = \left(\frac{\partial \ell nJ}{\partial T}\right)^2 \mathrm{Var}(T) + \left(\frac{\partial \ell nJ}{\partial S}\right)^2 \mathrm{Var}(S) \qquad (56)$$

Estimating the error in S and T at 22°C and a supersaturation of 6.0, the variance in ℓnJ is

$$\mathrm{Var}(\ell nJ) = K_1 \mathrm{Var}(T) + K_2 \mathrm{Var}(S)$$
$$= 1.45\times10^{3} + 1.31\times10^{1}.$$

The variance in T is two orders of magnitude larger than the variance in S. Fluctuations in T have a large effect upon the measurement of the rate and related thermodynamic parameters. For this reason the $CaSO_4 \cdot 2H_2O$ experiments with a

constant driving force were conducted at controlled, constant temperatures.

Temperature Probe Experiments: The calibrated probe described in section II-4 was inserted into the oil near the bottom of the Nessler cup which was positioned in the thermostatted cell holder. The constant temperature bath was set at a certain temperature and measurements of the oil temperature were taken. The results are found in Table III-B1. After each measurement, the cup and holder were cooled with cold tap water (< 20°C). When the oil temperature reached 22°C, the constant temperature bath pump and a stop watch were turned on simultaneously. Temperature-time measurements made with constant temperature bath temperatures of 30, 40, and 50°C are plotted in Figure III-B1. The reliability of the lag time measurements depends upon the length of time required for the oil in the Nessler cup to reach a maximum temperature after the constant temperature bath pump is switched on. Lag times at the highest experimental temperatures and supersaturations are very short, whereas, the times required for the oil to come to thermal equilibrium are longest. The end of an apparent lag time, therefore, may pass before the contents of the Nessler cup reach their final experimental temperature.

Solubility Measurements: The solubility product was measured using a technique described in section III-A3(b) and at constant temperature bath temperatures of 20, 30, 40, and 50°C. The results are shown in Table III-B1 and Figure III-B2. Other than measured Ksp values were determined by interpolation.

Figure III-B1. Plots of Nessler cup oil temperatures measured with time after the constant temperature bath pump was switched on.

Legend	Bath Temperature
●	30°C
■	40°C
▲	50°C

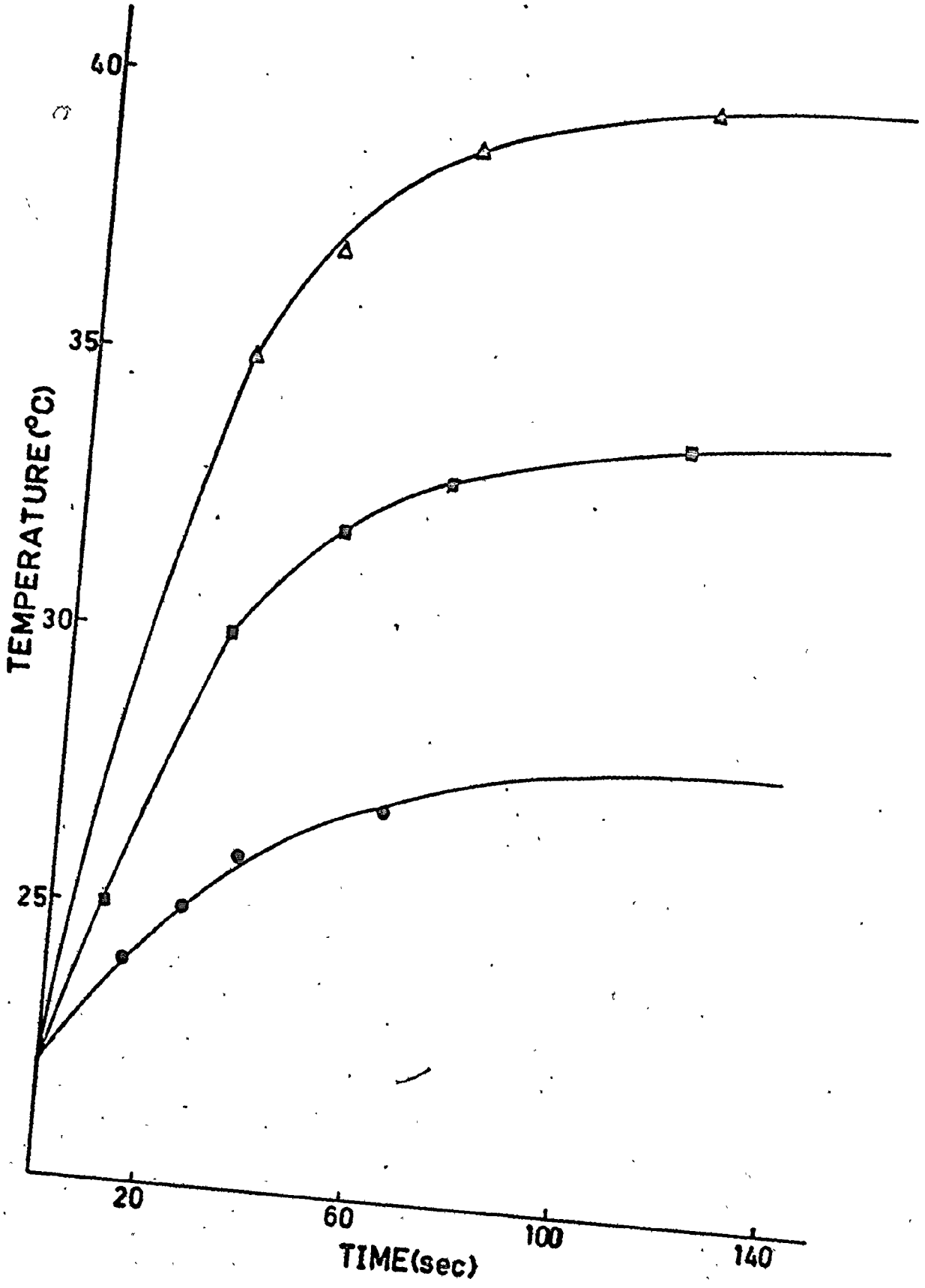
40
35
30
25
TEMPERATURE(°C)
20
60
100
140
TIME(sec)

TABLE III-B1

Temperature and solubility measurements

CTB temperature (°C)	Nessler cup T
20	21.8
30	28.1
40	31.3
50	40.4

CTB Temperature (°C)	Thermostatted beaker temperature (°C)	$[Ca^{2+}]$	Ksp
20	20.0	0.03888	1.512×10^{-3}
30	29.6	0.03951	1.561×10^{-3}
40	39.1	0.04044	1.635×10^{-3}
50	49.0	0.04133	1.708×10^{-3}

T°C	Ksp (by interpolation in Figure III-B-2)
21.8	1.521×10^{-3}
28.1	1.553×10^{-3}
34.3	1.592×10^{-3}
40.4	1.644×10^{-3}

CTB = constant temperature bath.

Figure III-B2. Plot of the calcium ion concentration in the matrix solution at certain temperatures.

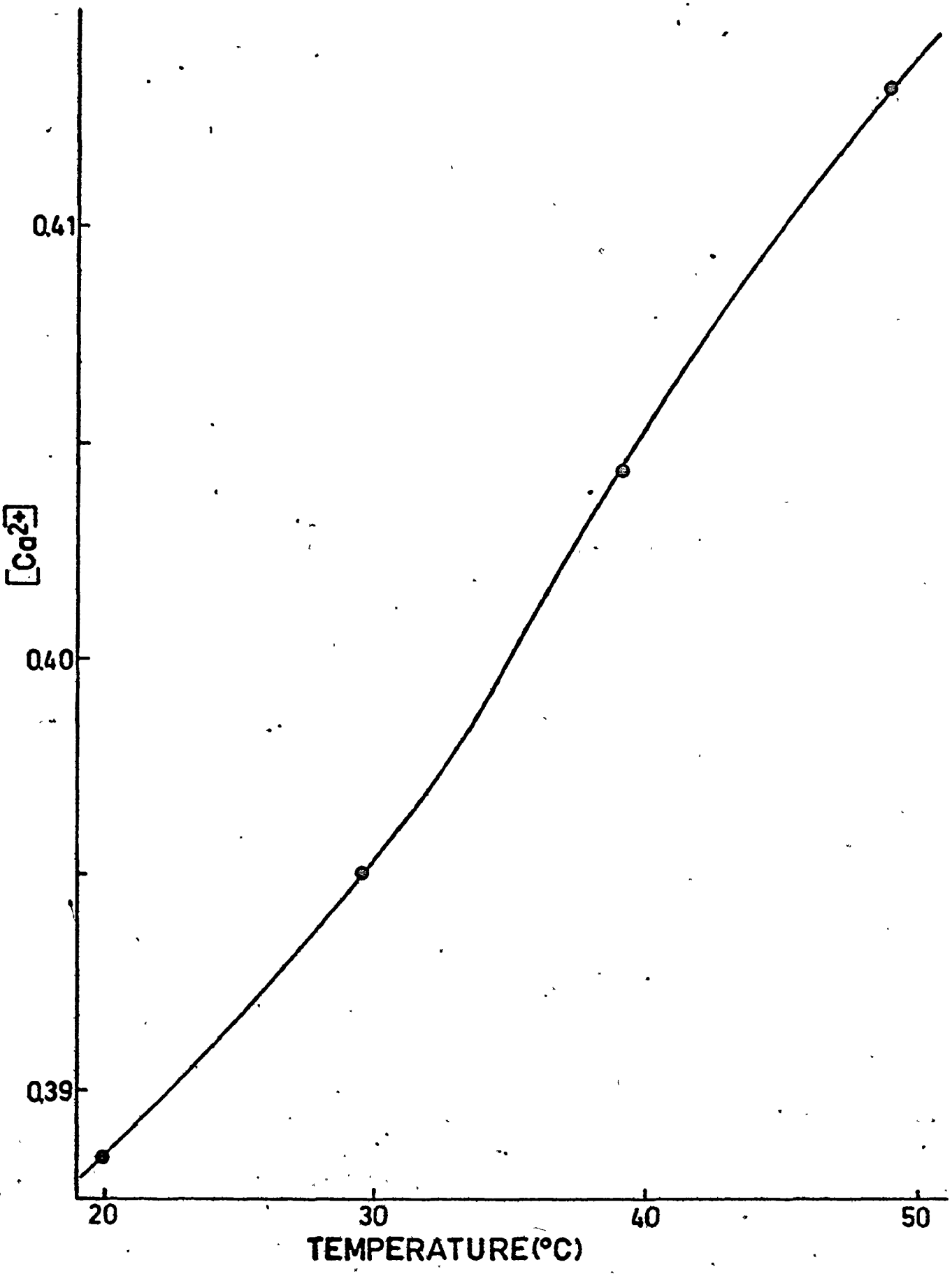
0.41
0.40
0.39
[Ca2+]
20
30
40
50
TEMPERATURE(°C)

The reaction: Excess iodide was used to reduce peroxydisulfate in the presence of a constant calcium concentration. To approximate a step function, an iodide concentration was selected which would give a high percent reaction completion in the time necessary to make droplets and to make an initial observation of them under the microscope (12 min). The procedure, found in section II-A2(b) was followed to determine the best initial iodide concentration. The transmittance vs. time data are plotted in Figure III-B3. The iodide concentration selected was 0.35 M. The supersaturation range to be used in the following experiments was estimated from the interpretation of the results of experiments described in section III-A.

Three ion products of calcium sulfate were selected; 0.03063, 0.04151, and 0.05423. These ion products gave a supersaturation high enough at all temperatures such that $n_{t,v}/N \geq 0.5$ in a reasonable length of time (12 hours), and low enough to allow a reasonable number of photomicrographs to be taken. Droplet experiments were carried out at temperatures of 21.8, 28.1, 34.3, and 40.4°C.

III-B2 Nucleation Experiments

Droplets, ranging in size from 8 to 15 μ in diameter, were prepared at approximately 18°C for all experiments conducted at 28.1, 34.3, and 40.4°C. The lag times of the solutions at 18°C were extremely long compared to those at the experimental temperature. Crystals did not appear in the droplets until after the solutions were heated in the thermostatted cell holder. This technique made it easy to control t_o, the zero

Figure III-B3. Plot of percent reaction completion vs time at various initial iodide concentrations.

Legend	$[I^-]_i$
●	0.50
■	0.25
▲	0.40

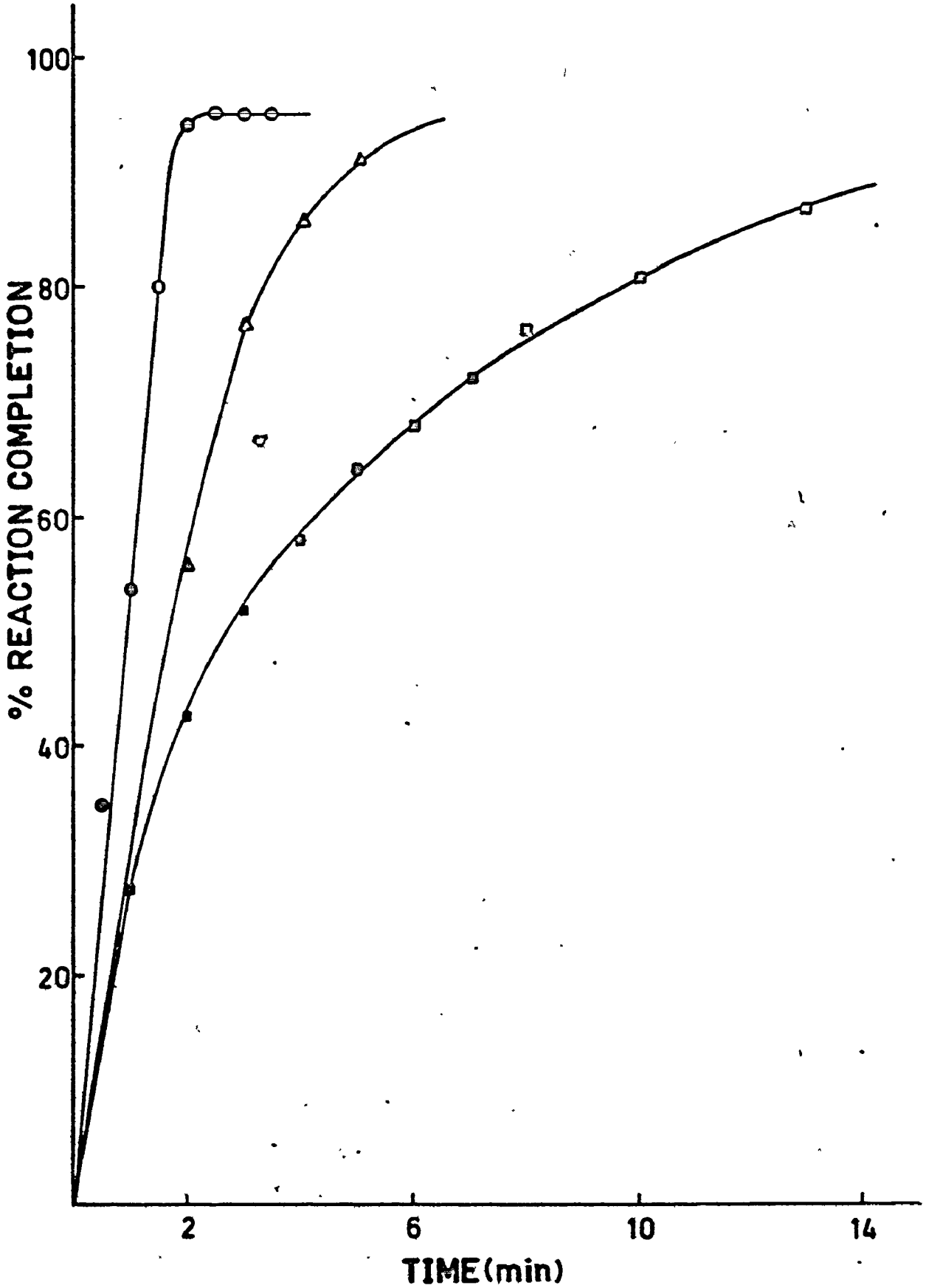
100
80
60
40
20
% REACTION COMPLETION
2
6
10
14
TIME(min)

experimental time, marked by that point in time that the constant temperature bath pump was switched on. For nucleation experiments conducted at 21.8°C, the droplets were prepared at 20°C and t_o was taken as the time of mixing of solutions A and B.

Photographs of any phase changes were taken as described in section II-B2. The M41 microscope was used with the dark field illumination technique because it was more sensitive to crystals in smaller droplets when compared with the polarized light technique. The slides were processed as described in section II-B3 giving $n_{t,v}$ data. The rate of nucleation was calculated using equation (39) and a non-linear least squares program, described in Appendix B, on a CDC 6400 computer.

Equation (39) may be made independent of the time by replacing the independent variable t by (t-L). Equation (57) is legitimate only when $t \geq L$.

$$n_{t,v} = N\{1-\exp[-Jv(t-L)]\} . \qquad (57)$$

Equation (57) was found to generate large positive and negative correlations among N, J, and L, and consequently, was not used.

Problems arose in the estimation of the two parameters in equation (39) due to the limitations of the droplet technique. Since the droplets were arranged in a number of volume ranges, the population within each range was small (15-40). Consequently, the $n_{t,v}$ vs time curves resembled step functions. Calculation of the nucleation rate based on these curves leads to a large error. To increase the population in a volume range

and thus to reduce the step-sizes, a number of fields of view were selected in each experiment.

There were two problems stemming from the form of equation (39). The first of these was the estimation of the rate of nucleation at very low supersaturations where the time required to complete an experiment was of the order of days. Droplets, however, have a limited life-time since they shrink with time, - the smaller droplets shrank more rapidly than the larger ones. At low supersaturations, therefore, the highest $n_{t,v}/N$ value will be much less than 1.0 leading to a high degree of negative correlation between the calculated parameters N and J. Only those supersaturations giving appreciable $n_{t,v}/N$ in a maximum time of 12 hours were selected for study.

The second problem arises from the time dependent nature of equation (39). The lag time or the induction time must be removed so that $n_{t,v} = 0$ when $t' = 0$, where $t' = t-L$ or $t-\tau$. This process is further complicated, however, by heterogeneous phase change data which usually is collected during the homogeneous lag time. The lag time, induction time, and heterogeneous nucleation data can usually be separated with any one of three methods. Visual observation of spontaneous new phase formation was accurate to 10%. Assuming that the initial portion of an $n_{t,v}$ vs t curve is linear and if only adjacent volume ranges are taken (ie. $n_{v_1 t} + n_{v_2,t}$) vs time can be graphically determined with a plot of $(n_{v_1,t} + n_{v_2,t})$ vs time. This technique, graphically shown in Figure III-B4(a), was used when the lag time was short. When the lag times are very long, heterogeneous nucleation is virtually complete before homogeneous nucleation begins. The

Figure III-B4. Various techniques used to measure pre-nucleation parameters; (a) the summation of $n_{t,v}$ when L is short, (b) distinguishing between heterogeneous and homogeneous nucleation when L is long, and (c) graphical measurement of τ.

a

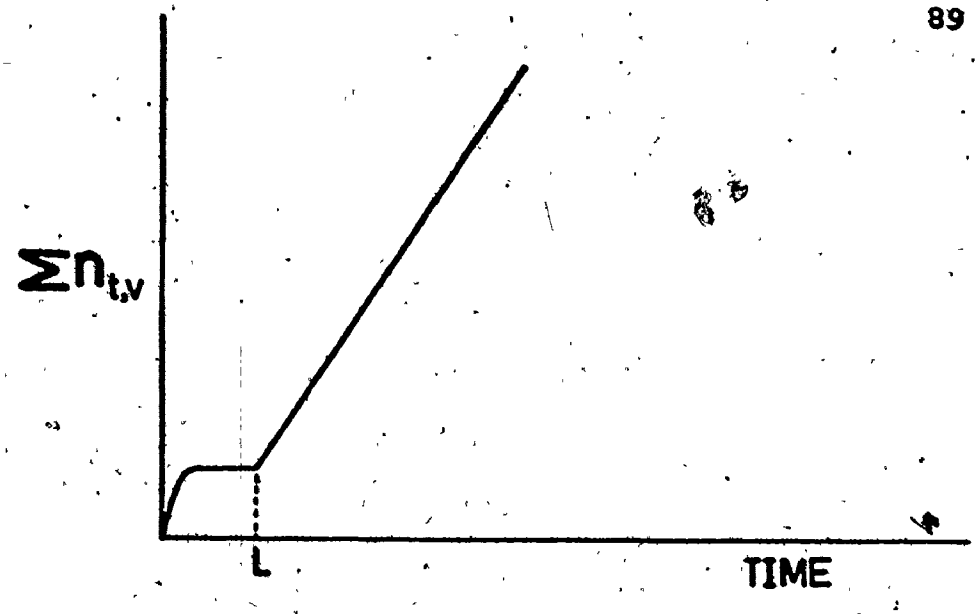

b

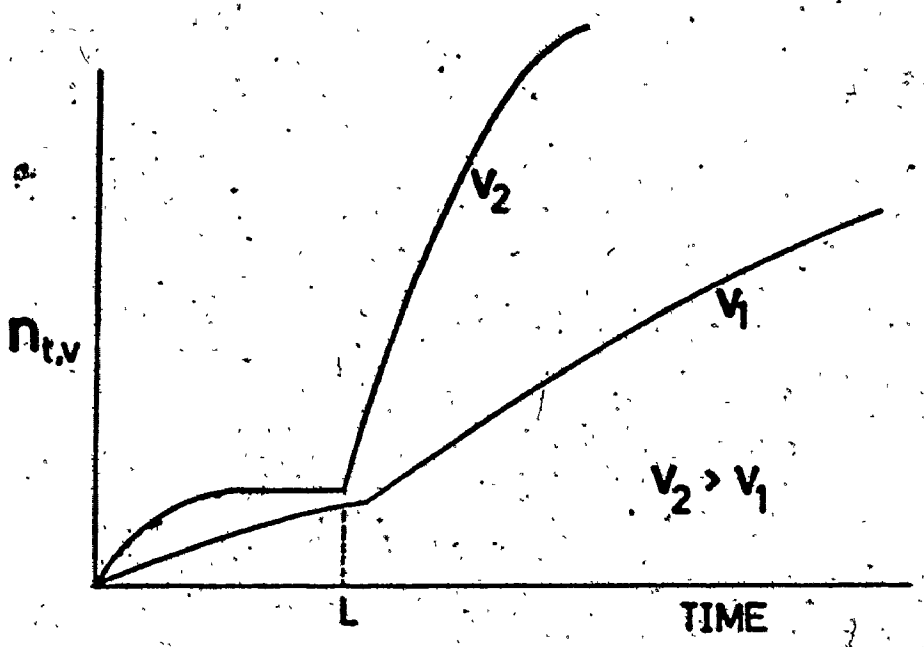

c

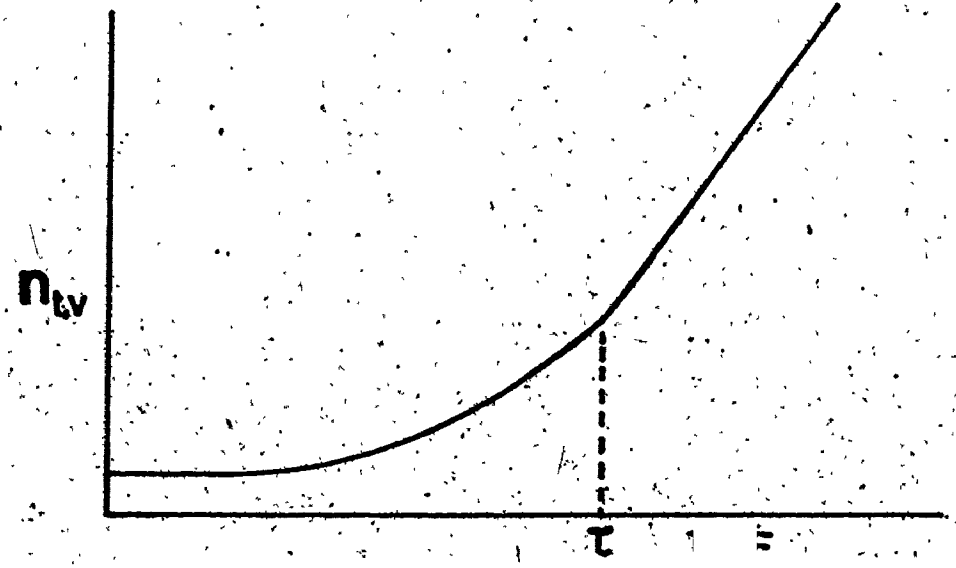

break in the two processes is represented for two droplet sizes in Figure III-B4(b). When there is an induction time, that is, a period of non steady-state nucleation rate, the induction time τ is measured graphically as shown in Figure III-B4(c), $n_{\tau,v}$ removed from $n_{\tau,v}$, τ removed from the time values (i.e. $t' = t-\tau$), and equation (39) used to calculate N' and J. In this case N' would be $N-n_{\tau,v}$.

Using the above techniques, the parameters J, and L were estimated and are reported in Table III-B2.

Thermodynamic Parameter Estimation: Plots of ℓnJ vs $(\ell nS)^{-2}$ at constant temperature are shown in Figure III-B5. From the values of the individual slopes and intercepts, σ, S^*, and ℓnA were calculated. ΔG^*, n^*, and r^* were calculated using equations (10), (21) and (22). These values are reported in Table III-B3.

The values of the surface tension term, σ, are significantly different at different temperatures and were used, justifiably, in the calculation of ΔG^*, n^*, and r^*. The values of the critical supersaturation at various temperatures, are not significantly different and ΔG^*, n^*, and r^* could not be calculated with any significance. A plot of ℓnJ vs ℓnS gave significantly different S* values, designated by S_b^* in Table III-B3. ΔG^*, n^*, and r^* were calculated using S_b^*.

The ℓnA values are statistically the same over the temperature range used. The pre-exponential factor, then, was found to be independent of the temperature.

The ΔG^* values are significant although they contain a

TABLE III-B2

Rates and lag times measured for experiments E_4 to E_{15}

(a) Nucleation Rates. (sec^{-1} cm^{-3})

Temperature (°C) \ Ion product	0.03063	0.04151	0.05423
21.8	5.80×10^{3}	1.90×10^{5}	5.27×10^{6}
28.1	4.67×10^{4}	4.27×10^{6}	1.36×10^{7}
34.3	2.22×10^{6}	3.25×10^{7}	1.23×10^{8}
40.4	3.67×10^{6}	5.77×10^{7}	3.14×10^{8}

(b) Lag times (sec)

Temperature (°C) \ Ion product	0.03063	0.04151	0.05423
21.8	15,600.	6,400.	1,854.
28.1	5,400.	703.	230.
34.3	420.	100.	27.
40.4	42.	21.	13.

Figure III-B5. Plots of ℓnJ vs $(\ell nS)^{-2}$ at various temperatures

Legend	Temperature (°C)
●	21.8
■	28.1
▲	34.3
O	40.4

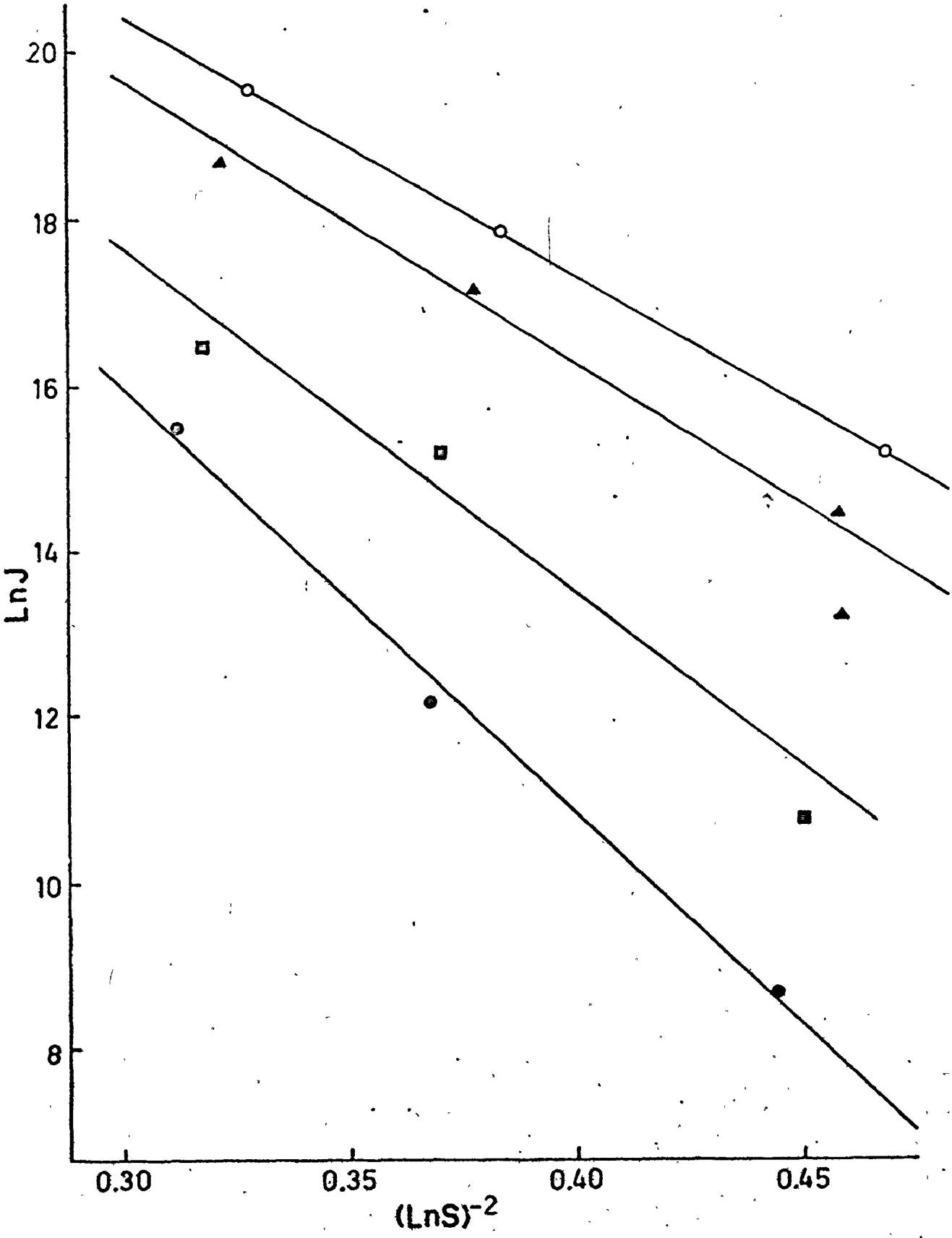
20
18
16
14
12
10
8
LnJ
0.30
0.35
0.40
0.45
(LnS)$^{-2}$

TABLE III-B3

Measured and derived thermodynamic parameters of $CaSO_4 \cdot 2H_2O$ at various temperatures

Parameter \ Temperature (°C)	21.8	28.1	34.3	40.4
Slope	-52.13	-41.61	-36.72	-31.67
σ (ergs cm^{-2})	24.01±.36	22.75±.60	22.26±.89	21.61±.39
ℓnA	30.0 ±0.5	30.7 ±1.3	29.9 ±1.0	31.6 ±.7
S*	3.29 ±.02	3.23 ±.10	3.12 ±.10	3.20 ±.09
n*	72±9	97±24	163±89	569±424
r* (Å)	12.9 ±.5	14.2±1.1	16.9±2.7	25.6 ±6.5
ΔG^* (10^{12} $\frac{ergs}{molecule}$)	1.66 ±.16	1.78±.34	2.5±1.0	5.9 ±3.0
S_b^*	3.10 ±.15	2.68±.14	2.20±.15	1.63 ±.16

S_b^* = critical supersaturation graphically measured from extrapolated ℓnJ vs ℓnS plots.

lot of uncertainty. The n* values, which increase with temperature, are not significantly different from each other at the lower three temperatures. All r* values have statistical significance.

It is very important that one step back at this point and contemplate the route we have taken to calculate the derived data. The calculation of σ, n*, r*, and ΔG^* is dependent upon two naive assumptions, that embryos are tiny pieces of crystal and that they have a spherical shape. Are we being misled by the classical model or can we actually use these derived values as a basis for mechanism discrimination?

The classical model makes definite shape restrictions. As a consequence, the only pathway for reduction of the surface tension at one temperature is addition of monomers to the embryo, This decreases the ratio of surface/bulk molecules.

An embryo, in the classical model, has a density and crystal structure indentical to a bulk crystal. These two properties are independent of temperature and supersaturation.

The non-classical model is more flexible. If embryos are solution density fluctuations containing loosely bound monomers, a change in shape should be a process involving very little energy. The free energy of an embryo of size n could have very many shape energy levels separated by small energy differences. Populations in any one energy level may be dependent upon temperature and supersaturation.

The non-classical model is not bound by density and crystal structure restrictions. The so-called "non-classical

surface tension" may decrease with temperature caused only by a decrease in the radius of the embryo. The size of the embryo and its density could decrease by means of a loss of water of hydration and/or internal rearrangement. If these processes are a function of temperature, the term $16\pi\bar{v}^2/3k^3$ in equation (20) is not constant and σ can not be separated from the slope of ℓnJ vs $(\ell nS)^{-2}$ plots. Without σ, the calculations of n^*, r^*, and ΔG^* are impossible. If the shape is in doubt, equation (20) should be simplified to

$$J = A \exp - \frac{\beta(T)}{T^3(\ell nS)^2} , \qquad (58)$$

where

$$\beta(T) = \frac{16\pi\bar{v}^2\sigma^3}{3k^2} .$$

If the number in the critical embryo is not a function of the temperature and supersaturation, an energy level diagram can be drawn, Figure III-B6, describing changes in embryo density and shape. At lower temperatures, embryos occupy lower density states, D_i, and shape states, S_{ij}. Embryos in these levels have densities and structures very unlike the crystal. The energy separation between shapes is very small. The energy barrier to nucleation, ΔG_n^*, is shown by the curved line joining embryo energy states to the crystal energy state.

As the temperature increases, embryos of size n begin to look more like crystals and occupy higher density states. The energy splitting between shape states becomes larger as it is more difficult for the more dense configurations to change shape

Figure III-B6. An energy level diagram of an embryo of size n relative to a crystal of size n.

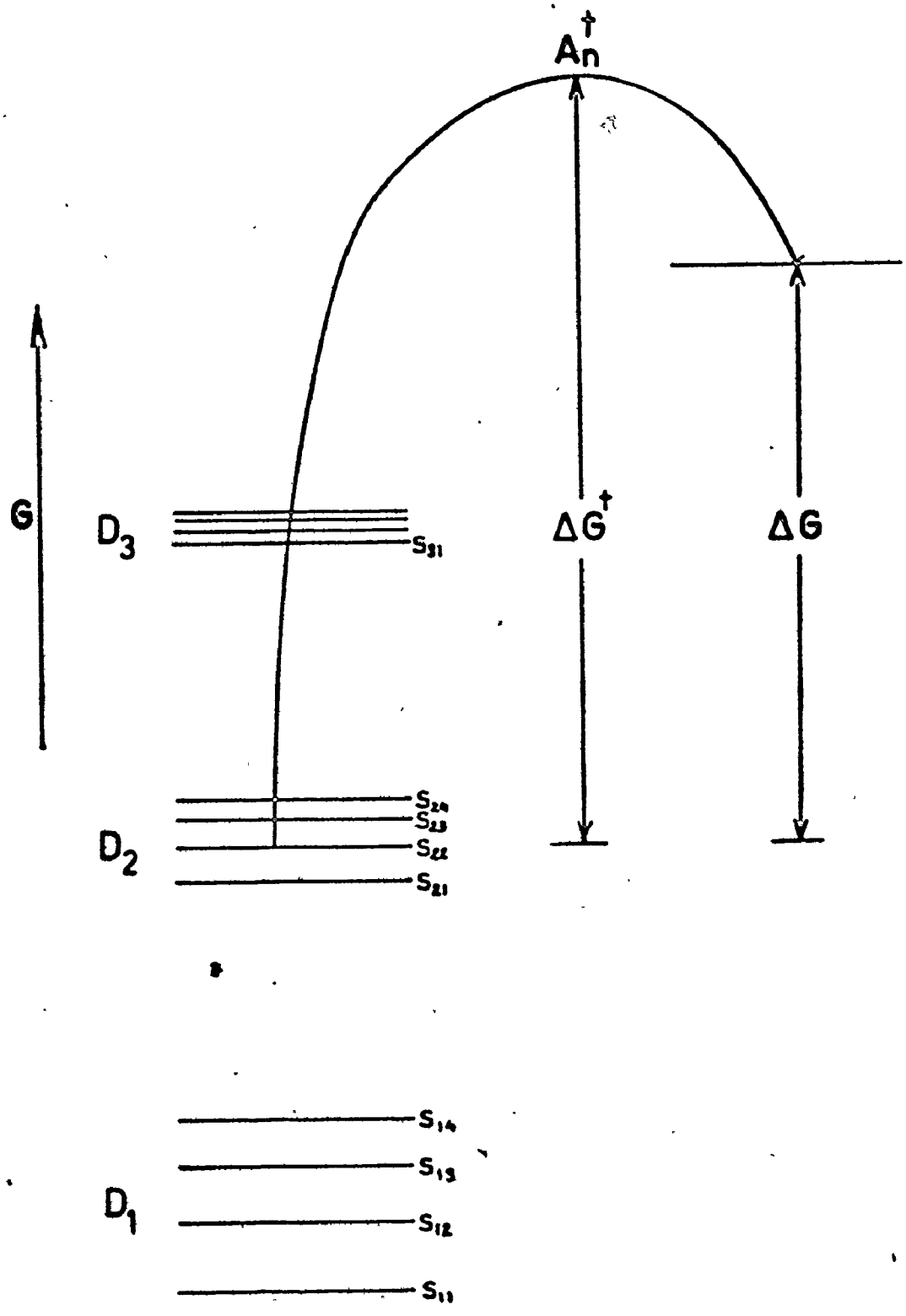
embryo A_n
cystal A_n
$A_n^{\dagger}$
G
D_3
S_{31}
$\Delta G^{\dagger}$
ΔG
S_{24}
S_{23}
D_2
S_{22}
S_{21}
S_{14}
S_{13}
D_1
S_{12}
S_{11}

and structure. The free energy of phase change, ΔG_n^*, decreases.

It may be concluded, then, that until more is known about embryos, it is very wise not to base any conclusions upon derived parameters such as n*, r* and ΔG^*.

Table III-B3 reports the values of S* found from graphical extrapolation of ℓnJ vs ℓnS curves shown in Figure III-B7. In Figure III-B8, the critical ion product is plotted against the temperature. The Ksp values are also plotted in the same figure resulting in an Ostwald solution phase diagram for $CaSO_4 \cdot 2H_2O$. As the temperature is increased, the critical ion product decreases quite rapidly.

Taking the logarithm of the classical nucleation equation gives

$$\ell nJ = \ell nA - \Delta G/kT = \ell nA + \frac{\Delta S}{k} - \frac{\Delta H}{T} \qquad (59)$$

where ΔH is the change in enthalpy of formation of a critical sized embryo and ΔS is the change in entropy in forming a critical sized embryo. ℓnJ vs 1/T is plotted in Figure III-B9 and ΔH and $\frac{\Delta S}{k} + \ell nA$ calculated from the slope and intercepts respectively. The entropy term was calculated by subtracting an average ℓnA, calculated from ℓnJ vs $(\ell nS)^{-2}$ plots from the intercept of ℓnJ vs 1/T and dividing by the Boltzmann constant. The values of ΔG^*, ΔS^* and ΔH^* are reported in Table III-B4.

The calculated enthalpy at various ion products were statistically the same giving an endothermic heat of formation of 3.2×10^{-12} ergs(molecule)$^{-1}$. The calculated entropy change was 8.87×10^{-15} erg deg^{-1} molecule^{-1}.

Figure III-B7. Plots of ℓnJ vs ℓnS at various temperatures.

Legend	Temperature (°C)
o	21.8
□	28.1
Δ	34.3
○	40.4

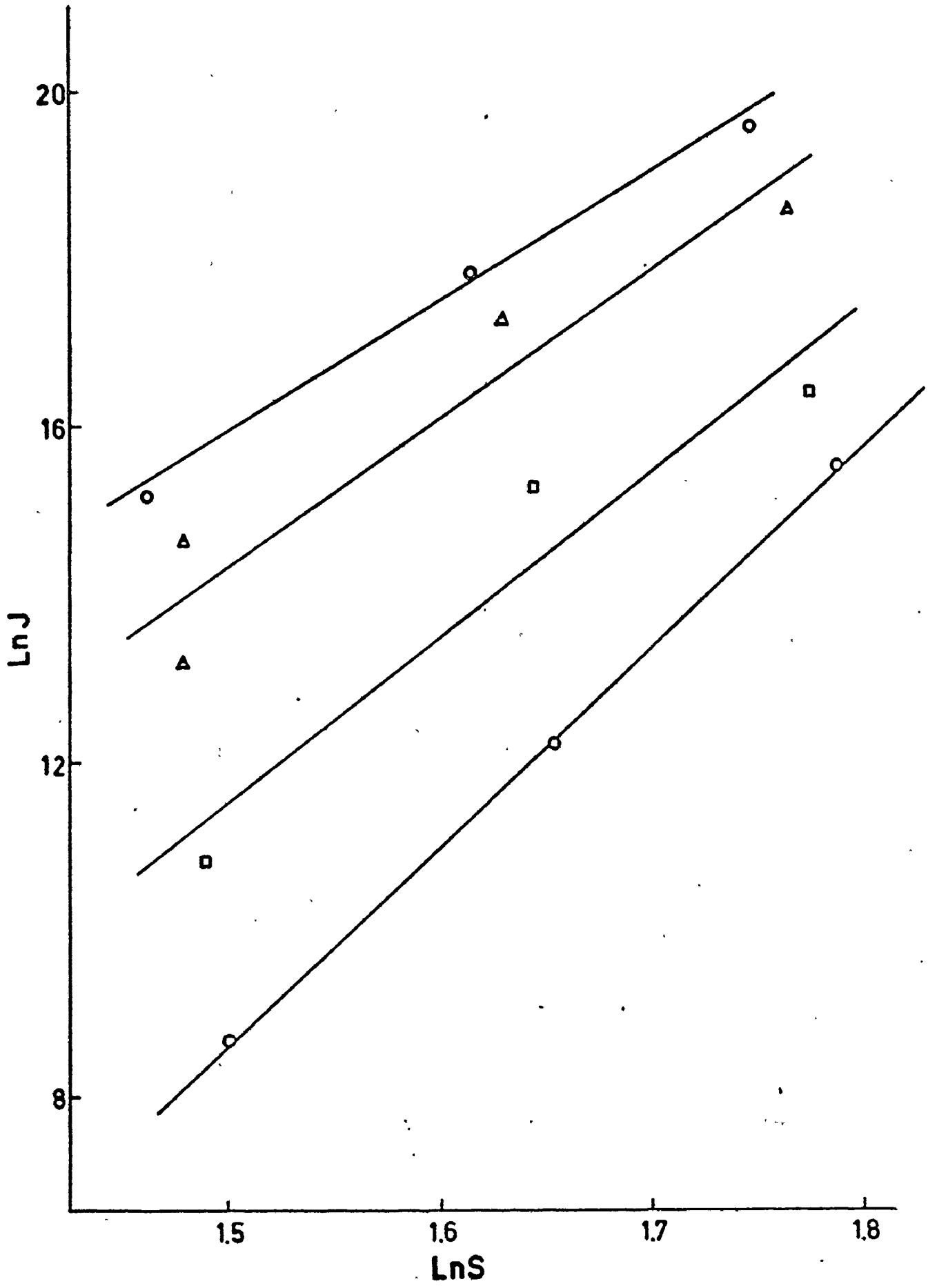
20
16
12
8
LnJ
1.5
1.6
1.7
1.8
LnS

Figure III-B8. The solution phase diagram for $CaSO_4 \cdot 2H_2O$ between 21.8 and 40.4°C.

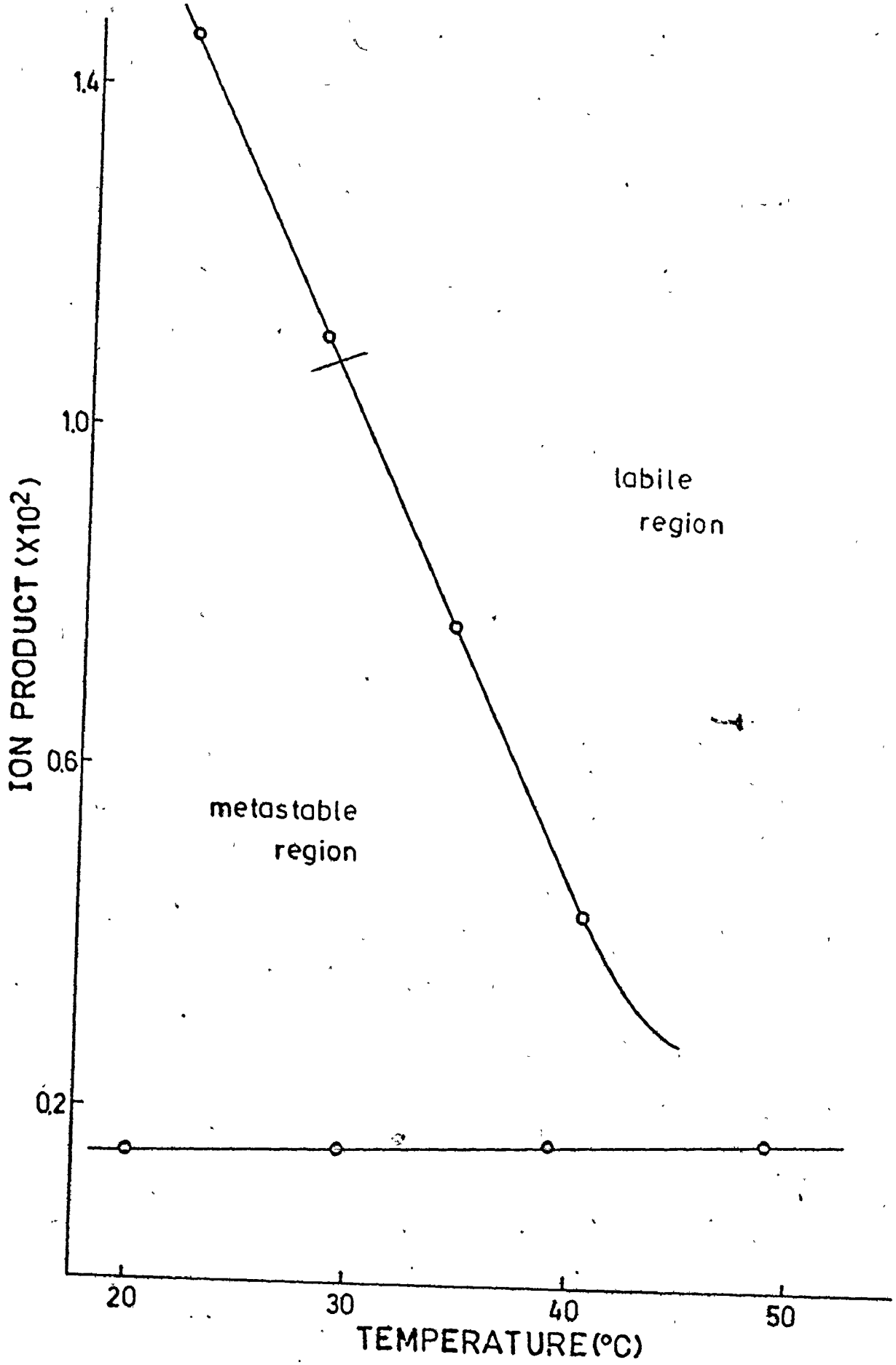
1.4
1.0
0.6
0.2
ION PRODUCT (X10²)
labile
region
metastable
region
20
30
40
50
TEMPERATURE (°C)

Figure III-B9. Plots of $\ell n J$ vs T^{-1} at three ion products

Legend	Ion product
o	0.03063
□	0.04151
Δ	0.05423

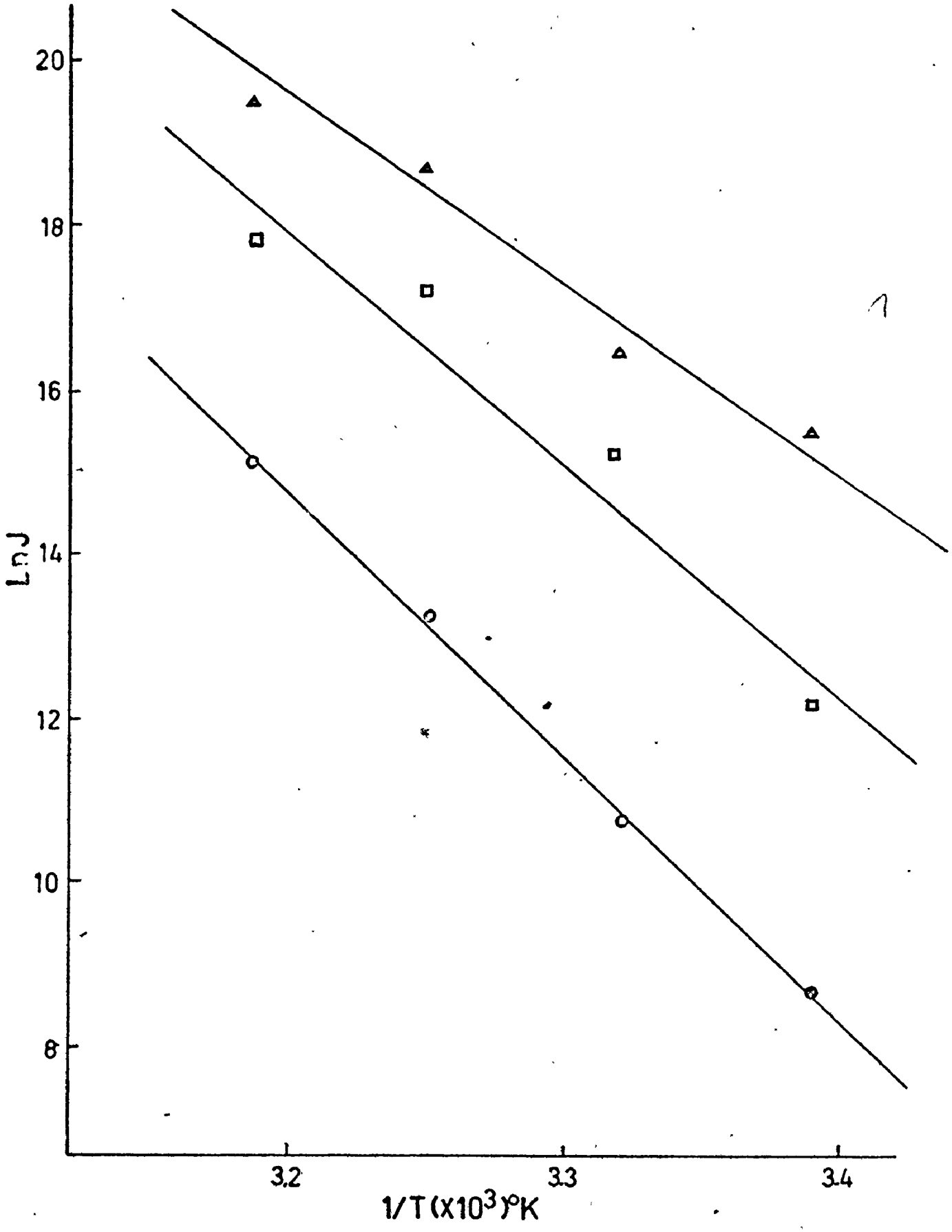
20
18
16
14
12
10
8
Ln J
3.2
3.3
3.4
1/T (x10³)°K

TABLE III-B4

Parameters calculated from ℓnJ vs T^{-1} data

parameter \ Ion product	0.03063	0.04151	0.05423
Slope ($\times 10^{-4}$)	-2.222	-2.708	-2.322
Intercept	86.2	104.2	93.9
ΔH ($\times 10^{12}$) (ergs.molecule^{-1})	3.07±.12	3.74±.50	3.21±.10
ΔS (ergs.deg.$^{-1}$ molecule^{-1})	$(8.9\pm9)\times10^{-15}$		

Temperature (°C)	ΔG^* (ergs. molecule^{-1})
21.8	5.84×10^{-13}
28.1	5.30×10^{-13}
34.3	4.77×10^{-13}
40.4	4.24×10^{-13}

It is noteworthy to look at the magnitude of ΔG^* as the temperature increases. The Gibbs free energy is positive at 21.8°C but becomes smaller (more spontaneous) as the temperature increases. It is interesting to compare the values of ΔG_n^* in Table III-B4 with those in Table III-B3. Using as a model equation (10), the free energy of the phase transformation increases with temperature. The free energy, calculated from ℓnJ vs 1/T plots, decreases with temperature, a result which is predicted by the non-classical model of nucleation described above in the discussion of ℓnJ vs $(\ell nS)^{-2}$ plots. The fact that calculations based on the classical model are misleading, may be one piece of evidence that the classical model is relatively limited in its description of nucleation of salts from solution. The effect of the assumptions made in its derivation finally surface in the calculation of ΔG_n^*.

LnJ vs ℓn 1/L is plotted in Figure III-B10. There is a linear relationship between ℓnJ and ℓn 1/L at constant temperature. The peculiarly small slope of the curve at 40.4°C is due to abnormally long lag times discussed below and in section III-D. This data, therefore, was discarded. The ℓnJ and ℓn 1/L values were fitted to a model given by equation (60).

$$\ell nJ = m\ell n\ 1/L + b. \qquad (60)$$

The calculated values of the slope, m, and the intercept, b, are reported in Table III-B5. Since both m and b are temperature dependent, equation (60) can be changed to include the relationship of ℓnJ and ℓn 1/L as the temperature and the super-

Figure III-B10. Plots of ℓnJ vs ℓn 1/L at four tempera-temperatures.

Legend	Temperature (°C)
o	21.8
□	28.1
▲	34.3
o	40.4

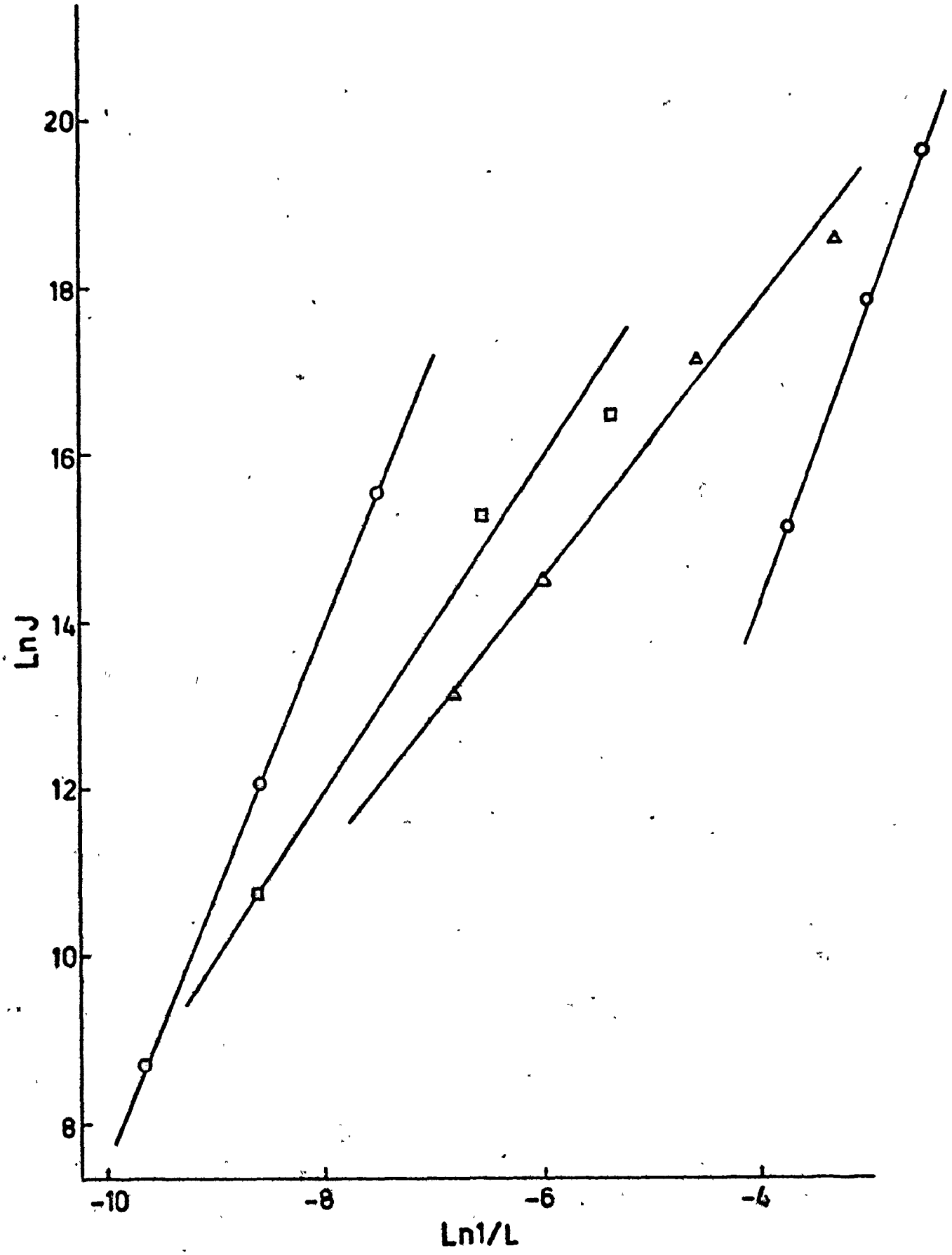
20
18
16
14
12
10
8
LnJ
-10
-8
-6
-4
Ln1/L

TABLE III-B5

Estimated values of the slope and intercept of equation (60) ℓnJ vs ℓn 1/L plots.

Temperature (°C)	Slope (m)	intercept (b)	relationship
21.8	3.213	-39.62	ℓnJ=3.213 ℓn 1/L+39.62
28.1	1.969	-27.59	ℓnJ=1.969 ℓn 1/L+27.59
34.3	1.640	-24.44	ℓnJ=1.640 ℓn 1/L+24.44

saturation changes

$$\ell nJ = f_1(T)\ \ell n\ 1/L + f_2(T) \qquad (61)$$

$f_1(T)$ is the value of m as a function of temperature, and $f_2(T)$ is the value of b as a function of temperature.

The linear relationship between ℓnJ and $\ell n\ 1/L$ is very important in that it demonstrates that the lag time is a real nucleation response (described in more detail in section III-D) and measurements of it can be used to estimate σ, ℓnA and S^*.

If equation (20) is substituted into equation (60) the following expression can be used at constant temperature.

$$\ell n\ 1/L = \frac{1}{m}\left[\ell nA - \frac{16\pi\bar{v}^2\sigma^3}{3k^2} \cdot \frac{1}{T^3(\ell nS)^2}\right] + \frac{b}{m}$$

$$= B - \frac{16\pi\bar{v}^2\sigma^3}{3mk^3} \cdot \frac{1}{T^3(\ell nS)^2} \qquad (62)$$

$\ell n\ 1/L$ is plotted against $T^{-3} \cdot (\ell nS)^{-2}$ in Figure III-B11 for temperatures of 21.8, 28.1, 34.3 and 40.4°C. Measured values of B, the intercept, the slope, and derived values of σ are listed in Table III-B6. The values of σ are not significantly different due to the fact that lag times are least reliable at higher temperatures and supersaturations. The use of equation (62) to calculate thermodynamic parameters is quite useful, however, at lower supersaturations where rate measurements fail due to droplet shrinkage and low $n_{t,v}/N$ values. The use of the droplet technique can be used to measure the nucleation rates, therefore, over an extended range of supersaturations and rates (from 10^2 - 10^8 sec^{-1}) and critical supersaturation can be calculated with more confidence.

Figure III-B11 Plots of $\ell n l/L$ vs. T^{-3} $(\ell nS)^{-2}$ at four temperatures.

Legend	Temperature (°C)
o	21.8
□	28.1
Δ	34.3
O	40.4

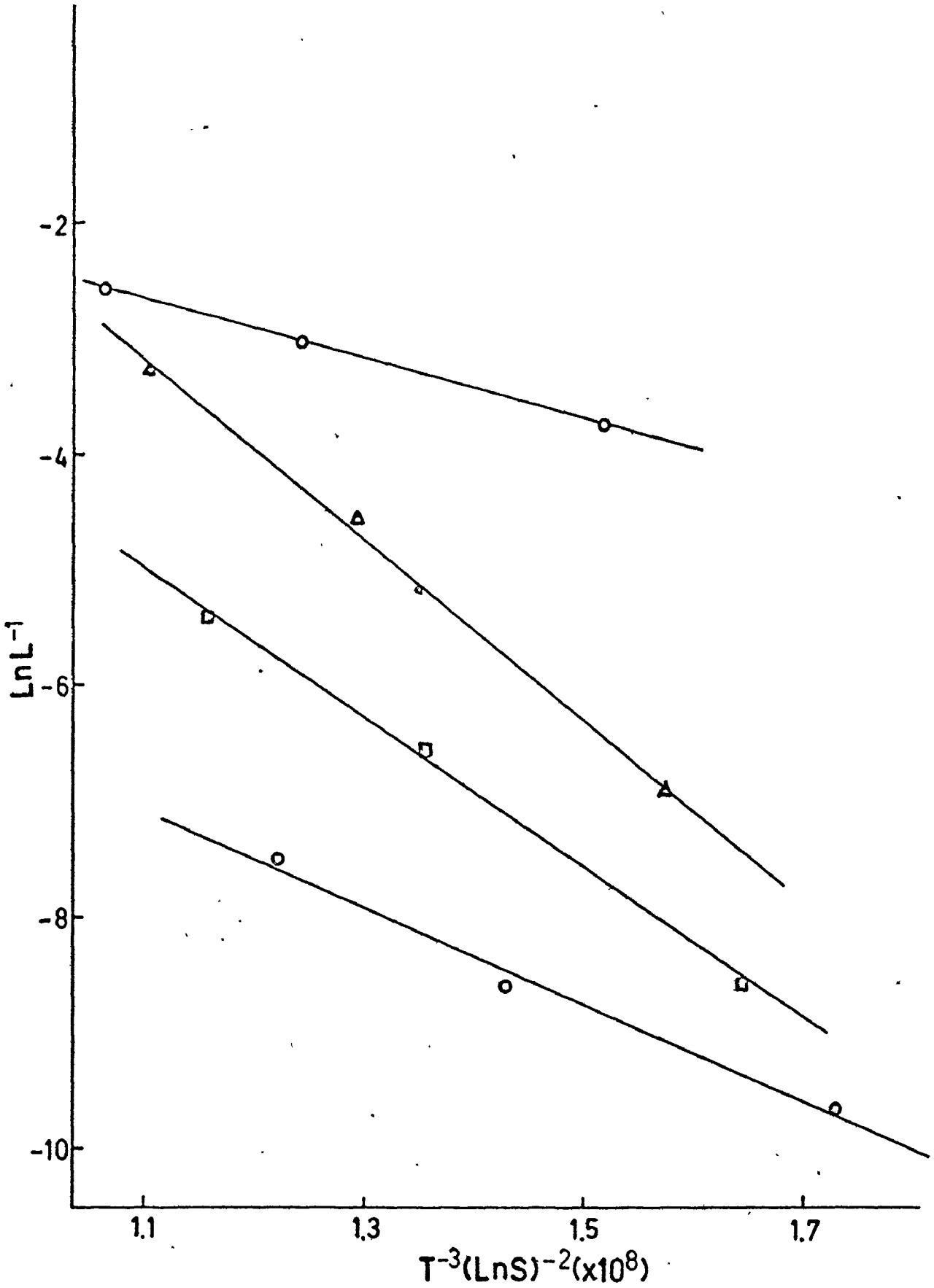
-2
-4
-6
-8
-10
LnL⁻¹
1.1
1.3
1.5
1.7
T⁻³(LnS)⁻²(x10⁸)

TABLE III-B6

Thermodynamic parameters calculated from plots of ℓn 1/L vs $T^{-3}.(\ell nS)^{-2}$

parameter \ Temperature (°C)	21.8	34.3	40.4
Slope ($\times 10^{-8}$)	-4.17	-6.44	-7.80
σ(ergs.cm^{2-})	24.01	23.59	23.65
Intercept	-2.49	2.83	5.41
b	-38.6	-25.0	-21.7
ℓnA	31.6	33.2	33.3

---

b = (Intercept × m)- ℓnA, m values taken from Table III-B5 and ℓnA average value from Table III-B3.

ℓnA = (Intercept × m)- b, b values taken from Table III-B5.

Experiments with a Variable Driving Force: In section III-A the rate was calculated using equation (38). There were a number of assumptions made, the consequences of which were not fully understood. It was estimated that one of the worst assumptions was the neglect of the lag time which affected the slope and intercepts of ℓnJ vs $(\ell nS)^{2-}$ plots leading to erroneous values of σ, S^* and ℓnA.

There are two routes that could be taken to extract meaningful data; either design experiments which minimize the supersaturation effects described in section III-A or derive a mathematical model which accounts for them.

Consider a droplet experiment with a high supersaturation being generated linearly by a chemical reaction. If we assume that the lag times are negligible and the supersaturation-time curve can be represented by a step function, the $n_{t,v}$ vs t curve can be approximated by the summation of steady-state rates over small time intervals Δt. $n_{t,v}$ calculations are given in the following for unit volume.

$$n_{i\Delta t} = N_1[1-\exp(-J,\Delta t)]+N_2[1-\exp(-J_2\Delta t)]+\ldots+N_i[1-\exp(-J_i\Delta t)] + \ldots\ldots \quad 0 \qquad (63)$$

After a time $t = 2\Delta t$

$$n_{2\Delta t} = N_1\{1-\exp[-\Delta t(J_1+J_2)]\}$$

after a time $t = 3\Delta t$

$$n_{3\Delta t} = N_1\{1-2\exp[-\Delta tJ_1)-2\exp[-\Delta t(J_1+J_3)]-\exp[-\Delta t(J_1+J_2+J_3)]\}$$

When the supersaturation is lower, however, the lag time becomes significant and the number of crystals forming with time at constant supersaturation can be approximated by equation (57). Summation over the small intervals, Δt, where the supersaturation is assumed to remain constant is now

$$n_{i\Delta t} = N_1\{1-\exp[-J_1(\Delta t-L_1)]\}+N_2\{1-\exp[-J_2(\Delta t-L_2)]\} + \ldots$$

$$\ldots+N_i\{1-\exp[-J_i(\Delta t-L_i)]\} + \ldots. \quad 0. \qquad (64)$$

The term $(\Delta t-L_i)$ may be replaced by Δt_i in equation (64). It fails when $L \geq \Delta t$. Using equations (20) and (62) for the rate and the lag time we can find an expression for $J_i\Delta t_i$

$$J_i\Delta t_i = A\{\Delta t \exp[-\frac{16\pi v^{-2}\sigma^3}{3k^3T^3(\ell nS)^2} - B]\} \qquad (65)$$

Substitutuion of equation (65) into (64) for $J_i\Delta t_i$ leaves a very complicated expression, the result of which is further confused when the rate of change of supersaturation is not linear. In this case, Δt would also be a function of the supersaturation.

The use of the equation proposed above requires that the duration of the lag time be known at every supersaturation along with the prexponential factor B described in equation (62). In cases where designed experiments cannot be performed and a suitable reaction cannot be found for step like generation of the supersaturation, the equations suggested above must be used with an estimation of some parameters.

From the results in this section the following conclusions can be made about the design of variable driving force experiments

(1) The rate equation (38) can be used with a changing supersaturation only when the lag time is small, $\partial L/\partial S = 0$, and there is a steady-state rate. If there is an induction time, (lag time until L plus a non-steady-state rate until τ), the steady-state rate is calculated from the $n_{t,v}$ information from time τ to infinity with the total number of droplets equal to $N-n_{\tau,v}$.

(2) High supersaturations must be used in the rate experiments with a variable driving force. This gives high rates of nucleation and negligible lag times yielding, however, poor extrapolated values of S* and more difficulty in measuring the rates.

(3) Care must be taken to keep $\frac{dS}{dt}$ as low as possible in order that the rate may be calculated as a function of supersaturation. Experiments at constant S are more time consuming but they remove most of the difficulties described above.

III-C NUCLEATION OF SALTS FROM SOLUTION AND CATION-ANION RATIO

Several authors[57] [58], have examined the homogeneous nucleation of some ionic salts and found that the critical supersaturation was independent of the ratio of cation to anion in the original mixture. The purpose of this section was to design and carry out experiments which nucleate calcium sulfate from aqueous solution at various cation-anion ratios at constant temperature and with a constant ion product. Observations of phase changes occurring in the droplets were photomicrographical-

ly recorded and the rate of nucleation, lag times, and induction times calculated.

III-C1 Experimental Design

The supersaturation was generated using the iodide-peroxydisulfate reaction. The iodide concentration was 0.35 M in all experiments and the ion product of calcium sulfate was set at a value of 0.03063 by carefully weighing out various amounts of reagent $Ca(NO_3)_2$ and $K_2S_2O_8$ to make up solution A. Solution A was prepared such that after reaction with iodide was complete, the calcium-sulfate ratios were 0.33, 0.50, 0.60, 0.75, 0.90, 1.00, 1.50, 1.75, 2.00, 3.00 and 4.00. The Nessler cup temperature was 34.3°C as water from the constant temperature bath, set at 40°C, was pumped through the thermostatted cell holder described in section II-B2.

III-C2 Nucleation Experiments

Droplets were prepared in each case for experiments E_{16} to E_{26} by a procedure described in section III-B2. The nucleation events were observed and recorded using the dark field illumination technique and the M41 microscope. The slides were processed, as described in section II-B3, giving $n_{t,v}$ data. The lag or induction times were separated using the procedure described in section III-B2 and the rate of nucleation calculated using equation (39) and a non-linear least squares program.

The experimental values of the rate of nucleation, reported in Table III-C1, were plotted against the cation-anion

TABLE III-C1

Rate and lag time measurements at various calcium-sulfate ratios

Ca^{2+}/SO_4^{2-}	L(sec)	τ(sec)	$J(sec^{-1})(\times 10^{-4})$
0.33	660		39.2
0.50	540		35.8
0.60	300		398.
0.75	300		146.
0.90	300		359.
1.00	420		222.
1.50	720	60	71.1
1.75	840	1080	35.1
2.00	1320.		9.07
3.00	4200	15,000	-
4.00	4800		9.59

ratio in Figure III-C-1. There are three important qualitative aspects of these rate-ratio data which are listed below:

1. The classical rate equation breaks down, in the case of calcium sulfate, since the rate is not constant with variable Ca^{2+}/SO_4^{2-} ratio and constant S. The supersaturation term "S" must be described in a more comprehensive expression.
2. The rate of nucleation is higher with excess anion compared with excess cation.
3. A maximum in the nucleation rate occurs when the calcium-sulfate ratio is 0.72 and not 1.0, as expected.

On the microscopic scale, it is quite obvious that the rate of nucleation should be a function of the cation-anion ratio, since the rate will depend upon the "effective monomer concentration". Since fluctuations, in the non-classical model, have a very short life-time , growth will be of lesser importance and the effective monomer concentration of more importance in their formation.

For example, if a supersaturated solution contained $[Ca^{2+}] = A$ and a $[SO_4^{2-}] = A+X$, the maximum concentration of monomers is A. The classical model, which depends upon growth, predicts a rate, at these conditions, equal to the rate when $[Ca^{2+}] = [SO_4^{2-}] = \sqrt{A(A+X)}$. The non-classical model, however, predicts a rate which is dependent upon the effective monomer concentration, A, and the ratio of cation-anion.

The trend to higher rates of nucleation with an excess of sulfate ion may be argued from either a growth or a diffu-

Figure III-C1. Plot of ℓnJ vs Ca^{2+}/SO_4^{2-}.

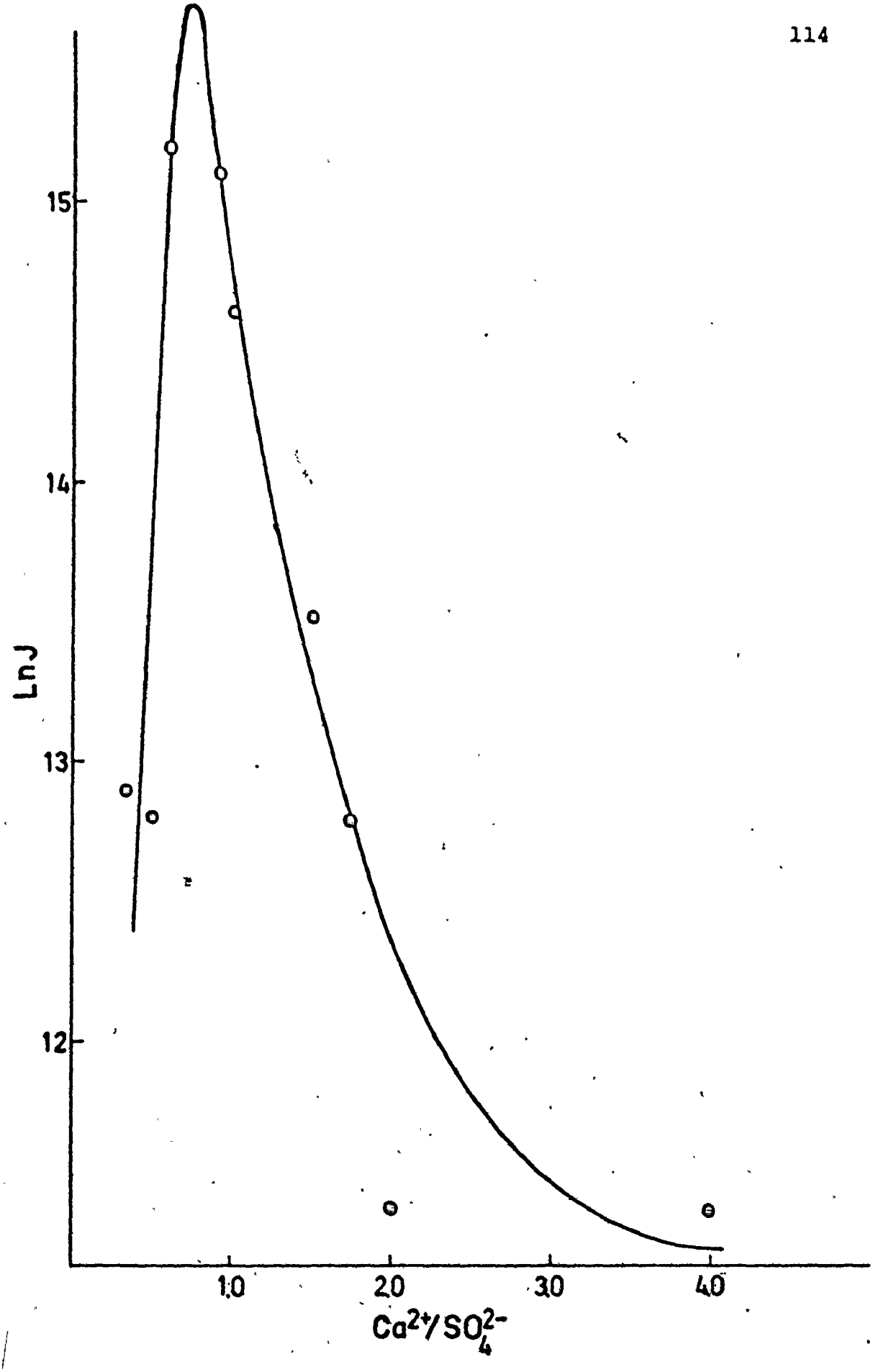
15
14
13
12
Ln J
1.0
2.0
3.0
4.0
Ca2+/SO42-

sional point of view. If the rate controlling step to nucleation is growth, which means that embryos have very long lifetimes, the rate measurements should follow very closely the results of crystal growth rate measurements at various cation-anion ratios. According to Nancollas et al[59], the growth rate of $CaSO_4 \cdot 2H_2O$ is surface controlled and independent of the diffusion. Their results, shown in Figure III-C2, show that the growth rate increases when sulfate is in excess but that the variation in the rate is small and there is no maximum. Comparing Figures III-C1 and III-C2, growth, if it is at all involved, is not a major factor governing the rate of nucleation.

A diffusional argument is particularly agreeable with the non-classical model since density fluctuations depend upon the mobilities and concentrations of monomers and ions. One can argue that because the rate is a function of the ratio of ions in solution the relative mobilities of ions is most important in governing nucleation phenomena. Some measure of the relative mobilities of the calcium and sulfate ions can be obtained from the diffusion coefficients measured by polarography. $D_{SO_4^{2-}} = 1.08 \times 10^{-5}$ and $D_{Ca^{2+}} = 0.79 \times 10^{-5}$ measured at infinite dilution and 25°C. Since sulfate ion is more mobile than calcium ion in aqueous solution, the formation of embryos should be facilitated when sulfate ion is in excess. The difference in the coefficients is small on the macroscopic scale but this may be magnified many times on the microscopic level.

The maximum rate at a calcium-sulfate ratio of 0.72 is more difficult to understand. The ratio of diffusion coefficients

Figure III-C2. Growth rates of $CaSO_4 \cdot 2H_2O$ as a function of Ca^{2+}/SO_4^{2-}.

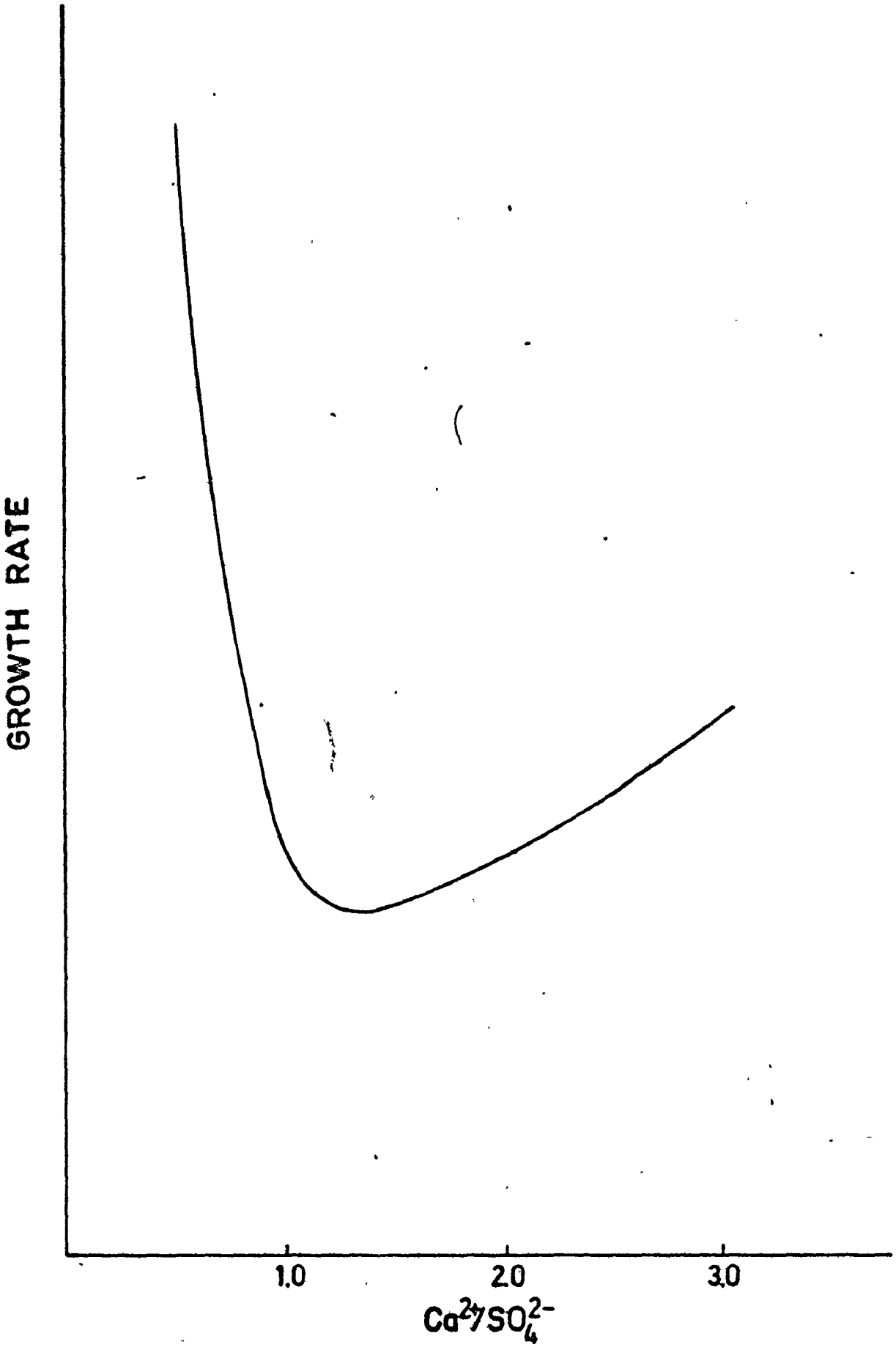
GROWTH RATE
1.0
2.0
3.0
Ca^{2+}/SO_4^{2-}

$D_{Ca^{2+}}/D_{SO_4^{2-}}$ is 0.73. This may be coincidence or it may suggest that the relative mobility governs the rate maximum.

The activity coefficients of calcium and sulfate, at an ionic strength of 1.40 are 0.189 and 0.114 respectively. The activity cation-anion ratio corresponding to the rate maximum is 1.19 which really doesn't solve any problems. These calculations of the activity coefficients, however, are only very approximate.

Quantitative results: The plot of the calcium-sulfate ratio in Figure III-C1 shows a skewed distribution about a maximum. We can redefine the independent variable by allowing

$$\left(\frac{Ca^{2+}}{SO_4^{2-}}\right)' = \left(\frac{Ca^{2+}}{SO_4^{2-}}\right) - 1 \quad , \quad \text{when} \quad \frac{Ca^{2+}}{SO_4^{2-}} > 1, \quad \text{and}$$

$$\left(\frac{Ca^{2+}}{SO_4^{2-}}\right)' = -\left(\frac{Ca^{2+}}{SO_4^{2-}}\right)^{-1} + 1 \quad \text{when} \quad \frac{Ca^{2+}}{SO_4^{2-}} < 1.$$

The ℓnJ vs $(Ca^{2+}/SO_4^{2+})'$ curve, shown in Figure III-C3 resembles a normal distribution. The data were fitted to the model given by equation (67) using a nonlinear least squares program described in section III-B.

$$J = B \exp\{-C[(Ca^{2+}/SO_4^{2-})' - D]^2\}. \qquad (67)$$

The estimated parameters were B = 15.3, C = 0.3, and D = -0.40. The parameter B represents the maximum rate and should be a function of the ion product and the temperature as predicted by classical theory. The parameter C describes how sharply the rate depends upon the calcium-sulfate ratio and it too may

Figure III-C3. Plot of ℓnJ vs $(Ca^{2+}/SO_4^{2-})'$.

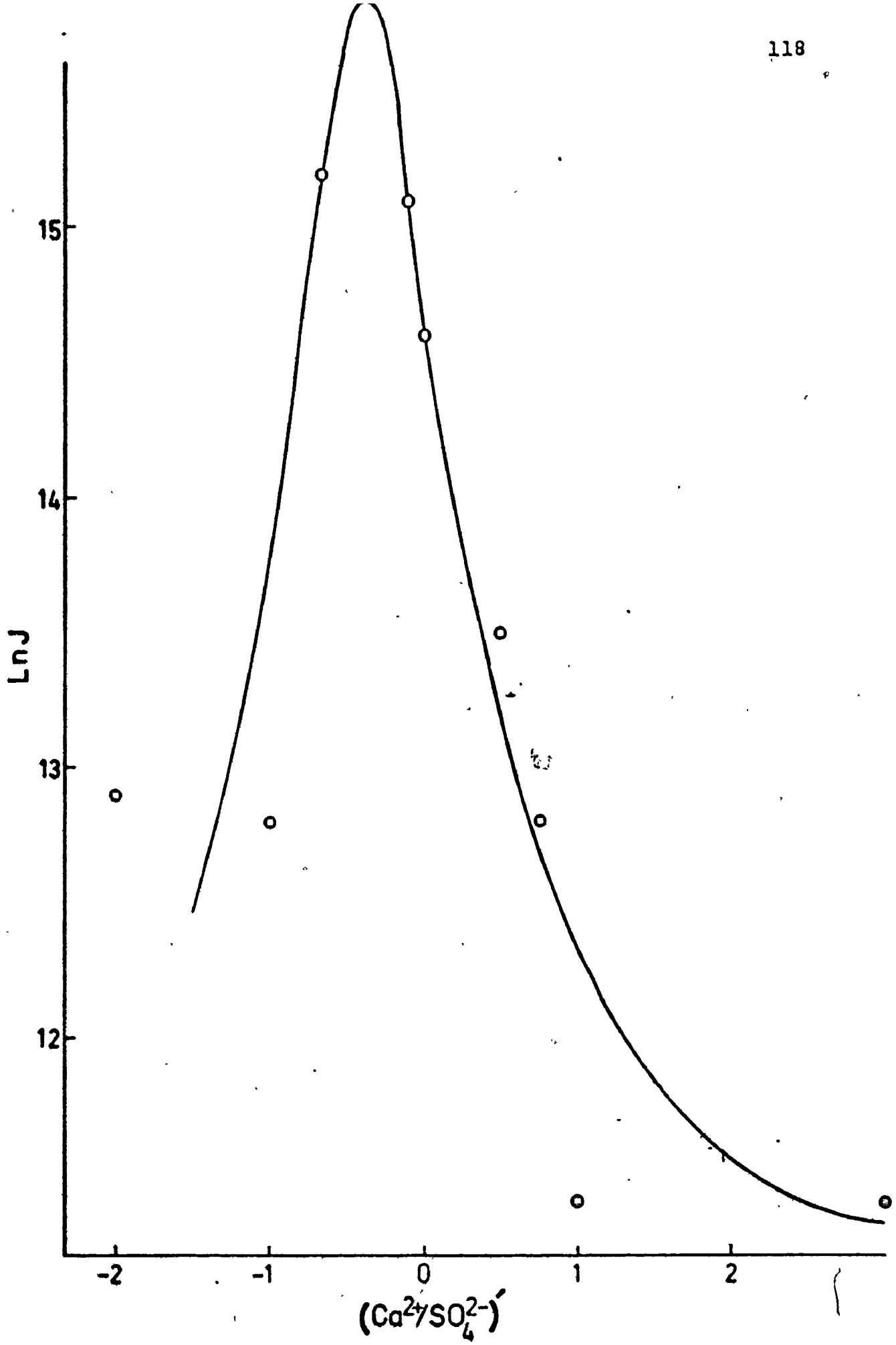
15
14
13
12
LnJ
-2
-1
0
1
2
$(Ca^{2+}/SO_4^{2-})'$

be a function of the I.P. and T.

If C and D are constants, independent of I.P. and T, equation (20) may be written

$$J = A \exp\left[\frac{-16\pi\sigma^{3}v^{2}}{3k^{3}T^{3}(\ell nS)^{2}}\right] \cdot \exp\left\{-C\left[\left(\frac{Ca^{2+}}{SO_4^{2-}}\right)' - D\right]^{2}\right\} \quad (68)$$

If in a set of experiments the calcium-sulfate ratio equalled D and if the supersaturation and temperature were varied, equation (20) is identical to equation (68). When the Ca^{2+}/SO_4^{2-} varies during the observation of $n_{t,v}$, disregard of the last exponential term in equation (68) will result in low measurements of the rate. Since the condition above will be present in all variable driving force experiments of the nucleation of ionic salts, their derived thermodynamic parameters A, σ, and S* will be affected.

The experimental values of the lag time, found in Table III-C1, were plotted against the calcium-sulfate ratio in Figure III-C4. There are three important aspects of the lag time ratio data. These are listed below:

1. Lag times vary with the cation-anion ratio. Equation (62) is only applicable, then, to sets of experiments with constant calcium-sulfate ratios and with temperature and supersaturation as changeable variables.
2. Lag times are shorter with an excess of sulfate ion over calcium ion present in solution. In Table III-C1, τ only appears when the cation-anion ratio is very high. The induction time, by definition will equal L in all other

Figure III-C4. Plot of ℓn L vs Ca^{2+}/SO_4^{2-}.

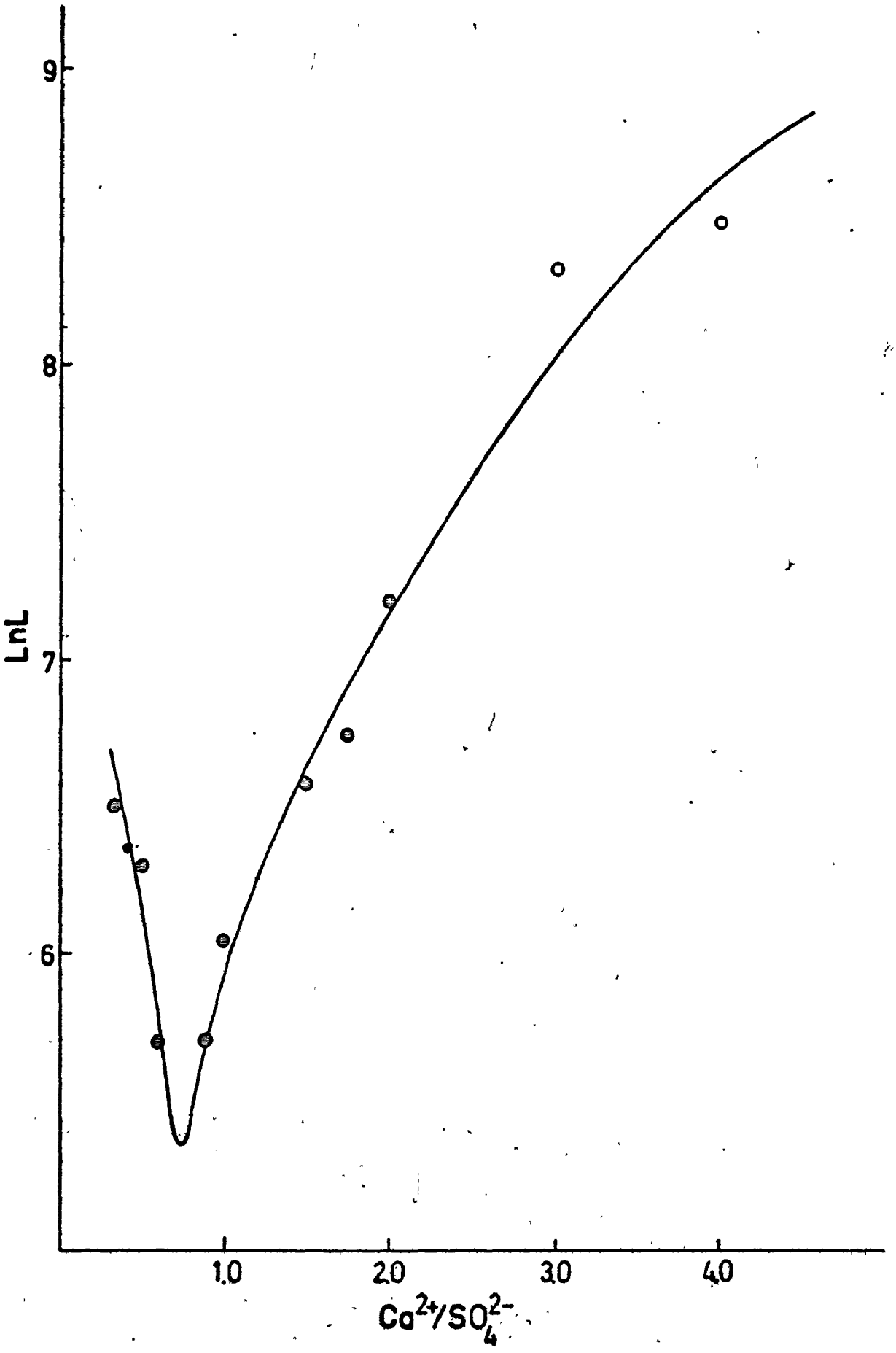
9
8
7
6
LnL
1.0
2.0
3.0
4.0
Ca^{2+}/SO_4^{2-}

3. A minimum lag time is estimated at a $Ca^{2+}/SO_4^{2-} = 0.72$, the same ratio which gave a maximum rate.

The same type of arguments used in explaining the rate-ratio data may be used here. The nucleation of $CaSO_4 \cdot 2H_2O$ seems to be controlled by diffusion, a fact more consistent with the non-classical theory.

A new piece of information not yet discussed springs from the observation of induction times at high values of the calcium-sulfate ratio. Equation (24), describing the induction time in terms of three microscopic components may be redefined in terms of the lag time and a component "M". This is shown by equation (69).

$$\tau = L + M = t_i + t_n + t_g. \qquad (69)$$

The "M" term corresponds to the duration of time required, after the appearance of a new phase, for the rate of nucleation to reach a steady-state value. In section III-D it will be shown that the lag time for $CaSO_4 \cdot 2H_2O$ has a major component of crystal growth. The M term may have components of nucleation and rearrangement time. If it is assumed that t_n is very small and $M = t_i$, then supersaturated solutions must exhibit long periods of time to arrange themselves.

Consider that there are two types of supersaturation, one a macroscopic type which is measured by gross terms such as Ksp and I.P., and the other a microscopic supersaturation determined by the solution structure. Assume that the build up of the microscopic supersaturation is rather sluggish but that it

speeds up as the supersaturation increases. If the critical supersaturation is passed very quickly and very high supersaturations are attained, the whole solution nucleates at the same microscopic supersaturation since rearrangement is fast and there should be a steady-state rate. If, however, the critical supersaturation is exceeded very slowly, the solution requires long rearrangement times and nucleation events occur at various microscopic supersaturations. The rate will increase with time (non steady-state). Not only is the solution rearrangement dependent upon the supersaturation but also on the calcium-sulfate ratio. The build-up of microscopic supersaturation is retarded, in the case of $CaSO_4 \cdot 2H_2O$, by excess calcium ion. This seems quite logical when one considers that calcium ion is less mobile due to tremendous solvent effects such as hydration and complexation.

Quantitative results: The lag-ratio data were used to calculate the parameters X, Y, and Z in equation (70).

$$1/L = X \exp\{-Y[(\frac{Ca^{2+}}{SO_4^{2-}})' - Z]^2\} \qquad (70)$$

The values of the parameters were X = 120 sec, Y = 0.32 and Z = -0.400. The parameter X, representing minimum lag time, can be equated with the right side of equation (62). If Y and Z are constants independent of I.P. and T we can write for 1/L,

$$\frac{1}{L} = K \exp[\frac{-16\pi \bar{v}^2 \sigma^3}{3k^3T^3(\ell nS)^2}] \cdot \exp\{-Y[(\frac{Ca^{2+}}{SO_4^{2-}})' - Z]^2\} \qquad (71)$$

The lag time dependence upon the cation-anion ratio and the appearance of non steady state rates at high ratio values

will further complicate ℓnA, σ, and S* measurements when the supersaturation is changing.

III-D pH EFFECT ON THE NUCLEATION OF CALCIUM SULFATE

It is very tempting to associate the lag time with the time required for nuclei to grow to detectable size. In this section, the pH effect upon the lag time and the rate of nucleation will be studied in hopes that t_g may be separated from L and that $\partial J/\partial pH$ is very small. As a consequence of the change in Ksp with pH, some statements are made about the change in the rate of nucleation with the Ksp.

III-D1 Experimental Design

The experiments, E_{27} and E_{28}, were carried out with solution conditions identical except for the pH. The following conditions were constant for both: T = 34.3°C, I.P. = 0.03063, Ca^{2+}/SO_4^{2-} = 1.0, and $[I^-]$ = 0.35 M.

The pH of the solution numbered experiment E_{27} was 3.23, whereas, the pH of the mixture of solutions A and B in experiment E_{28} was 7.60. The pH was raised by the addition of enough NaOH to solution B to raise the pH of the mixture of A and B, when diluted with solution A.

The Ksp of $CaSO_4 \cdot 2H_2O$ at a pH of 7.60 was measured using the technique reported in section III-B1. The pH of the matrix solution plus added $CaSO_4 \cdot 2H_2O$, contained in a thermostatted beaker, was adjusted to a pH of 7.60. The solution temperature was adjusted to 34.3°C and the solution was stirred for 12 hours. Aliquots of this solution were removed and the calcium

ion concentration determined by EDTA titration.

III-D2 Nucleation Experiments

Droplets were prepared for Experiments E_{27} and E_{28} by a procedure described in section III-B2. The nucleation events were observed and recorded using the dark field illumination technique and the M41 microscope. The slides were processed, as described in section II-B3, giving $n_{t,v}$ data. The lag times are separated using a procedure described in section III-B2 and the rate of nucleation calculated using equation (39) and a non-linear least squares program. The results are listed below.

Experiment	pH	Ksp	ℓnJ	L (sec)
E_{27}	3.23	1.592×10^{-3}	14.61±.15	420±20
E_{28}	7.60	1.674×10^{-3}	14.35±.39	240±15

In section III-B, it was observed that the rate change of the rate of nucleation per degree Celsius was about 1 at an I.P. of 0.03063 and 34.3°C. The Ksp change per degree at this I.P. and T was 0.40×10^{-3}. The change in the Ksp with pH in experimental E_{28}, however, was 0.8×10^{-3} while the rate remained statistically the same. The fact that $\partial J/\partial Ksp$ is very small, compared with the values of $\partial J/\partial T$ and $\partial J/\partial S$ which are of the order of 20, is very important to the calculations of ΔG^* from ℓnJ and 1/T data. The slopes of these curves at various supersaturations were in doubt because the Ksp was also changing with temperature. Since the Ksp effect is small, i.e. a small $\partial J/\partial Ksp$, the entropy calculation of $CaSO_4 \cdot 2H_2O$

was not drastically affected by a changing Ksp.

An important conclusion can also be drawn from the results of the lag times. It has been reported in the literature[60] that the growth rate of $CaSO_4 \cdot 2H_2O$ is accelerated as the pH increases, and levels off at about pH 7. In experiment E_{28}, the measured lag time was smaller than that measured at the lower pH. This may indicate that the experimentally measured lag times contain components of growth of the nuclei to detectable size as discussed in section I-C4.

If it is assumed that the growth rate at a pH of 7.60 is very large compared with that at pH 3.23, then at the lower pH $t_g/L = \frac{L_{7.60} - L_{3.23}}{L_{3.23}} = .43$. The growth time is at least 43% of the measured lag time at a pH of 3.23. At lower temperatures or lower values of the ion product, the percentage of growth time in L will decrease since it is expected that the change in growth rate to detectable size is much smaller than the change in the lag time with either the ion product or the temperature. The lag time of experiment E_4, for instance, was 14,400 sec.

It is important to point out that t_g may be an even larger percentage of the lag time at 34.3°C and an I.P. of 0.03063. The crystal growth rates from the literature are measured by seeding supersaturated solutions with macroscopic crystals. The rate of growth of submicroscopic growing nuclei, however, may be much smaller, since it is assumed that very small crystals have no surface imperfections, high energy sites which catalyze the growth process.

Figure III-D1. (a) Surface controlled growth and
(b) diffusional controlled growth of
crystals to macroscopic size.

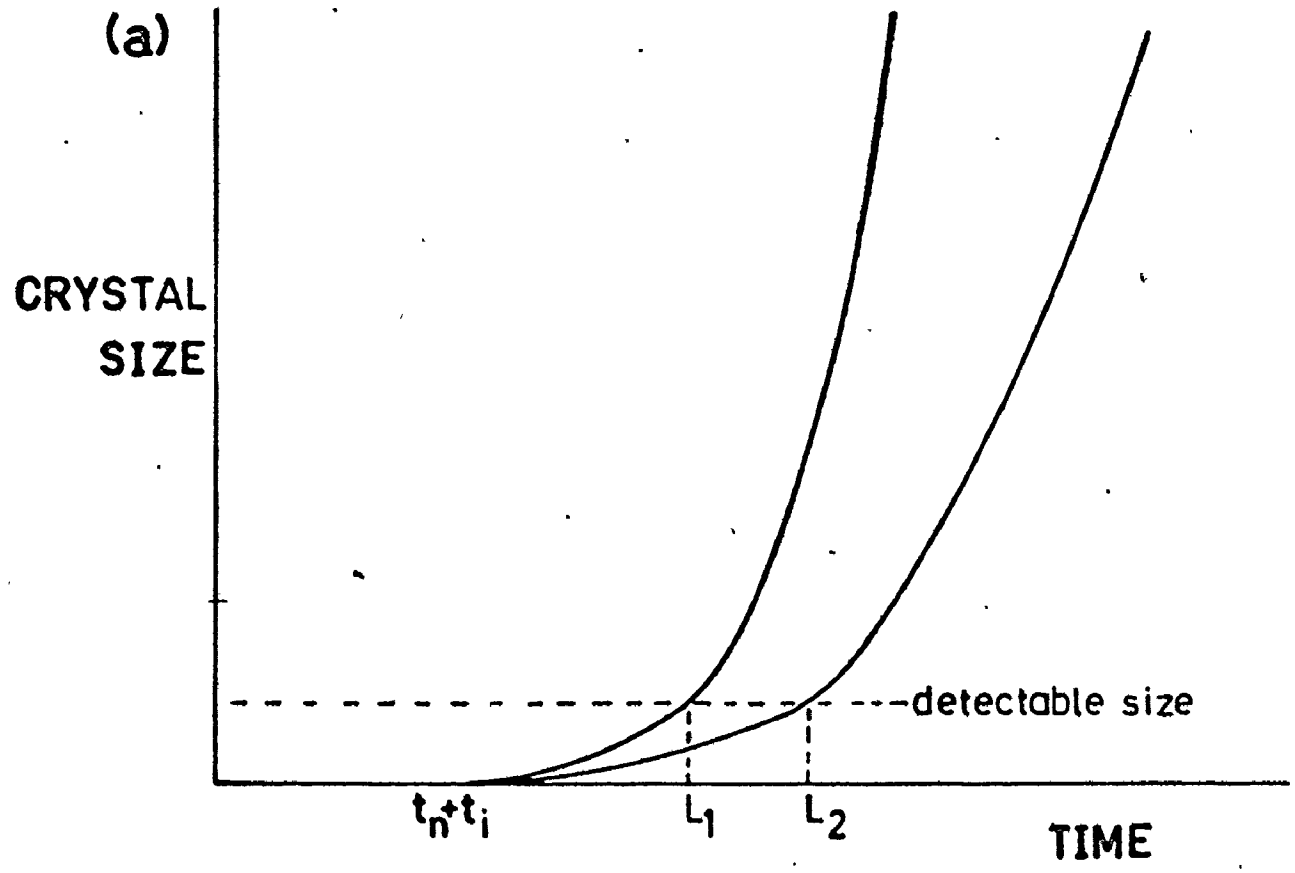
(a)
CRYSTAL SIZE
detectable size
t_n+t_i
L_1
L_2
TIME

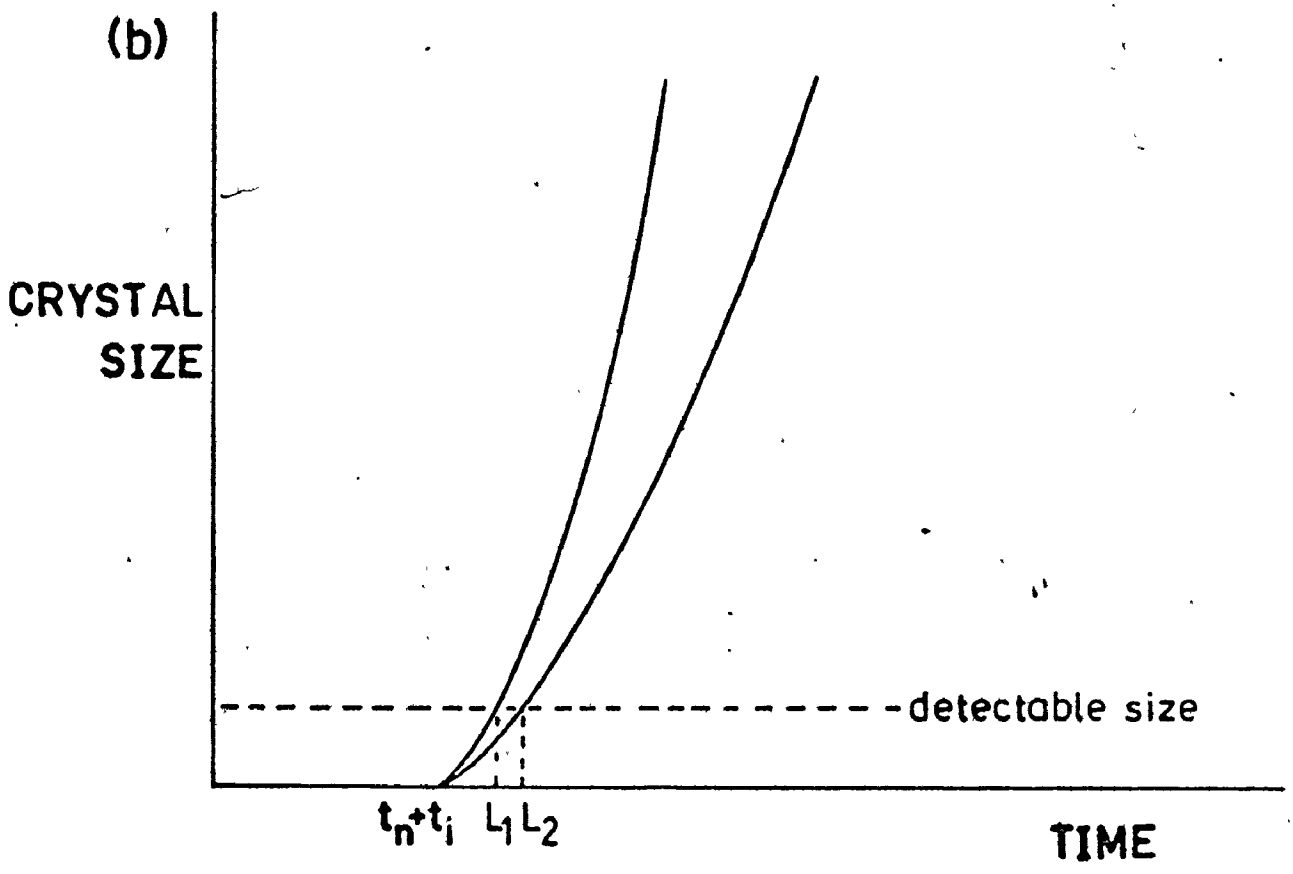
(b)
CRYSTAL SIZE
detectable size
t_n+t_i
L_1
L_2
TIME

The growth of nuclei to macroscopic size is represented in Figures III-D1 (a) and (b).

(a) If the period of surface controlled growth is very long, then t_g is a large percentage of the measured lag time.

(b) If the growth is diffusionally controlled, the period of growth to detectable size will be relatively short and t_g is of minor consideration. With an increase in the sensitivity of the detection device, more information about the magnitudes of t_g and L could be obtained.

The significance of experiments E_{27} and E_{28} is that they have provided evidence which proves that there is a component in experimental values of the lag time that is a "real" nucleation phenomena.

$$L = L' + t_g \tag{72}$$

L' is related to the rate of nucleation through equation (60). The growth time t_g is not related to the rate of nucleation. Lag time measurements are more meaningful when taken at low supersaturations where t_g/L is small. This criterion can be used to design experiments to estimate σ, ℓnA, and S^* using equation (62).

IV CONTRIBUTIONS

An exhaustive study of the nucleation phenomena of $CaSO_4 \cdot 2H_2O$ under various experimental conditions was undertaken in order that 1) the droplet technique could be evaluated, 2) an understanding of the mechanism of phase changes in aqueous solutions could be uncovered and (3) the

classical model could be tested for adequacy.

One of the contributions made was the derivation of a mathematical expression equating the rate of nucleation to the experimental response $n_{t,v}$. From this, a set of limiting equations applicable in various experimental situations were developed. These equations are particularly useful for the calculation of the rate from droplet technique data collected from variable driving force experiments. For a number of years it has not been clear whether the measured rate was a function of supersaturation and/or time when the supersaturation changes with time. These equations, with their limitations, described the nucleation rate as a function of both.

The rate of nucleation and the lag time were measured as functions of single independent variables T, S, and Ca^{2+}/SO_4^{2-} by careful experimental design. Most notable were the results of the work with the calcium-sulfate ratio. Comments on the classical definition of the supersaturation and expansion of equation (20) to include Ca^{2+}/SO_4^{2-} effects were two of the results of this study along with a proposal that diffusion was possibly the nucleation rate controlling step.

One severe limitation of the droplet technique, as it was discovered, is that the measurement of lag times is impossible when the supersaturation is changing. A chemical reaction was found which generated sulfate ion fast enough to approximate a step function. This turned out to be very bene-

ficial in that it allowed measurement of rates of nucleation and lag times at constant supersaturation and temperature and from these data an empirical relationship was uncovered between J and L. Using the correlation between these two fundamental nucleation responses we now can show that the droplet technique can be extended to much lower supersaturations and this leads to more accurate measurements of the critical supersaturation.

In the literature there is confusion about the definition of the pre-nucleation period labelled either the lag or the induction time. This author has found evidence for two distinct processes; a lag time, the time required for the new phase to appear, and the induction time, the time required until attainment of a steady-state nucleation rate. A new term, "M", was introduced where $M = \tau - L$, which is the time interval between appearance of a new phase and the attainment of a steady-state rate. L and M are symbols for two distinct phenomena.

A series of experiments at constant supersaturation and temperature were carried out and the various classical thermodynamic nucleation parameters calculated. Most significant of these was the critical ion product and Ksp vs temperature plot. This is a solution phase diagram for calcium sulfate with a curve near to that predicted by Ostwald at the turn of the century but never confirmed by experiment. Some comments were made about the usefulness of deriving ΔG^* from equation (10) in a comparison with those obtained graphically from ℓnJ vs $1/T$ plots.

The goal of experimental design is to extract the most information from the least amount of experimental work. When data are collected during variable driving force experiments, the droplet technique is most effective. To this end, a substantial effort was made to understand the criterion involved in the design of experiments. The factors found to be most critical were $\frac{dS}{dt}$, L, Ca^{2+}/SO_4^{2-}, and M. The effects of each upon the the data evaluation were studied individually and this information was gathered together to form a framework of experimental design for variable driving force droplet techniques.

Woven into the fabric of the thesis is a discussion of the mechanism of nucleation of salts from aqueous solution. Criticism of the classical model was presented as some experimental evidence seemed to be in conflict with is predictions. Paralleling this, a new model was introduced which seemed consistent not only with the results reported here but also with certain of those reported in the literature.

V FUTURE WORK

1. It would be interesting to measure the rate of nucleation and the lag time as a function of temperature, ion product, and the calcium-sulfate ratio. The nucleation phenomena, η, could be fit to equation (73)

$$\eta = \beta_o + \beta_1[Ca^{2+}] + \beta_2[SO_4^{2-}] + \beta_3[Ca^{2+}][SO_4^{2-}] \qquad (73)$$

where the β_i are functions of the temperature. A new definition for the supersaturation may evolve from such a study.

2. The development of practical equations to describe $n_{t,v}$ as a function of L, S, Ca^{2+}/SO_4^{2-} and t would be beneficial to data processing.
3. Since a sound method of studying the nucleation of $CaSO_4 \cdot 2H_2O$ has been developed, it may prove fruitful to delve into the field of nucleation inhibition. Besides being of universal interest, a study of nucleation inhibition may provide some understanding of the mechanism of phase changes in aqueous solution.
4. The experimental parameters used to study $CaSO_4 \cdot 2H_2O$ at constant T and S can easily be adapted to a study of $SrSO_4$.
5. The droplet technique can be used to study the nucleation of $CaCO_3$. A convenient photodecomposition reaction of a nitrated phenylacetic acid producing carbonate could be adapted to our microscopic observation techniques.

APPENDIX A

VARIANCE OF NON-LINEAR FUNCTIONS OF RANDOM VARIABLES:

A function $f(y_1, y_2, \ldots y_n)$ with random variables y_1, $y_2, \ldots y_n$ can be expanded in a Taylor series about a point described by y_1^o, y_2^o, ... y_n^o. This is shown in equation (A-1).

$$f(y_1, y_2 \cdots y_n) = f(y_1^o, y_2^o, \ldots y_n^o) + \sum_{i=1}^{n} \left.\frac{\partial f}{\partial y_i}\right|_{y_i^o} + \text{second order terms} \quad \text{(A-1)}$$

The expectation of the function is

$$E\{f(y_1, y_2 \cdots y_n)\} = f(y_1^o, y_2^o, \ldots y_n^o) + \sum_{i=1}^{n} \left.\frac{\partial f}{\partial y_i}\right|_{y_i^o} E(y_i - y_i^o). \quad \text{(A-2)}$$

The variance in the function is then

$$\begin{aligned} \text{Var}(f) &= E\{f(y_1, y_2, \ldots y_n) - E\{f(y_1, y_2, \ldots y_n)\}^2 \\ &= E\{\sum_{i=1}^{n} \left.\frac{\partial f}{\partial y_i}\right|_{y_i^o} [y_i - y_i^o - E(y_i - y_i^o)]\}^2 \\ &= \sum_{i=1}^{n} \left(\left.\frac{\partial f}{\partial y_i}\right|_{y_i^o}\right)^2 \text{Var}(y_i) + 2 \sum_{i=1}^{n} \sum_{j=1}^{n} \left.\frac{\partial f}{\partial y_i}\right|_{y_i^o} \text{Cov}(y_i y_i). \end{aligned} \quad \text{(A-3)}$$

Using the natural logarithm of equation (20) the variance in the rate is

$$\begin{aligned} \text{Var}(\ell n J) &= \left(\frac{\partial \ell n J}{\partial S}\right)^2 \text{Var } S + \left(\frac{\partial \ell n J}{\partial T}\right)^2 \text{Var } T \\ &= \left[\frac{32\pi\bar{\nu}^2\sigma^3}{3k^3T^3(\ell n S)^3, S}\right]^2 \text{Var } S + \left[\frac{16\pi\bar{\nu}^2\sigma^3}{k^3T^4(\ell n S)^2}\right]^2 \text{Var } T. \end{aligned} \quad \text{(A-4)}$$

Assuming the following values, components of Var $\ell n J$ were determined.

$S = 6.0$,

$\sigma^3 = 1.20\times10^4$,

$T = 295°K$ and,

$\bar{v}^2 = 1.52\times10^{-44}$.

$\text{Var}(\ell nJ) = 8.20\times10^4 \text{ Var } S + 2.27\times10^2 \text{ Var } T.$

Estimates of variances in S and T are 1.6×10^{-4} and 6.4 respectively. The components of the variance in ℓnJ are 1.31×10^1 for the supersaturation component and 1.45×10^3 for the temperature component.

APPENDIX B

NON-LINEAR LEAST SQUARES PROGRAM (GAUSHAUS)

The purpose of this program is to obtain least squares estimates of parameters entering non-linear equations in n unknowns. An iterative technique is used; the estimates at each iteration are obtained by a method due to Marquardt (1963) which combines the Gauss (Taylor series) method and the method of steepest descent. Since any type of mathematical model can be used, the user must specify its form by providing a subroutine to compute its values. The user must also provide a main program to read input data from cards and to initialize certain constants. Output from Gaushaus is a printed report which includes a description of the problem, a summary of each iteration, and information relating to the precision of the estimates and possibly to the adequacy of the mathematical model. Provision is made for multiple problem runs and for passing different models over the same data.

CO-OP Class/Index Code E2

CO-OP Organ. Code WISC.

University of Wisconsin Computing Center December 1965

UWCC I.D. Code C0017-00/S0017-00

LITERATURE CITED

1. D. B. Fahrenheit, Phil. Trans. Roy. Soc. 39, 78 (1724).
2. J. T. Lowitz, Crells Chemische Annalen, 1, 3 (1795).
3. H. Schröder and von Dusch, Leibigs Annalen, 89, 232 (1853); 109, 35 (1859).
4. Lecoq de Boisbaudran, Compt. Rend., 63, 95 (1866).
5. L. C. de Coppet, Ann. Chim. Phys. (5), 6, 275 (1875).
6. W. Ostwald, Z. Phys. Chem., 22, 289 (1897); 34, 493, (1900).
7. H. A. Miers and F. Isaac, J. Chem. Soc., 89, 413, (1906); 93, 927, (1908); Isaac ibid, 93, 384, (1908).
8. G. Tamman, Z. Physik. Chem. (Leipzig), 25, 441, (1898); Kristallisicren und Schmelzen, Leipzig (1903), p. 151; P. Othmer, Z. Anorg. Allgem. Chem., 91, 200, (1915).
9. C. Despretz, Compt. Rend. 4, 124, (1837); Ann. Physik, 41, 492 (1937).
10. L. Dufour, Ann. Chim. Phys., 68, 370, (1863).
11. D. Turnbull, J. Appl. Phys., 20, 817, (1949).
12. D. Turnbull, J. Chem. Phys. 20, 411, (1952).
13. R. Becker and W. Döring, Ann. Phys., 24, 317 (1935).
14. R. Becker, Discuss. Faraday Soc., 5, 55, (1949).
15. L. Farkas, Phys. Chem., 125, 236, (1927).
16. J. B. Zeldovich, Acta Physiochem. USSR, 18, 17, (1943).
17. J. Frenkel, Kinetic Theory of Liquids, Oxford Univ. Press (1946).
18. A. Kantrowitz, J. Chem. Phys., 17, 1097 (1951).
19. J. W. Christian, The Theory of Transformation in Metals and Alloys, Pergamon Press, Oxford (1965).

21. H. Garabedian and R. F. Strickland-Constable, J. Crystal Growth, 12, 53, (1972).

22. W. G. Hoover, A.C. Hindmarsh, and B.L. Holian, J. Chem. Phys. 57, 1980, (1972).

23. F. C. Frank, J. Crystal Growth 13/14, 154, (1973).

24. D. Turnbull and J. C. Fisher, J. Chem. Phys. 17, 91, (1949).

25. J. W. Mullin and C. L. Leci, J. Crystal Growth, 5, 75, (1969).

26. A.E. Nelson, Kinetics of Precipitation, Pergamon Press, New York, (1964).

27. H.A.C. Thijssen, M.A.G. Vorstman and J.A. Roels, J. Crystal Growth 3, 4, 355, (1968).

28. N. H. Fletcher, J. Chem. Phys. 29, 572, (1958).

29. I. Markov and D. Kaschiev, J. Crystal Growth, 16, 170, (1972).

30. A. A. Chernov and B. J. Lyubov, Rost Kristallov, Vol. 5

B. Lewis and D. Campbell, J. Vacuum Sci. Technol. 4, 209, (1967).

32. R. A. Sigsbee and G. M. Pound, Advan. Colloid Interface Sci. 1, 335, (1967).

33. V. Halpern, J. Appl. Phys. 40, 4627, (1969).

34. B. Lewis, Surface Sci. 21, 273,(1970).

35. I. Markov, Thin Solid Films 8, 281, (1971).

36. R. A. Sigsbee, J. Appl. Phys., 42, 3904, (1971).

37. I. Markov, A. Boynov and S. Toschev, Electrochim. Acta in print*.

38. L. Rosenstein, U.S. Patent 2,038,316, 1936.

39. G. L. Illig, J. Am. Water Works Assoc., 49, 805 (1957).

40. O. Rice and E. P. Partridge, Ind. Eng. Chem., 31, 58, (1939).

41. R. W. Liddell, U.S. Patent 2,782,162, 1957.

42. A. Glasner and S. Skurnik, Israel J. Chem.,6, 69 (1968).

43. M. N. Elliot,Desalination, 8, 221, (1970).

44. P. F. Rolfe, Desalination, 1, 359, (1966).

45. B. R. Smith, Desalination, 3, 263, (1967).

46. A. G. Walton, W.J. Bodin, H. Furedi, and A. Schwartz, Can. J. Chem. 45, 2695, (1967).

47. H. Garabedion and R. F. Strickland-Constable, J. Crystal Growth, 12, 53, (1972).

48. S. Tochev and I. Markov, J. Crystal Growth, 3,4,436, (1968).

49. I. E. Kuhns and B. J. Mason, Proc. Roy. Soc. A 302 , 437, (1968).

51,3435, (1973).

50. O. A. Bempah and O. E. Hileman, Can. J. Chem.

51. G. Gallo, Ann. Chim. Appl., 25, 628, (1935).

52. Gmelin Handbuch der Anorganischen Chemie Verlag Chemic, GMBH, Weinheim/Bergstrasse p. 256.

53. A.E. Carte, Proc. Phys. Soc. London, 73, 324 (1959).

54. E. K. Bigg, Phys. Soc. Proc. 66B, 688 (1953).

55. A. E. Carte, Proc. Phys. Soc. London, 73, 324, (1959).

56. I. E. Kuhns and B. J. Mason, Proc. Roy. Soc. A302, 437, (1968).

57. A. E. Nielsen, Crystal Growth, Pergamon Press, Oxford, 419, (1967).

58. D. Mealor and A. Townshend, Talanta, 13, 1069, (1966).

59. S. T. Liu and G.H.Nancollas, J. Crystal Growth, 6, 281, (1970).

60. O. J. Schierholtz, Can. J. Chem., 36, 1057, (1958).